



HAL
open science

Confinement and driving effects on continuous and discrete model interfaces

Paul Gersberg

► **To cite this version:**

Paul Gersberg. Confinement and driving effects on continuous and discrete model interfaces. Fluid mechanics [physics.class-ph]. Université de Bordeaux, 2020. English. NNT : 2020BORD0084 . tel-02977844

HAL Id: tel-02977844

<https://theses.hal.science/tel-02977844>

Submitted on 26 Oct 2020

HAL is a multi-disciplinary open access archive for the deposit and dissemination of scientific research documents, whether they are published or not. The documents may come from teaching and research institutions in France or abroad, or from public or private research centers.

L'archive ouverte pluridisciplinaire **HAL**, est destinée au dépôt et à la diffusion de documents scientifiques de niveau recherche, publiés ou non, émanant des établissements d'enseignement et de recherche français ou étrangers, des laboratoires publics ou privés.

École doctorale 209 : Sciences physiques et de l'ingénieur

THÈSE

pour obtenir le grade de docteur délivré par

Université de Bordeaux

Spécialité doctorale "Laser, Matière, Nanosciences"

présentée et soutenue publiquement par

Paul Gersberg

le 16 juillet 2020

Confinement and driving effects on continuous and discrete model interfaces

Directeur de thèse : **David S. Dean**

Co-directeur de thèse : **Peter C.W. Holdsworth**

Jury

Steve Bramwell, University College London,

Jorge Kurchan, ENS Paris,

Pierre Pujol, LPT Toulouse ,

Jérôme Cayssol, LOMA,

Professeur

Directeur de recherche

Professeur

Professeur

Rapporteur

Rapporteur

Examinateur

Président

Effets d'écoulements et de confinement dans les modèles discrets et continus d'interfaces

Cette thèse examine les propriétés de l'interface entre deux phases dans un système de phases séparées. Nous regardons comment les effets de taille finies modifient les propriétés statistiques de ces interfaces, en particulier comment la dépendance de l'énergie libre par rapport à la taille du système donne lieu à des interactions de Casimir critique à longue portée proche du point critique. Souvent, les interfaces sont décrites par des modèles simplifiés ou coarse-grained dont les seuls degrés de liberté sont les hauteurs de l'interface. Nous rappelons comment les propriétés statiques et dynamiques de ces interfaces sont retrouvées à partir de modèles microscopiques de spins et de la théorie statistique des champs. Nous étudions ensuite les effets de taille finie pour les interfaces continues comme le modèle Edwards-Wilkinson ou discrètes comme le modèle Solid-On-Solid, et discutons leur pertinence dans le cadre de l'effet Casimir critique.

Dans la seconde partie de la thèse, nous examinons des modèles d'interfaces sous écoulement possédant des états stationnaires hors-équilibre. Nous développons ces équations dans le cadre du modèle C d'une interface, ayant un état stationnaire hors-équilibre lorsque soumis à un écoulement uniforme. L'état stationnaire hors-équilibre résultant exhibe des propriétés retrouvées dans les expériences sur des colloïdes sous cisaillement, notamment la suppression des fluctuations de la hauteur de l'interface et une augmentation de la longueur de corrélation des fluctuations. Finalement, nous proposons un nouveau modèle pour des interfaces uni-dimensionnelles qui est une modification du modèle Solid-on-Solid contenant un terme supplémentaire d'entropie, dont la correspondance à des systèmes physiques reste à être trouvée.

Mots-clés : Modèles d'interface, Théorie d'ordonnancement des phases, Modèle d'Ising, Modèle Solid-On-Solid, Force de Casimir, Écoulements stationnaires hors-équilibre

Confinement and driving effects on continuous and discrete model interfaces

This thesis examines the properties of the interface between two phases in phase separated systems. We are interested in how finite size effects modify the statistical properties of these interfaces, in particular how the dependence of the free energy on the system size gives rise to long range critical Casimir forces close to the critical point. Often the interfaces in phase separated systems are described by simplified or coarse grained models whose only degrees of freedom are the interface height. We review how the statics and dynamics of these interface models can be derived from microscopic spin models and statistical field theories. We then examine finite size effects for continuous interface models such as the Edwards Wilkinson model and discrete models such as the Solid-On-Solid model and discuss their relevance to the critical Casimir effect.

In the second part of the thesis we examine models of driven interfaces which have nonequilibrium steady states. We develop a model C type model of an interface which shows a nonequilibrium steady state even with constant driving. The resulting nonequilibrium steady state shows properties seen in experiments on sheared colloidal systems, notably the suppression of height fluctuations but an increase in the fluctuations' correlation length. Finally we propose a new model for one dimensional interfaces which is a modification of the solid-on-solid model and containing an extra entropic term, whose correspondance with physical systems is yet to be found.

Keywords : Interface models, phase ordering dynamics, Ising model, Solid-On-Solid model, Casimir force, driven nonequilibrium steady states

Résumé en français

La majorité des systèmes statistiques peuvent être décrits par un paramètre d'ordre, comme la magnétisation moyenne dans les systèmes magnétiques, la densité dans un fluide ou l'orientation moyenne des polymères dans les cristaux liquides. Les propriétés statiques et dynamiques de tels systèmes sont bien décrites par la théorie statistique des champs. Dans cette théorie, le champ ϕ est soumis à un hamiltonien $H(\phi)$, et ses propriétés peuvent être dérivées de la fonction de partition Z . Lorsque ces systèmes possèdent une transition de phase au point critique, il y a une discontinuité de l'énergie libre due à la modification des micro-configurations possibles ; dans les systèmes magnétiques on passe ainsi d'une magnétisation nulle à une magnétisation finie, les liquides qui étaient auparavant mélangés se séparent, et les polymères adoptent une direction moyenne commune. Dans la phase ordonnée on retrouve alors des composantes connexes où la valeur de ϕ est quasi-constante. Entre ces composantes connexes se situe l'interface entre les phases. Dans cette thèse, nous nous intéressons particulièrement aux propriétés statiques et dynamiques des interfaces dans des modèles continus et discrets soumis à des contraintes telles que le confinement et le cisaillement.

Description d'une interface

La première partie de cette thèse est consacrée à la description des interfaces à partir de la théorie statistique des champs. L'utilisant un champ externe ϕ^4 dans l'Hamiltonien induit une séparation de phase en dessous de la température critique, ce qui donne une interface dont le profil peut-être calculé grâce aux équations dynamiques du modèle A dans le cas stationnaire. L'énergie libre associée à cette interface est directement reliée à la tension superficielle σ par la relation de Cahn-Hilliard. Depuis les équations de théorie statistique des champs, en considérant une interface d'épaisseur nulle, on retrouve les équations d'Edwards-Wilkinson pour le modèle A et le modèle B. La réduction du nombre de degrés de liberté par cette transformation d'un volume en surface permet leur étude grâce à des intégrales de chemin.

Ensuite nous expliquons le modèle le plus simple sur réseaux - le modèle d'Ising - qui décrit un réseau orthonormé de spins avec une interaction entre plus proches voisins plus un champ externe. Ce modèle, où chaque site du réseau prend la valeur $\sigma_i = \pm 1$, permet de modéliser un système de gaz sur réseau ou de liquides binaires en faisant un changement de variable sur σ_i . En appliquant la même approximation d'interface d'épaisseur nulle que précédemment, on trouve cette fois-ci le modèle Solid-On-Solid. La fonction de partition SOS a l'avantage d'être diagonalisable grâce à la matrice de transfert. Dans la limite thermodynamique, seul l'état fondamental (qui possède la plus grande valeur propre de la matrice de transfert) est nécessaire pour obtenir toutes les observables du système.

Dans ce premier chapitre, une grande importance est également donnée quant à la différence entre les différents ensembles statistiques. La complexité de l'ensemble canonique provient de la contrainte sur la hauteur totale de l'interface qui ne peut être intégrée au formalisme des matrices de transfert issus de l'ensemble grand-canonique. Pour étudier ces différences, il faut donc utiliser des méthodes numériques. Dans l'ensemble canonique, il est également possible d'introduire des états stationnaires hors-équilibre grâce à l'advection d'un champ de vitesse.

Méthodes numériques

Dans le second chapitre, nous développons les simulations de Monte Carlo Métropolis, qui permettent d'explorer l'espace des configurations et ainsi obtenir les valeurs moyennes d'observables. Ces méthodes sont particulièrement adaptées aux systèmes sur réseau comme le modèle d'Ising ou Solid-On-Solid, dont les implémentations de Glauber ou de Kawasaki fixent l'ensemble thermodynamique du système.

Néanmoins, l'énergie libre n'est pas une valeur mesurable directement dans les simulations de Monte Carlo, et il faut alors utiliser des méthodes indirectes. La méthode de Vasilyev consiste à découpler progressivement une rangée du système afin d'obtenir la dérivée de l'énergie libre par rapport à la taille du système. Cette méthode ne fonctionnant pas dans le cas du modèle SOS à cause de l'absence de terme de volume dans l'hamiltonien, la méthode Lopes-Jacquin-Holdsworth développée dans le cas d'un champ magnétique uniforme est plus pertinente. Puisque l'intensité du champ magnétique est la valeur conjuguée de la magnétisation totale, l'intégrale de la magnétisation entre deux intensités permet d'obtenir la différence entre l'énergie libre des deux systèmes. Cette méthode utilisant la magnétisation, elle ne peut être utilisée lorsque le paramètre d'ordre est conservé. Il n'existe dans la littérature aucune méthode pour mesurer l'énergie libre dans des simulations numériques de Kawasaki pour le modèle SOS.

Le chapitre se termine avec une petite liste d'astuces pour optimiser et paralléliser le code numérique.

Interfaces à l'équilibre et effets de taille finie

Lorsque la longueur de corrélation est du même ordre de grandeur que la taille du système, la contrainte imposée sur les modes mous de fluctuations ajoute une partie singulière à l'énergie libre. Cette dépendance de l'énergie libre en fonction de la taille du système implique une force thermodynamique qui s'appelle force de Casimir dans le cas des fluctuations du champ électromagnétique entre deux plaques diélectriques parfaitement conductrices, ou effet Casimir critique dans les systèmes critiques. Après avoir exposé ces deux effets grâce à la mécanique quantique et le groupe de renormalisation, cette force de confinement est étudiée dans le cas des interfaces confinées.

En utilisant le formalisme de Matsubara pour l'équation du propagateur de l'hamiltonien dans le cas d'une interface continue soumise à un champ externe, la distribution de probabilité de l'interface, l'énergie libre, la fonction de corrélation à deux points et la longueur de corrélation sont explicités en fonction de l'énergie de l'état fondamental et du premier état excité. En appliquant ce formalisme à une interface libre et confinée, nous retrouvons des

résultats connus sur la force thermodynamique. Dans le cas où cette interface ne possède pas de tension superficielle (comme c'est le cas dans les systèmes critiques), la correction de taille finie à la tension superficielle proposée par Privman nous permet de retrouver quantitativement le même comportement que pour la force de Casimir critique, ce qui jette un lien intéressant entre la physique des interfaces et celle des systèmes critiques. Nous utilisons également ce formalisme dans le cas où l'interface est confinée à cause d'une pression afin de trouver la hauteur de moyenne de l'interface et sa variance.

Puisque la méthode Lopes-Jacquín-Holdsworth de calcul de l'énergie libre dans les simulations de Monte Carlo n'est pas utilisable dans la dynamique de Kawasaki et que la méthode de Vasilyev ne l'est pas non plus pour les modèles SOS, nous généralisons la méthode LJH pour des champs externes non-uniformes, permettant ainsi l'intégration sur une magnétisation généralisée qui n'est plus conservée dans une dynamique de Kawasaki. La généralisation de cette méthode permet de démontrer numériquement une ressemblance forte entre les ensembles canoniques et grand-canoniques dans le modèle SOS et ouvre la voie à des études plus poussées de l'effet Casimir critique sur les modèles d'Ising dans l'ensemble canonique.

Ce troisième chapitre s'achève par la diagonalisation exacte de la matrice de transfert du modèle SOS en absence de potentiel externe, généralisant ainsi les résultats de Privman, avec une étude des limites à faible et haute température ainsi que dans la limite thermodynamique.

Le modèle Particles-Over-Particles

Le modèle SOS est un modèle d'interface provenant de l'approximation à basse température du modèle d'Ising. Nous développons dans ce quatrième chapitre un nouveau modèle prenant en compte le terme d'entropie associé aux simulations numériques dans le modèle d'Ising et faisant défaut dans SOS, que l'on nomme Particles-Over-Particles. Ce terme d'entropie apparaît lorsque l'on considère non plus juste la hauteur de l'interface (comme dans SOS), mais également le nombre de particules en dessous. En labellisant ainsi les particules, il devient possible de créer des modèles avec M types différents de particules, chacune étant régie par un coefficient cinétique ou un coefficient de diffusion dans le cas où elles appartiennent à des ensembles thermodynamiques différents. De nombreuses difficultés surviennent lors de l'implémentation de Metropolis sur dans ce modèle et les applications physiques sont laissées en suspens. Ces deux questions sont laissées comme exercice pour les lecteurs.

Interfaces stationnaires hors-équilibre

Lorsqu'une interface est advectée par un champ de vitesse, sa largeur et sa longueur de corrélation sont modifiées. Le cinquième et dernier chapitre s'intéresse à un écoulement uniforme et constant.

À cause de l'invariance galiléenne de translation dans le référentiel de l'écoulement, l'équation dynamique du modèle B reste inchangée. Le cas d'un champ soumis au modèle B et couplé à un autre champ soumis au modèle A (afin de briser l'invariance galiléenne) a été l'objet d'un article publié dans **Journal of Statistical Mechanics: Theory and Experiment** en mars 2020, et la première partie de ce chapitre est une reproduction de l'article original. À partir

des équations couplées donnant le modèle C, une relation fermée pour la dynamique d'une interface soumis à un écoulement uniforme et constant dans l'espace de Fourier est trouvée. Le résultat principal de cet article est la preuve que des systèmes hors-équilibre peuvent avoir des propriétés similaires à celles des systèmes à l'équilibre via un redimensionnement effectif des observables. Dans les systèmes où l'écoulement est uniforme, conformément aux expériences de Derks et aux simulations numériques de Smith, nous trouvons que la tension superficielle effective de l'interface augmente avec l'intensité de l'écoulement. De plus, nous montrons comment ce modèle permet de décrire l'interface entre deux phases de colloïdes ayant une activité différente en jouant sur la température de chaque phase.

Dans le cas où l'écoulement n'est pas appliqué qu'au niveau de l'interface, des études numériques du modèle SOS montrent une diminution de la tension superficielle en fonction de l'intensité de l'écoulement, contrairement aux calculs précédents, mais en accord avec la génération de vagues par le vent sur l'eau. Des pistes de réflexion sont apportées sur la différence entre les deux types de cisaillement.

Remerciements

Cette thèse n'a pas duré quatre années mais bien vingt-six. C'est pour cela qu'il m'est impossible de ne pas remercier toutes les personnes avec qui j'ai interagi et qui m'ont mené là où je suis.

Je tiens particulièrement à remercier mes deux directeurs de thèse, l'un gallois et l'autre britannique. Je n'avais pas compris la difficulté que représente une thèse jusqu'à ce que je la fasse : j'ai eu énormément de moments de doutes, et bien que mes proches m'aient soutenu pour ne pas abandonner, ceux qui apportaient les arguments les plus convaincants furent toujours David et Peter. Je n'oublierais pas tout ce qu'ils ont fait pour moi dès le début, et pour ça, je leur dédie cette thèse. Bien que certaines fois la communication ait été "un peu trop russe" (sic), je conseille aux futurs doctorants qui liront la présente de leur faire confiance.

Je dédie également cette thèse à ma mère, qui a relu le manuscrit plusieurs fois pour les coquilles et m'a soutenu tout du long, et à mon père, qui dès ma plus jeune enfance a cultivé mon esprit curieusement scientifique. Un gran abrazo también a mi hermana, por ser, por estar y por amar. Los amo a los tres! También agradezco un montón a toda la familia argentina, a les tías y primes, et à tous les amis de la famille qui se sont enquis de mon avancement durant le périple.

Du collègue et du lycée, je retiens d'abord deux professeurs qui m'ont honoré de leur présence lors de la soutenance en ligne, treize ans plus tard : S. Borde (SVT) et J. Abauzit (Physique-Chimie). Je suis fier d'être officiellement le premier docteur du Club Sciences de Marcel Roby. Je remercie également Morgane, Xavier, Pierre pour leur soutien et Guillaume pour son cours d'algèbre des groupes qui m'a aidé à valider la L3.

De l'UPMC, je remercie Driss-kohai, José Alejandro, Jean-Baptiste, Maxime, William et Sami pour avoir partagé les bancs avec moi durant les interminables cours de thermodynamique ou de physique non-linéaire, ainsi que Massil et Paul qui m'ont donné des idées pour ma carrière professionnelle. Un grand bisou à Quentin et à Matthieu, deux danseurs aux styles atypiques qui m'ont accompagné dans la salsa, et à Nicolas, qui a libéré le geek en moi. Si je pouvais recommencer depuis la L1 et aller en prépa au lieu de la fac, pour tous vous avoir connu, je refuserai.

Au LOMA, mention spéciale à mes deux co-bureau successifs, Quentin et Alexandre (à qui j'ai promis de placer le mot cabestan dans ce manuscrit qui a finalement été rédigé en anglais), pour toutes les discussions de bureau sur la politique, la science et la vie en général. Je remercie également Mathieu, précédent doctorant de David, qui a cédé afin de m'accompagner à Bruneck et pour son aide technique concernant le MCIA. Je suis également reconnaissant à toute la clique lomienne, changeante au fil des années, dont mon groupe était constitué de Quentin (il est partout!), Julie, Goce, Marion, Alizée, Alexandre, Houssem et un peu Mathilde. Merci pour le vidéoprojecteur, j'avais presque réussi à oublier ce pas-

sage honteux de ma vie. Je n'oublie pas non plus Stéphan, qui était avec moi en M2 et avec qui l'on s'est retrouvés incroyables dans le même laboratoire de Bordeaux pour une thèse, devenant de fait mon colocataire pendant deux ans et demi. Parmi les membres permanents du laboratoire, je remercie J. Parzych pour son suivi administratif, Jean-Pierre et Joseph pour leurs anecdotes interminables à l'heure du repas et Thomas pour m'avoir emmené faire du surf en crocs-chaussettes.

Du côté de Lyon, où je suis resté huit mois lors de ma seconde année, je remercie particulièrement L. Mauduit pour le suivi administratif lors de mon séjour, Samuel et Jérôme, avec qui j'ai passé d'excellents moments, ainsi que Pol et Alexandre, collègues de fait dans le monde du divertissement ludique. Et Riad, envoie-moi une carte depuis l'ISS !

Je continue avec Eileen, ex-présidente de l'association des doctorants SPIDoc pour la peluche qu'elle m'a offerte, ainsi qu'avec Nelson - qui n'aura qu'à lire les remerciements de sa propre thèse pour se souvenir pourquoi il est dans les miens !

Je finis cette section en remerciant chaleureusement la Section Jeune et la Société Française de Physique, pour la tenue du French Physicists' Tournament¹. Ce tournoi - auquel j'ai participé en M1 avec Joao et William et qui m'a profondément convaincu de l'amusement que procure la Philosophie Naturelle - consiste en une série de problèmes de physique de coin de table que les étudiants doivent résoudre au mieux en un semestre, avant de présenter leurs résultats devant les équipes des autres universités et écoles. Pour la tenue de ces événements, je remercie les Présidents successifs : Daniel, Arnaud et Lorenzo. Cette aventure, j'ai pu la réitérer en tant qu'encadrant lors de mes années de thèse, portant l'équipe de Bordeaux avec Simon, Thomas et Maxime. Je prierai en 2021 pour que l'on obtienne la médaille d'argent ! J'invite tous les physiciens, permanents et doctorants, et former leur équipe et à participer dans cette aventure palpitante qu'est le FPT.

Et pour tous ceux que je n'ai pas mentionné, sachez que si vous êtes assez proches de moi pour regarder si vous êtes cités dans les remerciements, je vous assure qu'au moment de rédiger ces lignes, je pense à vous !

NB: étant très nostalgique, j'écris un message pour mon futur moi. Malgré les difficultés du moi passé à achever la thèse, sache que je suis très fier maintenant, et que les portes que j'espère m'ouvriront seront bel et bien ouvertes. J'espère pour toi que tu trouveras un travail qui te plaira vraiment, alliant physique, informatique et utilité climatique.

¹<https://france.iptnet.info/>

Contents

Contents	xi
Introduction	xiii
1 Equilibrium interface dynamics	1
1.1 Models for equilibrium fields	2
1.1.1 Statics of systems with a finite number of degrees of freedom	2
1.1.2 Statistical field theory	4
1.1.3 Surface tension	7
1.2 Models for equilibrium interfaces	8
1.2.1 Basic continuous model	8
1.2.2 Effective dynamics of interface heights	10
1.2.2.1 Model A dynamics	10
1.2.2.2 Model B dynamics	12
1.3 Lattice models	15
1.3.1 The Ising model	15
1.3.2 The Solid-On-Solid Model	19
1.3.3 Transfer matrix	21
1.4 Systems driven by imposed hydrodynamic flows	24
1.5 Conclusion	26
2 Numerical methods	27
2.1 Estimator	28
2.2 Monte Carlo Metropolis algorithm	28
2.2.1 Glauber dynamics	29
2.2.2 Kawasaki dynamics	32
2.3 Computing size dependent free energy	33
2.3.1 The Layer method	33
2.3.2 The Lopes-Jacquin-Holdsworth method	35
2.4 Tips and tricks	35
2.5 Conclusion	36
3 Equilibrium Interface models and their finite size effects	37
3.1 The Casimir effect	37
3.1.1 Quantum Casimir effect	37
3.1.2 Lifshitz Theory	40
3.1.3 Critical Casimir effect	42

3.1.3.1	Bulk scaling for near critical systems	42
3.1.3.2	Finite size scaling	43
3.2	Finite size scaling in one dimensional interface models	45
3.2.1	Continuous models in one dimension	45
3.2.2	The confined elastic line	47
3.2.3	The Airy line	50
3.3	The generalized Lopes-Jacquín-Holdsworth Method	53
3.4	The confined Solid-On-Solid model	57
3.5	Conclusion	64
4	Beyond Solid-On-Solid : the Particles-Over-Particles model	67
4.1	The model	67
4.2	M-particles POP system	70
4.3	Continuum Theory	72
4.4	Conclusion	73
5	Driven interfaces	75
5.1	The effect of driving on model C interfaces	75
5.1.1	The underlying two field model	77
5.1.2	Effective interface dynamics	79
5.1.3	A model of active interfaces	83
5.1.4	Conclusion	85
5.2	Driven SOS model	86
5.3	Conclusions	89

Introduction

Most statistical mechanical models can be described using an order parameter, such as the mean magnetization in a magnetic system, the density of a liquid or gas or the average orientation of liquid crystals [1]. During a continuous phase transition, the correlation length diverges [2]. When the correlation length becomes of the same order of magnitude as the experimental or numerical system size, finite size effects become stronger, leading to interesting new physics, for example the critical Casimir effect [3].

In a system where the order parameter is conserved, or when it is fixed at values corresponding to two different phases, an interface is formed between both phases. In systems with a rectangular geometry this interface is flat at first order as the system tends to minimize the area between the two phases to minimize the interfacial energy generated by the surface tension. However thermal fluctuations induce fluctuations of the interface. From a theoretical point of view, one can study the statistical properties, both static and dynamic, of interfaces between two phases through different though complementary methods. Historically, the first method was through lattice models, and more precisely the Ising model [4, 34]. Those models are well-suited for numerical analysis due to their discrete nature, while posing analytical challenges due to the large number of degrees of freedom. Analytic studies of the interface are limited to two dimensional systems [5]. Numerical simulations of phase separated Ising models are straightforward, whilst the identification of the interface and unambiguous definition of the interface's position are not obvious. For this reason coarse grained models of the interface have been proposed. The Solid-On-Solid model [6] is an approximation of the Ising model in d dimensions which describes the position of an interface under certain simplifying circumstances. For two dimensional Ising systems this means that the transfer matrix method can be applied either analytically or numerically and the results are directly comparable with numerical simulations.

Coarse graining the Ising model leads to the Landau-Ginzburg Hamiltonian description in terms of a continuous field [7]. Using this description one can derive the equations for both the dynamics and statics of the interface. In particular, within this formalism the effective partition function of the interface describes a random walker in a potential, then using path integrals [8] two dimensional systems can be analysed using a quantum mechanical treatment.

When modeling experiments using statistical mechanics it is important to identify the correct thermodynamic ensemble to describe the system. For instance in an Ising spin which describes interacting spins with $s = \pm 1$ the total magnetisation is not necessarily conserved as a single spin can change its sign. However if the spins' sum is fixed and each spin can exchange with each other by swapping sites (to describe a lattice gas for example), the two ensembles are clearly different. It is thus interesting to study how ensemble differences in

the underlying lattice model affect the statics and dynamics of interfaces in these models.

The thesis' outline is as following :

- In the first chapter we explain how the interface's statics can be modeled in terms of various discrete and continuous interface models. In particular we review phase ordering kinetics for the evolution of the order parameter in coarse grained systems, from which one can deduce the equilibrium dynamics of the interface using a method introduced by Bray and coworkers [9]. Discrete models are convenient for numerical studies of the interfaces. The most famous one is the Ising model, which can be studied in both the canonical and grand-canonical ensembles, even though the interface has no formal numerical definition. The interface approximation of the Ising model is called the Solid-On-Solid model, which can be addressed through the transfer matrix method. After explaining how those discrete models work, we discuss the case of out-of-equilibrium interfaces, and how the driving affect the properties in experimental and numerical studies.
- In the second chapter we discuss the basics of numerical simulations [10] for lattice systems, and in particular two methods to compute the free energy for equilibrium systems. In the first method by Vasilyev et al, its derivative is computed with respect to the system size by decoupling a layer of the system [11], a method which does not work for SOS models . For SOS models it is thus more convenient to use the Lopes-Jacquin-Holdsworth method [12] which gives the difference of free energy between two points in parameter-space by integrating over the total magnetization. We also discuss some numerical tips we have found particularly useful.
- The third chapter is devoted to finite size effects for various models. A particularly interesting manifestation of finite size effects is the so called Casimir interaction [13]. For completeness we describe the original quantum calculation of Casimir for two perfectly conducting plates at zero temperature [14], the generalization to arbitrary dielectric materials [15] and the critical Casimir effect which was first predicted by Fisher and de Gennes which is due to thermal fluctuations in critical or near critical systems. A natural question to ask is whether interface models can capture the same finite size scaling as predicted by Fisher and de Gennes. To this end we analyse finite size effects in the continuous elastic line model where the underlying interface is described by a Brownian motion in an external potential. These models have been studied extensively in the literature but we find a number of new results. First we consider an elastic surface (corresponding to the Edwards-Wilkinson model) confined between two hard walls. The resulting free energy is well known and does not correspond to what is expected from the critical Casimir effect, whilst we show that by including a phenomenological finite size correction to the surface tension (or line stiffness) proposed by Privman [16] one can recover the quantitative form predicted by the critical Casimir effect. We also derive the statistics of the equilibrium interface, in particular the fluctuations of the integrated height (corresponding to the average magnetisation in a spin model). Then we analyse the so called Airy line, corresponding to an interface above a hard wall but with a linear potential (corresponding to an applied pressure in the constant pressure ensemble) pushing the interface toward the wall.

Then, we generalize the LJH method [12] for the free energy's measurement in numerical simulations for any external field, which allows to use it in conserved dynamics. The method is used in the case of an exotic potential in SOS, both in Glauber and Kawasaki dynamics, in agreement with transfer matrix results.

Finally we examine finite size effects in the Solid-on-Solid model. While first analysed by Privman [16], we give a complete derivation allowing to compute the correlation length and to show that for large systems the physics is essentially the same as for continuum Brownian models, while determining the effective surface tension.

- In the fourth chapter we introduce a new $d - 1$ lattice model similar to SOS in which we have taken into account the entropy. This model, that we call Particles-Over-Particles, takes the literal definition of the height of the interface by assuming the existence of particles under it. Through this lens, we are able to form systems with many different types of particles which are in different statistical ensembles and different activities, and show the numerical limitations that have to overcome.
- The last chapter explains how uniform driving alters the properties of the interface. The first section is essentially a published paper [17], where we consider an interface model which can be driven out of equilibrium by a uniform driving field. In order for a uniform field to have an effect on the system we introduce two fields, a colloidal field with model B conserved dynamics and a solvent field with model A dynamics. This combination of dynamics is called model C dynamics [18]. The system is driven out of equilibrium by assuming that the driving acts only on the colloidal field. Using the method of Bray et al [9] we derive the interface dynamics and compute its correlation function in the resulting non-equilibrium steady state. The properties are considerably different to the standard capillary wave properties of equilibrium surfaces and some of the results can be interpreted in terms of an effective surface tension. The calculations exhibit some of the phenomenology seen in experiments on sheared interface [19]. Finally we discuss the same model without driving but with different temperatures for the two fields to simulate active colloid systems, again a rich phenomenology of non-equilibrium states emerges. Afterwards we show how uniform driving in SOS model decreases surface tension and discuss briefly the physical difference between this system and model C dynamics stated prior.

This thesis has been possible thanks to the ANR's grant FISICS, the Laboratoire Onde Matière d'Aquitaine from Université de Bordeaux, and the Laboratoire de Physique at ENS Lyon. The numerical simulations benefited from the numerical resources of the Mésocentre de Calcul Intensif Aquitain [20], with the help of Nguyen Ky Nguyen. All my numerical codes can be found on Github [21]. I also wish to thank Josiane Parzych (LOMA) and Laurence Mauduit (ENS LYON) for all the administration procedures and their support.

Chapter 1

Equilibrium interface dynamics

This chapter is a review of the dynamics of statistical systems, and how phase transitions - in particular those who possess a phase separation - occur dynamically [18]. The most famous example is the Ising model without any external field, its order parameter being the total magnetization.

In the high temperature phase, the system is homogeneous and its total magnetization is zero, while below the critical temperature there will be phase separation. When the order parameter is not conserved (Glauber dynamics or Model A), one of the two phases takes over the whole system due to spontaneous symmetry breaking. In a continuous phase transition where the critical point is reached from the disordered state to the ordered state, the domain size - equal to the system's correlation length - diverges close to the critical temperature T_C . In a thermodynamical system it becomes infinite, implying that the system takes an infinite amount of time to reach equilibrium : it's the critical slowing down. The process of domain growth is known as coarsening and phase ordering kinetics is the theory that has been developed to understand the phenomenon of coarsening[22]. In Fig 1.1, we show an example of coarsening in the Ising model with respect to time, where one phase will take over the whole system due to its finite size. In the case of an infinite system, we talk about spinodal decomposition. When the order parameter is conserved (Kawasaki dynamic or Model B), the system locally separates into two phases of opposite mean magnetization divided by an interface whose surface minimizes the energy between both phases. This interface is characterised by its surface tension and its average position.

While the phase diagram of a system can be determined via its Hamiltonian and equilibrium statistical mechanics, the dynamics of coarsening depend on the details that do not show up in single time thermodynamic observables. Therefore, one needs to construct dynamical models that capture the underlying evolution of the state of the system. In particular, there is a big difference between equilibrium systems where the order parameter is conserved and those where it is not conserved in the thermodynamic limit.

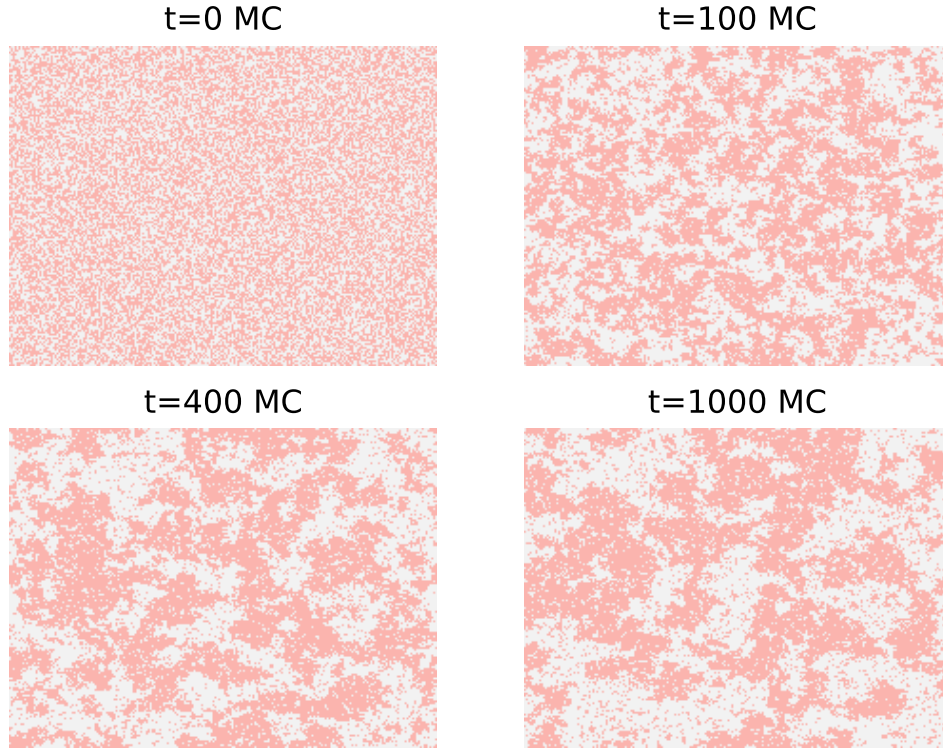


Figure 1.1: Numerical simulations of coarsening from a quench from a disordered state $T = \infty$ to an ordered state $T = T_{2D,C}$ [23] for different times, in Monte Carlo steps, for a 600×600 system with non-conserved Glauber dynamics and periodic boundary conditions.

1.1 Models for equilibrium fields

1.1.1 Statics of systems with a finite number of degrees of freedom

Measuring observables in experimental setups means to measure the derivative of the partition function Z with respect to its conjugate variable. This measure is done with a certain degree of spatial and temporal resolution, which means in a statistical language that they measure the average of the observable over some space and time. If $\Phi(\mathbf{x}, t)$ is the physical field of our system, our device having a temporal resolution of Δt and a spatial resolution over a volume V will measure

$$\phi(\mathbf{x}, t) = \frac{1}{V\Delta t} \int_{t-\Delta t}^t dt' \int_V d\mathbf{x}' \Phi(\mathbf{x}', t') \quad (1.1)$$

This means that one is naturally lead to consider statistical field theories where the system is described in terms of a local field $\phi(\mathbf{x}, t)$. We start to examine the case of a system with a finite number of degrees of freedom.

Consider a system in the canonical ensemble with a Hamiltonian $H(\mathbf{q})$ where q_i for $1 \leq i \leq N$ represent a finite number of continuous spatial degrees of freedom and where in a classical

system we have already integrated over the corresponding momenta. The partition function for the system is given by

$$Z = \int d\mathbf{q} \exp(-\beta H(\mathbf{q})) \quad (1.2)$$

In general the integral which gives the partition function cannot be computed analytically. In equilibrium, the probability density function $P_{eq}(\mathbf{q})$ of the degrees of freedom is given by

$$P_{eq}(\mathbf{q}) = \frac{\exp(-\beta H(\mathbf{q}))}{Z} \quad (1.3)$$

The simplest approximation to compute Z is the mean field approximation where the integral is approximated by the integrand at its largest value - in mathematics this is the Laplace method for approximating an integral and in this context it is just an expansion about the minimum energy configuration of the system. The mean field approximation is thus

$$Z_{MF} = \exp(-\beta H(\mathbf{q}^*)) \quad (1.4)$$

where \mathbf{q}^* is the value of \mathbf{q} which minimises H (note that the approximation becomes exact in the zero temperature limit - $\beta \rightarrow \infty$ - as the system will minimise its energy). The values q_i^* are determined from

$$\left. \frac{\partial H}{\partial q_i} \right|_{\mathbf{q}=\mathbf{q}^*} = 0 \quad (1.5)$$

Within this approximation any thermodynamic observable is given by

$$\langle f(\mathbf{q}) \rangle = f(\mathbf{q}^*) \quad (1.6)$$

In order to reach the correct equilibrium Gibbs-Boltzmann distribution, the following Langevin equation

$$\frac{dq_i}{dt} = -L_{ij} \frac{\partial H(\mathbf{q})}{\partial q_j} + \eta_i(t) \quad (1.7)$$

needs to satisfy some conditions. Here, L_{ij} is a matrix operator which has to be carefully chosen and $\eta_i(t)$ is zero mean Gaussian white noise with correlation function

$$\langle \eta_i(t) \eta_j(t') \rangle = \Gamma_{ij} \delta(t - t') \quad (1.8)$$

The Gaussian white noise represents the effects of thermal fluctuations on the system, and we assume that the correlation time of these fluctuations is extremely short with respect to the dynamics of the degrees of freedom q_i (in fact due to critical slowing down, the dynamics become very slow close to the critical point). There is no momentum term in this Langevin equation and for this reason it is often called the overdamped Langevin equation.

As Eq. (1.8) is for a correlation function, the matrix Γ_{ij} must be symmetric and cannot have any negative eigenvalues.

In the absence of noise or thermal fluctuations, so at zero temperature, the system minimises its energy. Therefore if

$$\frac{\partial H(\mathbf{q})}{\partial q_j} = 0 \quad (1.9)$$

with no noise then we have $\frac{dq_i}{dt} = 0$, that is to say it is the term $\frac{\partial H(\mathbf{q})}{\partial q_j}$ that drives the dynamics in that case. As long as the matrix L_{ij}^{-1} exists the zero temperature dynamics will take the

system to the local minimum of H and to the absolute minimum in absence of metastable configurations.

Under these assumptions, the Fokker-Planck equation for the probability density function of the degrees of freedom is

$$\frac{\partial p(\mathbf{q}, t)}{\partial t} = \frac{\partial}{\partial q_i} \left[\frac{1}{2} \Gamma_{ij} \frac{\partial p(\mathbf{q}, t)}{\partial q_j} + p(\mathbf{q}, t) L_{ij} \frac{\partial H(\mathbf{q})}{\partial q_j} \right] \quad (1.10)$$

This can be written as

$$\frac{\partial p(\mathbf{q}, t)}{\partial t} + \frac{\partial}{\partial q_i} J_i(\mathbf{q}, t) = 0 \quad (1.11)$$

where the $\mathbf{J}(\mathbf{q}, t)$ is the probability current. Since the system is in equilibrium with zero current when $p(\mathbf{q}, t) = P_{eq}(\mathbf{q})$ as given by Eq. (1.3), this gives

$$\left[-\frac{\beta}{2} \Gamma_{ij} + L_{ij} \right] \frac{\partial H(\mathbf{q})}{\partial q_j} = 0 \quad (1.12)$$

which holds for any choice of H is we chose

$$\Gamma_{ij} = 2TL_{ij} \quad (1.13)$$

where Boltzmann's constant has been set to $k_B = 1$.

1.1.2 Statistical field theory

The partition function of a system with Hamiltonian $H[\phi]$ depending on a continuous field $\phi(\mathbf{x})$ is given by a functional integral

$$Z = \int d[\phi] \exp(-\beta H[\phi]), \quad (1.14)$$

the functional integral over all possible fields ϕ can be taken as a limit where ϕ is defined at a finite number of points on a lattice where the lattice spacing is taken to zero. In many cases, the system has been coarse-grained and ϕ represents a spatially varying order parameter, for instance the local density averaged over some small volume. In this case the Hamiltonian H is strictly speaking a free energy and contains terms that depend on the temperature.

The mean field approximation to partition function is then given by

$$Z_{MF} = \exp(-\beta H[\phi_{MF}]) \quad (1.15)$$

where ϕ_{MF} is the mean field solution which minimises H . By definition of a functional derivative

$$F[\phi + \delta\phi] - F[\phi] = \int d\mathbf{x} \frac{\delta F}{\delta\phi(\mathbf{x})} \delta\phi(\mathbf{x}), \quad (1.16)$$

if a field ϕ maximises H we must have

$$\frac{\delta H}{\delta\phi(\mathbf{x})} = 0 \quad (1.17)$$

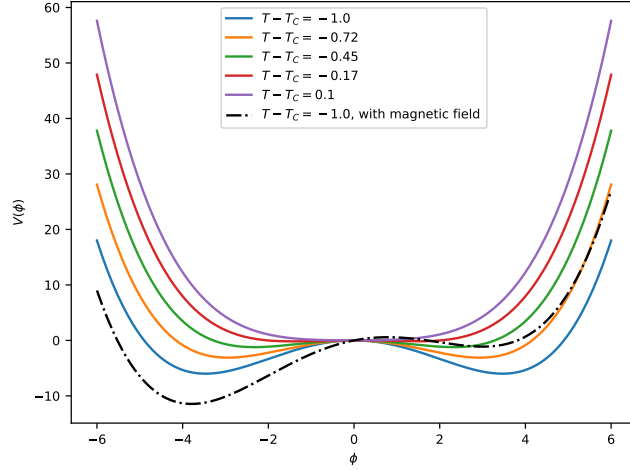


Figure 1.2: Double-well potential (1.19) for $\lambda = 1$ in function of the temperature difference with respect to the critical temperature with $m^2 = T - T_C$. In the ordered phase, the minima are at $\phi_C = \pm\sqrt{-\frac{6m^2}{\lambda}}$, while for the ordered phase it is at $\phi_C = 0$. In black, the addition of a uniform magnetic field $h(\mathbf{x}) = 1$ makes the positive phase metastable.

We now consider the standard Landau-Ginzburg Hamiltonian [1] describing Ising like systems where

$$H[\phi] = \int d\mathbf{x} \frac{\kappa}{2} [\nabla\phi]^2 + V(\phi) \quad (1.18)$$

The first term represents an energetic cost of varying the field ϕ . The second potential term has two minima at $\phi = \pm\phi_c$, and, in the low temperature or phase separated phase, without loss of generality we can chose $V(\phi_c) = V(-\phi_c)$, while it has a single minimum at $\phi = 0$ in the high temperature phase.

The standard potential for phase separations, called the ϕ^4 model, is given by the double-well

$$V(\phi) = \frac{1}{2}m^2\phi^2 + \frac{\lambda}{4!}\phi^4 \quad (1.19)$$

where $m^2 = T - T_C$. For $m^2 < 0$, the minima are at $\phi_C = \pm\sqrt{-\frac{6m^2}{\lambda}} \pm$, while at $m^2 \geq 0$, the single minimum is at $\phi_C = 0$, as shown in Fig 1.2. We can also couple our system with the magnetic field of Hamiltonian

$$H_1 = - \int d^d x h(\mathbf{x})\phi(\mathbf{x}) \quad (1.20)$$

in order to favorise one phase over the other one. As the only important feature of this potential is to have phase separation in two phases, the absolute value of ϕ_C is irrelevant. For example, if ϕ describes a density field, the ϕ^4 potential will have two minima at $\phi_C = 0$ and $\phi_C = 1$, while for spin systems it will be $\phi_C = \pm 1$.

It is easy to see that

$$\frac{\delta H}{\delta\phi(\mathbf{x})} = -\kappa\nabla^2\phi(\mathbf{x}) + V'(\phi) \quad (1.21)$$

By analogy with discrete systems from Eq. (1.7), the continuous Langevin equation has the form

$$\frac{\partial \phi(\mathbf{x})}{\partial t} = -L \frac{\delta H}{\delta \phi(\mathbf{x})} + \eta(\mathbf{x}, t) \quad (1.22)$$

The white noise correlator should have the form

$$\langle \eta(\mathbf{x}, t) \eta(\mathbf{x}', t') \rangle = \delta(t - t') \Gamma(\mathbf{x}, \mathbf{x}') \quad (1.23)$$

where here $\Gamma(\mathbf{x}, \mathbf{x}')$ is an operator (before it was a matrix) defined by its action on functions f as

$$\Gamma f(\mathbf{x}) = \int d\mathbf{x}' \Gamma(\mathbf{x}, \mathbf{x}') f(\mathbf{x}') \quad (1.24)$$

and L is also an operator with

$$L f(\mathbf{x}) = \int d\mathbf{x}' L(\mathbf{x}, \mathbf{x}') f(\mathbf{x}') \quad (1.25)$$

Following the same arguments for systems with a finite number of degrees of freedom, both operations must follow the relation

$$\Gamma(\mathbf{x}, \mathbf{x}') = 2TL(\mathbf{x}, \mathbf{x}') \quad (1.26)$$

which is sometimes called the fluctuation dissipation theorem as it essentially is equivalent.

The simplest form of dynamics is given by $L(\mathbf{x}, \mathbf{x}') = \alpha \delta(\mathbf{x} - \mathbf{x}')$ which gives the **model A dynamics**

$$\frac{\partial \phi(\mathbf{x})}{\partial t} = -\alpha \frac{\delta H}{\delta \phi(\mathbf{x})} + \eta(\mathbf{x}, t) \quad (1.27)$$

with the noise correlator

$$\langle \eta(\mathbf{x}, t) \eta(\mathbf{x}', t') \rangle = 2T\alpha \delta(t - t') \delta(\mathbf{x} - \mathbf{x}') \quad (1.28)$$

The average value of ϕ

$$\bar{\phi}(t) = \frac{1}{V} \int d\mathbf{x} \phi(\mathbf{x}, t) \quad (1.29)$$

is clearly not generally conserved by this dynamics. Model A corresponds to a system in the grand-canonical ensemble, where α is the kinetic coefficient related to the relaxation time of the system [18].

Model B dynamics amounts to choosing

$$L(\mathbf{x} - \mathbf{x}') = -D\nabla^2 \delta(\mathbf{x} - \mathbf{x}') \quad (1.30)$$

The fact that L is a positive semi-definite operator can be seen by taking its Fourier transform. The evolution equation here is

$$\frac{\partial \phi(\mathbf{x})}{\partial t} = D\nabla^2 \frac{\delta H}{\delta \phi(\mathbf{x})} + \eta(\mathbf{x}, t) \quad (1.31)$$

where

$$\langle \eta(\mathbf{x}, t) \eta(\mathbf{x}', t') \rangle = -2TD \delta(t - t') \nabla^2 \delta(\mathbf{x} - \mathbf{x}') \quad (1.32)$$

By introducing the vectorial white noise with components $\eta_i(\mathbf{x}, t)$ such that

$$\langle \eta_i(\mathbf{x}, t) \eta_j(\mathbf{x}', t') \rangle = \delta_{ij} \delta(\mathbf{x} - \mathbf{x}') \delta(t - t') \quad (1.33)$$

where $\delta_{ij} = 1$ for $i = j$ and is zero otherwise, it can be rewritten as

$$\boldsymbol{\eta}(\mathbf{x}, t) = \nabla \cdot \boldsymbol{\eta}(\mathbf{x}, t) \quad (1.34)$$

As one can verify the two noises have the same correlation function. In this way Eq. (1.31) becomes

$$\frac{\partial \phi(\mathbf{x})}{\partial t} = \nabla \cdot \left[D \nabla \frac{\delta H}{\delta \phi(\mathbf{x})} + \boldsymbol{\eta}(\mathbf{x}, t) \right] \quad (1.35)$$

From this it is easy to see that the order parameter is conserved - thus model B describes conserved phase ordering dynamics. This model corresponds to the canonical ensemble, and is useful to describe diffusion or accretion systems.

Without the noise fluctuations, Eq. (1.27) and Eq. (1.31) are called the Time Dependent Ginzburg-Landau equation [24] and the Cahn-Hilliard equation [25] equations, which gives the mean field's dynamics.

1.1.3 Surface tension

Minimizing the free energy can be done by simply choosing $\phi(\mathbf{x}) = \phi_c$ or $\phi(\mathbf{x}) = -\phi_c$ everywhere, which amounts to a free energy of $F = H[\phi_c] = 0$. However in a system with a conserved order parameter

$$\int d\mathbf{x} \phi(\mathbf{x}) = 0 \quad (1.36)$$

the homogeneous solution cannot hold. In this case the system separates into two homogeneous phases where $\phi(\mathbf{x}) = \pm \phi_c$. By setting the interface at $z = 0$ and taking the field profile perpendicular to it $\phi(\mathbf{x}) = \phi_K(z)$ (K standing for kink as it is known as the kink solution in the literature) where $\lim_{z \rightarrow \infty} \phi_K = \phi_c$ and $\lim_{z \rightarrow -\infty} \phi_K = -\phi_c$, Eq. (1.21) gives

$$-\kappa \frac{d^2}{dz^2} \phi_K(z) + V'(\phi_K) = 0 \quad (1.37)$$

The interface Hamiltonian is written as

$$H[\phi_K] = A \int dz \frac{\kappa}{2} \left(\frac{d\phi_K(z)}{dz} \right)^2 + V(\phi_K(z)) \quad (1.38)$$

where A is the surface area of the system in the plane perpendicular to the direction z. Multiplying Eq. (1.37) by $d\phi/dz$ and by integrating we find

$$-\frac{\kappa}{2} \left(\frac{d\phi_K}{dz} \right)^2 + V(\phi_K) = C \quad (1.39)$$

where C is a constant. As $\phi_K(z) \rightarrow \pm \phi_c$ as $z \rightarrow \pm \infty$ and $V(\pm \phi_c) = 0$, the prior equation gives $C = 0$, which allows to rewrite the interface Hamiltonian as

$$H[\phi_K] = A \int dz \kappa \left(\frac{d\phi_K(z)}{dz} \right)^2 \quad (1.40)$$

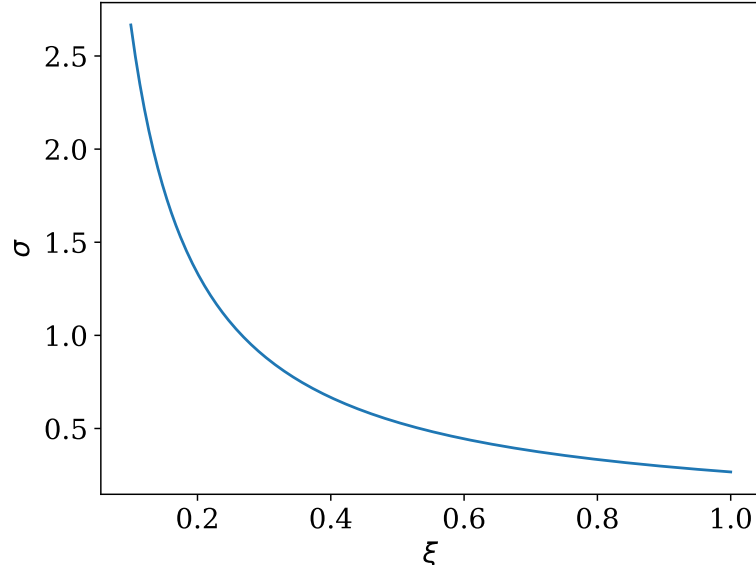


Figure 1.3: Surface tension (1.41) versus ξ for the ϕ^4 solution (1.43).

The Cahn-Hilliard estimate of the surface tension [25] is defined as the free energy per unit area

$$\sigma = \int dz \kappa \left(\frac{d\phi_K(z)}{dz} \right)^2 \quad (1.41)$$

In the case of the ϕ^4 model defined at Eq. (1.19), Eq. (1.37) becomes

$$\kappa \phi_K''(z) = m^2 \phi_K(z) (1 + \phi_C \phi_K(z)^2) \quad (1.42)$$

This potential is only defined by the ratio between m^2 and λ , so without loss of generality we set $\phi_C = 1$. The solution becomes

$$\phi_K(z) = \tanh\left(\frac{z}{\xi}\right) \quad (1.43)$$

where $\xi = \sqrt{\frac{-2\kappa}{m^2}}$. This correlation length diverges when $T \rightarrow T_C$. From Fig 1.3 we see that the bigger the correlation length of the system, the smaller the surface tension is. The experimental study of quasi-critical systems, which have fluctuations at a macroscopic length scale, is a good way to probe the properties of ultra-low surface tension systems [26]. Such systems are very susceptible to hydrodynamic instabilities caused by thermal noise, as in microfluidics for example [27].

1.2 Models for equilibrium interfaces

1.2.1 Basic continuous model

The simplest effective model of interface is to assume that the interface is parameterised by a height profile which is a single-valued function $h(\mathbf{r})$, where $\mathbf{x} = (\mathbf{r}, z)$. The interface hamil-

tonian is thus

$$H[h] = \sigma A[h] \quad (1.44)$$

where $A[h]$ is the area of the interface. The interface area is given by

$$A[h] = \int_A d\mathbf{r} \sqrt{1 + [\nabla h]^2} \quad (1.45)$$

where the integral is over the plane perpendicular to the z axis which is taken to be of area A . When the fluctuations of the interface are small, an expansion to quadratic order in h gives

$$H[h] = A\sigma + \frac{\sigma}{2} \int_A d\mathbf{r} [\nabla h]^2 \quad (1.46)$$

The first term is independent of the height, so the effective Hamiltonian for the surface becomes

$$H_{eff}[h] = \frac{\sigma}{2} \int_A d\mathbf{r} [\nabla h]^2 \quad (1.47)$$

The basic model describing the height of an interface at $z = h(\mathbf{r})$ above a plane with coordinates \mathbf{r} has the Hamiltonian

$$H[h] = \int d\mathbf{x} \frac{\sigma}{2} [\nabla h(\mathbf{x})]^2 + V(h(\mathbf{x})) \quad (1.48)$$

The first term corresponds to the surface energy. In principle surfaces can also have bending energies. While surface energies correspond to stretching the surface to increase its size, bending energies correspond to curving the surface. The standard bending energy for small surface energies [28] is given by

$$H_b[h] = \int d\mathbf{r} \frac{\kappa_b}{2} [\nabla^2 h(\mathbf{r})]^2 \quad (1.49)$$

where κ_b is called the bending rigidity. The term $V(h)$ represents the potential energy of the surface per unit area. For instance, if the surface interacts via an infinite hard-core potential with a solid surface at $z = 0$, it can be modelled by the potential $V(z) = 0$ for $z > 0$ and $V(z) = \infty$ for $z \leq 0$. Another example is where the surface describes the surface of a liquid such as water, again with a solid surface at $z = 0$, in the presence of gravity the potential energy of the water column above the area element $d\mathbf{x}$ is given by

$$\delta V = \int_0^{h(\mathbf{r})} dz \rho g z = \frac{1}{2} \rho g h^2(\mathbf{r}) \quad (1.50)$$

where ρ is the (mass) density of the liquid. This then gives

$$H[h] = \int d\mathbf{r} \frac{\sigma}{2} [\nabla h(\mathbf{r})]^2 + \frac{1}{2} \rho g h^2(\mathbf{r}) \quad (1.51)$$

The correlation length of the interface is given by

$$\xi = \left(\frac{\sigma}{\rho g} \right)^{\frac{1}{2}} \quad (1.52)$$

In the more general context, if $V(h)$ has a minimum at some point h_m , first order expansion gives $h = h_f(\mathbf{x}) + h_m$, where $h_f(\mathbf{x})$ represents the height fluctuations about the mechanically stable flat interface $h(\mathbf{x}) = h_m$, which gives the effective Hamiltonian for the fluctuations

$$H_{eff}[h_f] = \int d\mathbf{r} \frac{\sigma}{2} [\nabla h_f(\mathbf{r})]^2 + \frac{1}{2} V''(h_m) h_f^2(\mathbf{r}) \quad (1.53)$$

where the constant term $AV(h_m)$ is dropped. The above field theory is Gaussian and so, when the approximations made to derive it are valid, all of the statistical properties of the height fluctuations can be deduced. However for general potentials $V(h)$ the model cannot be solved exactly in two dimensions but can in principle be solved in one dimension as we will see below.

1.2.2 Effective dynamics of interface heights

From the original phase ordering kinetics, one can derive an approximation for the dynamics of the interface's height. Here we use the method of Bray and Cavagna [9, 29], which was used to study the dynamics of sheared interfaces, in the absence of shear to determine the dynamical properties of interfaces in phase separated systems for both model A and model B dynamics.

Imagining that the system is phase separated in the z direction by an interface whose average is set to be at $z = 0$, we set

$$\phi(z, \mathbf{r}, t) = f(z - h(\mathbf{r}, t)) \quad (1.54)$$

where $f(z) = \phi_K(z)$ is the kink solution from mean field theory.

1.2.2.1 Model A dynamics

For model A dynamics, substituting Eq. (1.54) into Eq. (1.27) and making use of the following results

$$\frac{\partial f(z - h(\mathbf{r}, t))}{\partial t} = -f'(z - h(\mathbf{r}, t)) \frac{\partial h(\mathbf{r}, t)}{\partial t} \quad (1.55)$$

$$\nabla f(z - h(\mathbf{r}, t)) = [\mathbf{e}_z - \nabla h(\mathbf{r}, t)] f'(z - h(\mathbf{r}, t)) \quad (1.56)$$

$$\nabla^2 f(z - h(\mathbf{r}, t)) = f''(z - h(\mathbf{r}, t)) - \nabla^2 h(\mathbf{r}, t) f'(z - h(\mathbf{r}, t)) + [\nabla h(\mathbf{r}, t)]^2 f''(z - h(\mathbf{r}, t)) \quad (1.57)$$

we find

$$-f'(z - h(\mathbf{r}, t)) \frac{\partial h(\mathbf{r}, t)}{\partial t} = \alpha \kappa [f''(z - h(\mathbf{r}, t)) - \nabla^2 h(\mathbf{r}, t) f'(z - h(\mathbf{r}, t)) + [\nabla h(\mathbf{r}, t)]^2 f''(z - h(\mathbf{r}, t))] \quad (1.58)$$

$$- \alpha \nabla' (f'(z - h(\mathbf{r}, t))) + \eta(\mathbf{r}, z, t) \quad (1.59)$$

After multiplying both sides of this equation by $f'(z - h(\mathbf{r}, t))$ and defining $\zeta = z - h(\mathbf{r}, t)$, we integrate ζ over $[-\infty, \infty]$ while using the following identities

$$\int_{-\infty}^{\infty} d\zeta f'(\zeta) f''(\zeta) = \left[\frac{1}{2} f'^2(\zeta) \right]_{-\infty}^{\infty} = 0$$

$$\int_{-\infty}^{\infty} d\zeta f'(\zeta) V'(f) = \int_{-\infty}^{\infty} d\zeta \frac{dV(f)}{d\zeta} = [V(f(\zeta))]_{-\infty}^{\infty} = 0$$

Note that the first relation above holds as $f(\zeta) = \pm\phi_c$ as $\zeta \rightarrow \pm\infty$ and the second as $V(\phi_c) = V(-\phi_c) = 0$. The terms that are left then give

$$-\int_{-\infty}^{\infty} f'^2(\zeta) d\zeta \frac{\partial h(\mathbf{r}, t)}{\partial t} = -\alpha \int_{-\infty}^{\infty} f'^2(\zeta) d\zeta \kappa \nabla^2 h(\mathbf{r}, t) + \int_{-\infty}^{\infty} d\zeta \eta(\mathbf{r}, \zeta + h(\mathbf{r}, t)) f'(\zeta) \quad (1.60)$$

Now using the Cahn-Hilliard estimate of the surface tension, Eq. (1.41) thus becomes

$$\frac{\sigma}{\kappa} \frac{\partial h(\mathbf{r}, t)}{\partial t} = \alpha \sigma \nabla^2 h(\mathbf{r}, t) + \xi(\mathbf{r}, t) \quad (1.61)$$

where the noise term is given by

$$\xi(\mathbf{r}, t) = - \int_{-\infty}^{\infty} d\zeta \eta(\mathbf{r}, \zeta + h(\mathbf{r}, t)) f'(\zeta) \quad (1.62)$$

The noise term has zero mean and correlation function

$$\begin{aligned} \langle \xi(\mathbf{r}, t) \xi(\mathbf{r}', t') \rangle &= 2\alpha T \delta(t-t') \delta(\mathbf{r}-\mathbf{r}') \int_{-\infty}^{\infty} d\zeta d\zeta' \delta(\zeta-\zeta') f'(\zeta) f'(\zeta') \\ &= 2\alpha T \delta(t-t') \delta(\mathbf{r}-\mathbf{r}') \int_{-\infty}^{\infty} d\zeta f'^2(\zeta) = \frac{2\alpha T \sigma}{\kappa} \delta(t-t') \delta(\mathbf{r}-\mathbf{r}') \end{aligned} \quad (1.63)$$

This now gives

$$\frac{\partial h(\mathbf{r}, t)}{\partial t} = \kappa \alpha \nabla^2 h(\mathbf{r}, t) + \eta(\mathbf{r}, t) \quad (1.64)$$

where

$$\langle \eta(\mathbf{r}, t) \eta(\mathbf{r}', t') \rangle = \frac{2\alpha T \kappa}{\sigma} \delta(t-t') \delta(\mathbf{r}-\mathbf{r}') \quad (1.65)$$

Now defining $\alpha' = \frac{\kappa \alpha}{\sigma}$ we can write

$$\frac{\partial h(\mathbf{r}, t)}{\partial t} = \alpha' \sigma \nabla^2 h(\mathbf{r}, t) + \eta(\mathbf{r}, t) \quad (1.66)$$

This has the form of model A dynamics (as in Eq. (1.27)) for the height profile with Hamiltonian H_{eff} as given in (1.47), that is to say

$$\frac{\partial h(\mathbf{r}, t)}{\partial t} = -\alpha' \frac{\delta H_{eff}[h]}{\delta h(\mathbf{r})} + \eta(\mathbf{r}, t) \quad (1.67)$$

with

$$\langle \eta(\mathbf{r}, t) \eta(\mathbf{r}', t') \rangle = 2T \alpha' \delta(t-t') \quad (1.68)$$

This dynamical calculation is thus consistent with the idea of describing the surface in terms of a height variable with an energy given by the surface tension. The equation (1.67) is known as the Edwards-Wilkinson equation [30, 31]. This equation can be used to determine how the domains of a coarsening system grow at low temperatures. To do this we ignore the noise term and assume that at $t = 0$ the correlations of the height are short range, so

$$C(\mathbf{r}-\mathbf{r}', 0) = \langle h(\mathbf{r}, 0) h(\mathbf{r}', 0) \rangle = C_0 \delta(\mathbf{r}-\mathbf{r}') \quad (1.69)$$

In Fourier space the noiseless Edwards-Wilkinson equation becomes

$$\frac{\partial \tilde{h}(\mathbf{k}, t)}{\partial t} = -\alpha' \sigma k^2 \tilde{h}(\mathbf{k}, t) \quad (1.70)$$

and so

$$\tilde{h}(\mathbf{k}, t) = h(\mathbf{k}, 0) \exp(-\alpha' \sigma k^2 t) \quad (1.71)$$

The two point correlation function becomes

$$\langle \tilde{h}(\mathbf{k}, t) \tilde{h}(\mathbf{k}', t') \rangle = \langle h(\mathbf{k}, 0) h(\mathbf{k}', 0) \rangle \exp(-\alpha' \sigma [k^2 + k'^2] t). \quad (1.72)$$

Now recall that if

$$\langle h(\mathbf{r}, t) h(\mathbf{r}', t') \rangle = C(\mathbf{r} - \mathbf{r}', t) \quad (1.73)$$

then

$$\langle \tilde{h}(\mathbf{k}, t) \tilde{h}(\mathbf{k}', t') \rangle = (2\pi)^d \delta(\mathbf{k} + \mathbf{k}') \tilde{C}(\mathbf{k}, t) \quad (1.74)$$

where

$$\tilde{C}(\mathbf{k}, t) = \int d\mathbf{r} \exp(-i\mathbf{k} \cdot \mathbf{r}) C(\mathbf{r}, t) \quad (1.75)$$

is the Fourier transform of the correlation function, which is a function of a single position due to invariance by translation in space, and d is the dimension of space (so here $d = 2$ for a surface in 3d space and $d = 1$ for a surface in a 2d space). Putting all this together gives

$$\tilde{C}(\mathbf{k}, t) = C_0 \exp(-2\alpha' \sigma k^2 t) \quad (1.76)$$

Inverting the Fourier transform, we have

$$C(\mathbf{r}, t) = \frac{C_0}{(8\pi\alpha'\sigma t)^{\frac{d}{2}}} \exp\left(-\frac{\mathbf{r}^2}{16\pi\alpha'\sigma t}\right) \quad (1.77)$$

From this we see that if $C(\mathbf{r}, t) \sim g\left(\frac{\mathbf{r}}{\ell(t)}\right)r(t)$ then the length scale $\ell(t) \sim t^{\frac{1}{2}}$. This agrees with what is found in the Ising model under Glauber dynamics, where the growth exponent is also given by $z = \frac{1}{2}$ [32].

1.2.2.2 Model B dynamics

For model B dynamics, taking the same ansatz as in Eq. (1.54), model B dynamics is rewritten as

$$-\nabla^{-2} \frac{\partial \phi(\mathbf{x}, t)}{\partial t} = -D \frac{\delta H}{\delta \phi(\mathbf{x})} + \theta(\mathbf{x}, t) \quad (1.78)$$

Here $-\nabla^{-2}$ represents the Green's function G which obeys to

$$\nabla^2 G(\mathbf{x} - \mathbf{x}') = -\delta(\mathbf{x} - \mathbf{x}') \quad (1.79)$$

and

$$\theta(\mathbf{x}, t) = -\nabla^{-2} \eta(\mathbf{x}, t) = \int d\mathbf{x}' G(\mathbf{x} - \mathbf{x}') \eta(\mathbf{x}, t) \quad (1.80)$$

The correlation function of $\theta(\mathbf{x}, t)$ is given by

$$\begin{aligned}\langle \theta(\mathbf{x}, t)\theta(\mathbf{y}, t') \rangle &= -2DT\delta(t-t') \int d\mathbf{x}' G(\mathbf{x}-\mathbf{x}') d\mathbf{y}' G(\mathbf{y}-\mathbf{y}') \nabla^2 \delta(\mathbf{x}'-\mathbf{y}') \\ &= -2DT\delta(t-t') \int d\mathbf{x}' G(\mathbf{x}-\mathbf{x}') d\mathbf{y}' \nabla^2 G(\mathbf{y}-\mathbf{y}') \delta(\mathbf{x}'-\mathbf{y}') \\ &= 2DT\delta(t-t') G(\mathbf{x}-\mathbf{y})\end{aligned}\quad (1.81)$$

where we have integrated by parts in the second line and used

$$-\nabla^2 G(\mathbf{y}-\mathbf{y}') = \delta(\mathbf{y}-\mathbf{y}') \quad (1.82)$$

in the third.

Now multiplying by $f'(z-h(\mathbf{r}, t))$ and integrating z over $[-\infty, \infty]$, we find

$$-\int dz f'(z-h(\mathbf{r}, t)) \int dz' d\mathbf{r}' G(z-z', \mathbf{r}-\mathbf{r}') f'(z'-h(\mathbf{r}', t)) \frac{\partial h(\mathbf{r}', t)}{\partial t} = -D\sigma \nabla^2 h(\mathbf{r}, t) + \chi(\mathbf{r}, t), \quad (1.83)$$

with the noise

$$\chi(\mathbf{r}, t) = \int dz f'(z-h(\mathbf{r}, t)) \theta(\mathbf{r}, z, t). \quad (1.84)$$

Assuming that the height fluctuations are small, only the lowest order terms in h in the deterministic terms and the noise are kept, which we will see later is compatible thermodynamically. The equation becomes

$$-\int dz f'(z) \int dz' d\mathbf{r}' G(z-z', \mathbf{r}-\mathbf{r}') f'(z') \frac{\partial h(\mathbf{r}', t)}{\partial t} = -D\sigma \nabla^2 h(\mathbf{r}, t) + \chi(\mathbf{r}, t) \quad (1.85)$$

and now the noise is given by

$$\chi(\mathbf{r}, t) = \int dz f'(z) \theta(\mathbf{r}, z', t) \quad (1.86)$$

This equation which is linear in h can now be Fourier transformed in the plane \mathbf{r} . In terms of the Fourier transform of h we find

$$-\int dz f'(z) \int dz' d\mathbf{r}' \tilde{G}(z-z', \mathbf{k}) f'(z') \frac{\partial \tilde{h}(\mathbf{k}, t)}{\partial t} = Dk^2 \sigma \tilde{h}(\mathbf{k}, t) + \tilde{\chi}(\mathbf{k}, t) \quad (1.87)$$

The Fourier transform of G in the \mathbf{r} plane obeys

$$\frac{d^2 \tilde{G}(z-z', \mathbf{k})}{dz^2} - k^2 \tilde{G}(z-z', \mathbf{k}) = -\delta(z-z') \quad (1.88)$$

and the solution to this equation (with the boundary condition that $\tilde{G}(z-z', \mathbf{k}) \rightarrow 0$ as $|z-z'| \rightarrow \infty$) is

$$\tilde{G}(z-z', \mathbf{k}) = \frac{\exp(-k|z-z'|)}{2k} \quad (1.89)$$

where the notation $k = |\mathbf{k}|$ is used, so k is positive. Using the sharp interface approximation, we write

$$f(z) = 2\phi_c \delta(z) \quad (1.90)$$

that is to say we have replaced the smooth kink solution with a step like solution $f(z) = \phi_c \operatorname{sgn}(z)$. This then gives

$$-4\phi_c^2 \tilde{G}(0, k) \frac{\partial h(\mathbf{k}, t)}{\partial t} = Dk^2 \sigma \tilde{h}(\mathbf{k}, t) + \tilde{\chi}(\mathbf{k}, t) \quad (1.91)$$

which is rewritten as

$$\frac{\partial \tilde{h}(\mathbf{k}, t)}{\partial t} = -\frac{Dk^3 \sigma}{2\phi_c^2} \tilde{h}(\mathbf{k}, t) + \tilde{\xi}(\mathbf{k}, t) \quad (1.92)$$

with

$$\tilde{\xi}(\mathbf{k}, t) = -\frac{k}{2\phi_c^2} \tilde{\chi}(\mathbf{k}, t) \quad (1.93)$$

where

$$\tilde{\chi}(\mathbf{k}, t) = \int dz f'(z) \tilde{\theta}(\mathbf{k}, z, t) \quad (1.94)$$

The correlation function of $\tilde{\theta}(\mathbf{k}, t)$ is

$$\langle \theta(\mathbf{k}, t) \theta(\mathbf{k}', t') \rangle = 2DT(2\pi)^d \delta(t - t') \delta(\mathbf{k} + \mathbf{k}') \tilde{G}(z - z', k) \quad (1.95)$$

From this the correlation function in Fourier space is

$$\langle \chi(\mathbf{k}, t) \chi(\mathbf{k}', t') \rangle = 2DT(2\pi)^d \delta(t - t') \delta(\mathbf{k} + \mathbf{k}') \int dz dz' f(z) f(z') \tilde{G}(z - z', k) \quad (1.96)$$

Now, using the sharp interface approximation Eq. (1.90), we obtain

$$\langle \chi(\mathbf{k}, t) \chi(\mathbf{k}', t') \rangle = 2DT(2\pi)^d \delta(t - t') \delta(\mathbf{k} + \mathbf{k}') \frac{2\phi_c^2}{k} \quad (1.97)$$

and consequently

$$\langle \xi(\mathbf{k}, t) \xi(\mathbf{k}', t') \rangle = 2DT(2\pi)^d \delta(t - t') \delta(\mathbf{k} + \mathbf{k}') \frac{k}{2\phi_c^2} \quad (1.98)$$

The interface dynamics for model B in Fourier space is thus

$$\frac{\partial h(\mathbf{k}, t)}{\partial t} = -\frac{Dk^3 \sigma}{2\phi_c^2} \tilde{h}(\mathbf{k}, t) + \tilde{\xi}(\mathbf{k}, t) \quad (1.99)$$

which in real space this has the form

$$\frac{\partial h(\mathbf{r})}{\partial t} = -L \frac{\delta H_{eff}}{\delta h(\mathbf{r})} + \xi(\mathbf{r}, t) \quad (1.100)$$

where the operator L is defined via its Fourier transform

$$\tilde{L}(\mathbf{k}) = \frac{Dk}{2\phi_c^2} \quad (1.101)$$

Now if we look at Eq. (1.99) we see that the solution without noise is a function of $k^3 t$, which in real space corresponds to x^3/t . From this we see that the coarsening length scale grows as $\ell(t) \sim t^{1/3}$ and consequently the coarsening exponent is $z = \frac{1}{3}$. Coarsening for conserved

model B or diffusive dynamics is slower than that of model A [33]. One of the reasons for this slowing down with respect to nonconserved dynamics is that material must be physically transported by diffusion (by exchanging spins in the language of lattice spin models), where as for model A dynamics the composition can change at any given point by *spin flipping*. As a cautionary note, if we had taken the Hamiltonian in Eq. (1.47) and applied model B conserved dynamics, as in Eq. (1.31), for the height field we would not have obtained this equation.

Without using the sharp interface approximation, Eq. (1.87) can be written as

$$Q(k) \frac{\partial \tilde{h}(\mathbf{k}, t)}{\partial t} = -Dk^2 \sigma \tilde{h}(\mathbf{k}, t) - \tilde{\chi}(\mathbf{k}, t) \quad (1.102)$$

where

$$Q(k) = \int dz dz' f'(z) \tilde{G}(z - z', \mathbf{k}) f'(z') \quad (1.103)$$

Notice that from Eq. (1.102) that

$$\langle \chi(\mathbf{k}, t) \chi(\mathbf{k}', t') \rangle = 2DT(2\pi)^d \delta(t - t') \delta(\mathbf{k} + \mathbf{k}') Q(k) \quad (1.104)$$

and so

$$\frac{\partial \tilde{h}(\mathbf{k}, t)}{\partial t} = -\tilde{L}(k) \tilde{\mu}(\mathbf{k}) + \eta(\mathbf{k}) \quad (1.105)$$

where $\mu(\mathbf{x}) = \delta H_{eff} / \delta h(\mathbf{x})$, $\tilde{L}(k) = D/Q(k)$ and

$$\langle \eta(\mathbf{k}, t) \eta(\mathbf{k}', t') \rangle = 2T(2\pi)^d \delta(t - t') \delta(\mathbf{k} + \mathbf{k}') \tilde{L}(k) \quad (1.106)$$

1.3 Lattice models

1.3.1 The Ising model

The Hamiltonian of an Ising model of size $L' \times L' \times L$ and composed of N sites i whose value correspond to $\sigma_i = \pm 1$ is

$$H = - \sum_{\langle ij \rangle} J \sigma_i \sigma_j + B \frac{V(\sigma_i) + V(\sigma_j)}{2} \quad (1.107)$$

where $\sum_{\langle ij \rangle}$ is a sum over all pairs of nearest neighbours, and the external parameter B having the energy dimension is applied to the function of the internal variables $V(\sigma_i)$ which has been symmetrized. The Ising model [4, 34] is therefore a lattice model with short interactions between particles. Since all particles σ_i in the system are equal to ± 1 , this system is called a lattice based spin model. When σ_i is continuous, it is called the XY model [35]. J is the coupling parameter of the system and can be non-uniform if the nearest neighbours interaction is $J = J_{ij}$. If $J_{ij} < 0$, the system favors homogeneous phases and is called ferromagnetic. while if $J_{ij} > 0$, the system favors configurations where each spin has an opposite sign with respect to all of their neighbours, which modelises antiferromagnetic materials. We now set $J_{ij} = 1$.

The mean-field theory with a ϕ^4 potential has been developed from this model [36], and exact relationship between both of them has been found in 4 dimensions and above [37]. A

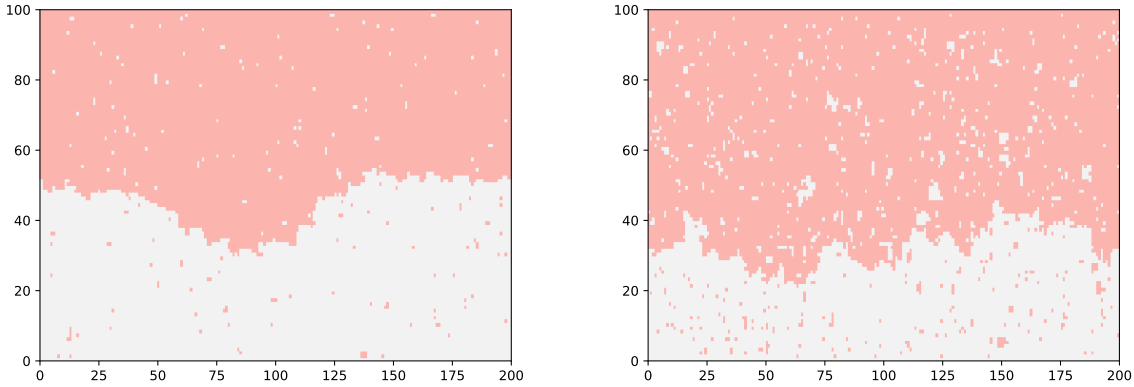


Figure 1.4: Snapshot of Monte Carlo simulations of the Ising model for two different temperatures in two dimensions ($T = 0.7T_C$ (left) and $T = 0.95T_C$ (right)) with periodic boundary conditions in x . The interface between both phases is set by the fixed boundary conditions on y .

fast way to convince ourselves is to take the finite difference derivative at first order of Eq (1.18). Supposing the sole role of the potential is to set the field to $\pm\phi_C$ on each site, then we have

$$\begin{aligned} [\nabla\phi(i)]^2 &= \left(\frac{\partial\phi(i)}{\partial x}\right)^2 + \left(\frac{\partial\phi(i)}{\partial y}\right)^2 + \left(\frac{\partial\phi(i)}{\partial z}\right)^2 \\ &= (\phi(x, y, z) - \phi(x+1, y, z))^2 + (\phi(x, y, z) - \phi(x, y+1, z))^2 + (\phi(x, y, z) - \phi(x, y, z+1))^2 \\ &= 2(1 - \phi(x, y, z)\phi(x+1, y, z)) + 2(1 - \phi(x, y, z)\phi(x, y+1, z)) + 2(1 - \phi(x, y, z)\phi(x, y, z+1)) \end{aligned} \quad (1.108)$$

where the distance between two sites is set to 1. From this we easily see some bulk energy to which we add the sites' nearest neighbours interactions in an Ising-like fashion.

This model precisely describes phase transitions in uniaxial magnetic systems[38, 39, 40]. It is also the simplest model of its eponymous universality class, which also contains liquid/gas transitions and binary fluids. In these mappings, the value $n_i = \frac{1}{2}(1 - \sigma_i) = 0, 1$ represents the occupation of a cell in a lattice fluid, and the value $\sigma_i = \pm 1$ gives the label of a binary species A or B. This model does not have a phase transition in 1D, but a phase transition in 2D was found in 1944[23] at the critical temperature

$$T_{2D,C} = \frac{2J}{k_B \ln(1 + \sqrt{2})} \simeq 2.27 \frac{J}{k_B} \quad (1.109)$$

The renormalization group approaches have deep connexions with the Ising model [41, 2]. Even though results have been found for $d = 4$ (which is the upper critical dimension), no analytical solution has been found in 3 dimensions. Numerous numerical simulations [42, 43] have shown that the 3-dimensional phase transition occurs at

$$T_{3D,C} \simeq 4.51 \frac{J}{k_B} \quad (1.110)$$

By making the transformation[2]

$$n_i = \frac{\sigma_i + 1}{2} \quad (1.111)$$

so that $n_i(\sigma_i = 1) = 1$ and $n_i(\sigma_i = -1) = 0$, the Hamiltonian liquid/gas Hamiltonian is

$$H = - \sum_{\langle ij \rangle} J_{ij} (4n_i n_j - 2(n_i + n_j) + 1) + B \sum_{\langle ij \rangle} \frac{V(\sigma_i) + V(\sigma_j)}{2} \quad (1.112)$$

Dropping the constant term $\sum_{\langle ij \rangle} J_{ij}$, it becomes

$$\begin{aligned} H_{LG} &= -4 \sum_{\langle ij \rangle} J_{ij} n_i n_j + 2 \sum_{\langle ij \rangle} J_{ij} (n_i + n_j) + B \sum_{\langle ij \rangle} \frac{V(\sigma_i) + V(\sigma_j)}{2} \\ &= -4J \sum_{\langle ij \rangle} n_i n_j + \mu_c \sum_i n_i + B \sum_{\langle ij \rangle} \frac{V(\sigma_i) + V(\sigma_j)}{2} \end{aligned} \quad (1.113)$$

where J_{ij} is set to J , and the intrinsic chemical potential for a liquid-gas system is $\mu_c = 4Jc$, with c the number of nearest neighbours depending on the dimensionality of the system. A positive magnetic phase is thus analogous to a high density state such as a liquid, while the negative magnetic phase is equal to a low density state such as a gas. An onsite potential $V(\sigma_i)$ further modifies the chemical potential, $\mu = \mu_c + \delta\mu[V(\sigma_i)]$ in the same fashion as in Fig 1.2. The chemical potential μ is the conjugate variable to the total number of particles $\sum_i n_i$, while the magnetic field B is the conjugate variable to the total magnetisation $\sum_i \sigma_i$. The two are connected through the mapping such that $B \sim \mu - \mu_c$, so that liquid-gas and Ising model systems share common thermodynamic features such as the universality class for critical fluctuations. For the fluid the grand canonical ensemble corresponds to the Gibbs ensemble with fixed T and μ and canonical ensemble with fixed T and N . In the magnetic system these ensembles correspond to fixed T, B and T, M respectively. The model also describes adsorption of a gas in a lattice or binary fluids between particles of different species A and B .

By imposing $+-$ boundary conditions in the z direction, the existence of an interface is forced, as seen in Fig 1.4. Those BC can be fixed, imposing $\sigma(z=0) = -1$ and $\sigma(z=L) = +1$, or free but with a local external field $V(z) = h(\delta_{0,z} - \delta_{z,L})$. An interface is characterized by its mean and its width. The easiest way to find it is to fit the magnetization profile

$$m(z) = \frac{1}{L^2} \langle \sum_{xy} \sigma(x, y, z) \rangle \quad (1.114)$$

to mean field results from Eq (1.43). The mean position of the interface is

$$m = \langle h \rangle = \frac{1}{L^2} \langle \sum_i \sigma_i \rangle \quad (1.115)$$

and the width of the interface is then defined as

$$w^2 = \langle h^2 \rangle - \langle h \rangle^2 \quad (1.116)$$

This can be rewritten [44] as

$$w^2 = 2 \frac{\int_0^L dz z \frac{dm(z)}{dz}}{\int_0^L dz \frac{dm(z)}{dz}} \quad (1.117)$$

The surface tension of the interface is now defined as the free energy difference between the bulk and the interface [45]. If Z^{++} is the partition function of a system with $(++)$ BC, and Z^{+-} with $(+-)$ BC, then the surface tension [46] is given by

$$\sigma = \lim_{L', L \rightarrow \infty} \frac{1}{L'^2} \ln \left(\frac{Z^{+-}}{Z^{++}} \right) \quad (1.118)$$

By diagonalization of the transfer matrix (which will be defined later), we find that the surface tension of a the interface between two pure phases $+$ and $-$ is given in a two-dimensional Ising model [5] by

$$\sigma = 2\beta J + \log(\tanh(\beta J)) \quad (1.119)$$

meaning that the hotter the system, the wider the interface becomes.

1.3.2 The Solid-On-Solid Model

In order to get the Edwards-Wilkinson equation of an interface from statistical field theory, the approximation

$$\phi(\mathbf{x}, t) = f(z - h(\mathbf{r}, t)) \quad (1.120)$$

was used. Its translation in lattice models is

$$\sigma_{i,j} = \text{sgn}(h_i - j) \quad (1.121)$$

where $\text{sgn}(x < 0) = -1$ and $\text{sgn}(x > 0) = 1$, and h_i is the height of the interface at site i . This is the low temperature approximation of the Ising model, where there are no overhangs from the + phase into the - phase and vice versa. If we note J_{\perp} the vertical bond energy between two Ising spins and J_{\parallel} the horizontal bond energy, this approximation becomes equivalent to a highly anisotropic Ising model where $J_{\perp} \gg J_{\parallel}$ [47].

In a slab or semi-infinite geometry as seen in Fig 1.5, the height of the interface corresponds to the number of spins - in the column i , while for an infinite geometry, h_i is interpreted as the number of excess spins - with respect to the mean height, set in the figure at $z = 0$ [48]. In this representation, height profiles represent an interface height and not a number of particles, since there is no entropy term associated with the number of ways that the h_i particles on each site can be chosen from the N particles available. In chapter 4, a model with those characteristics will be addressed. Using the identities

$$\min(a, b) = \frac{|a + b| - |a - b|}{2} \quad (1.122)$$

$$\max(a, b) = \frac{|a + b| + |a - b|}{2} \quad (1.123)$$

we have

$$\sum_{j=0}^L \text{sgn}(h - j) \text{sgn}(h' - j) = L - 2|h - h'| \quad (1.124)$$

which, from the 2-D Ising Hamiltonian (1.107) of size $L' \times L$, gives

$$H = 2JL'(1 - L) + 2J \sum_{i=0}^{L'} |h_i - h_{i+1}| + B \sum_{i=0}^{L'} V(h_i) \quad (1.125)$$

with external potential

$$BV(h_i) = B \sum_{j=0}^L V(\text{sgn}(h_i - j)) \quad (1.126)$$

For periodic boundary conditions, $h_{L'} = h_0$.

Another way to compute the energy for a SOS configuration is to directly count the number of energy bonds for a $L' \times L$ Ising model under the approximation (1.121). There are $L - 1$ vertical bonds per column, where all have an energy of $-J$, while the link that goes through the interface has an energy of $+J$. The total contribution to energy from vertical bonds is thus

$$E_{\perp} = -JL'(L - 2) \quad (1.127)$$

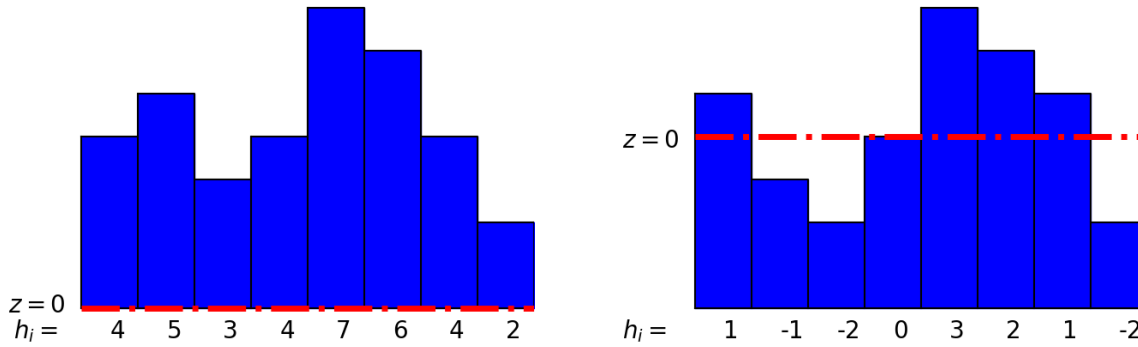


Figure 1.5: Possible configuration of the SOS model for a semi-infinite geometry (left) and infinite geometry (right). The red line shows the origin $z = 0$. In the i -th column the interface is at height h_i . Particles under the interface are from the Ising $-$ phase, while particles over it are from the $+$ phase.

There are $L' \times L$ horizontal bonds. In a pure phase system, the horizontal energy would be $-JL'/L$. Nevertheless, there are $\sum_i |h_i - h_{i+1}|$ bonds which have an energy of $+J$, which gives the horizontal energy contribution

$$E_{\parallel} = -JL'L + 2J \sum_i |h_i - h_{i+1}| \quad (1.128)$$

By adding both, we find back Eq (1.125).

By setting $2J = J$ and getting rid of the bulk energy, we obtain the **Solid-On-Solid Hamiltonian**

$$H = J \sum_{i=0}^{L'} |h_i - h_{i+1}| + B \frac{V(h_i) + V(h_{i+1})}{2} \quad (1.129)$$

The first system where the SOS model has been applied was crystals' growth in 1972 [6]. Since then, the model has been used with some success in naphthalene crystals[49], experimental epitaxial growth[50], polymer membranes [51, 52], or interfacial wetting [53], all of them being interface physical systems.

In the SOS model, the sites i of height h_i can take any value in $[0, L]$. The Restricted Solid-On-Solid model (RSOS) is a variation where sites can only take the value $h_{i+1} \in [h_i - 1, h_i, h_i + 1]$ [54]. This approximation works for very low temperatures or very smooth interfaces [55, 56].

Another model, closer to the continuous model of Hamiltonian (1.47) is the Discrete Gaussian model which has the following gaussian interaction

$$H = J \sum_{i=0}^{L'} (h_i - h_{i+1})^2 + B \frac{V(h_i) + V(h_{i+1})}{2} \quad (1.130)$$

and also has a restricted version. At low temperature, since height differences are typically small the typical energy cost of height differences $0, \pm 1$ is the same in every SOS model no matter the exponent, leading to similar qualitative features of all those models [59]. Because the SOS model has an exact relation with the XY model [57] no matter the power law used

for the interaction, even though GSOS is the direct discrete version of continuous models, we use SOS because its transfer matrix is easier to diagonalise, as we will show in Section 3.4. With a generalization of this model to continuous heights, it has been shown that extreme deviations statistics of the interface is described by a scaling function [58].

Since the dimensionality of the system has been reduced in only taking into account the height interface h_i at site i instead of the position of all particles, we can think of an interface as a partially self-avoiding walk. This idea, which will be developed in section 3.2, has proven quiet powerful in finding exact solutions of the generating function [60] or the extreme deviations statistics of the interface [61, 58].

In the canonical ensemble, the height interface is fixed to N , which is translated in the partition function as

$$Z(N) = \sum_{h_0 h_1 \dots h_{L'}} \exp(-\beta \sum_i H(h_i, h_{i+1})) \delta_{\sum_i h_i, N} \quad (1.131)$$

In the grand-canonical ensemble, the conjugate variable to the height interface is the chemical potential μ , and the grand partition function Ξ is related to the canonical partition function by

$$\begin{aligned} \Xi(\mu) &= \sum_N Z(N) \exp((\beta\mu N)) \\ &= \sum_{h_0 h_1 \dots h_{L'}} \exp(-\beta H_{eff}(h_0, h_1, \dots, h_{L'})) \end{aligned} \quad (1.132)$$

where

$$H_{eff} = J \sum_{i=0}^{L'} |h_i - h_{i+1}| + \sum_{i=0}^{L'} BV(h_i) - \mu h_i \quad (1.133)$$

In Fig 1.6, the mean number of particles per site with respect to the chemical potential is plotted, for different size of the system, in the thermodynamic limit $L' \rightarrow \infty$. When the chemical potential is too small, the Lagrange's multiplier of the mean height is negligible, allowing the interface to fluctuate freely, meaning that the mean value for $\mu = 0$ is $\frac{L}{2}$.

1.3.3 Transfer matrix

In a more general fashion, the SOS Hamiltonian takes the form

$$H = \sum_{i=0}^{L'} f(h_i, h_{i+1}) + BV(h_i, h_{i+1})$$

where $f(h_i, h_j)$ is the energy interaction between two nearest neighbours and $BV(h_i, h_j) = B \frac{V(h_i) + V(h_j)}{2}$ is the external potential. The partition function is

$$Z = \sum_{h_1=0}^L \sum_{h_2=0}^L \dots \sum_{h_{L'}=0}^L \exp(-\beta \sum_{i=0}^{L'} H(h_i, h_{i+1})) = \sum_{h_1 h_2 \dots h_{L'}} \prod_{i=0}^{L'} \exp(-\beta H(h_i, h_{i+1})) \quad (1.134)$$

We define the transfer matrix

$$T(h_i, h_j) = e^{-\beta H(h_i, h_j)} \quad (1.135)$$

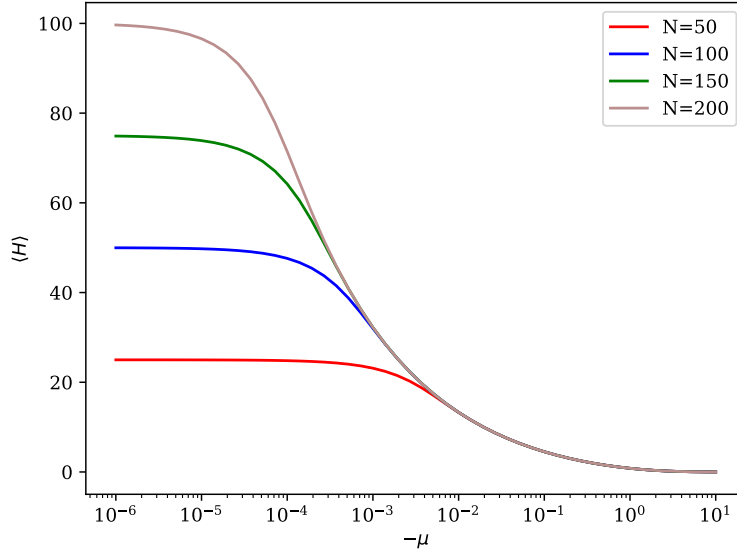


Figure 1.6: Mean height of the SOS interface (1.132) with respect to $-\mu$ through diagonalization of the transfer matrix for $\beta = 1$, in the limit $L' \rightarrow \infty$.

In Fig 1.7, an infinite matrix corresponding to the limit $L \rightarrow \infty$ is represented, where each site can take any value in $[-\infty, \infty]$. To diagonalize numerically such matrices, we translate the whole system with $h_i \rightarrow h_i - \frac{L}{2}$, where L is the matrix's size, which we tend to ∞ afterwards. The constraint (1.131) cannot be expressed in the transfer matrix formalism, which induces a change in properties from this ensemble with respect to the transfer matrix results [62].

Since the system has periodic boundary conditions $h_{L+1} = h_1$, we have $T(h_L, h_{L+1}) = T(h_L, h_1)$ [63]. The matrix is thus symmetric, meaning that it can be diagonalized with the eigenvectors and the eigenvalues

$$T|\lambda\rangle = \lambda|\lambda\rangle \quad (1.136)$$

Those eigenvectors are orthonormal

$$\langle \lambda | \lambda' \rangle = \delta_{\lambda \lambda'} \quad (1.137)$$

We set λ_0 as the biggest eigenvalue of T , by λ_1 the second biggest eigenvalue, and so on. The partition function can then be rewritten, in terms of the transfer matrix [5] as

$$Z = \sum_{h_1 h_2 \dots h_{L'}} \prod_i T(h_i, h_{i+1}) = \text{Tr}(T^{L'}) = \sum_{\lambda} \langle \lambda | T^{L'} | \lambda \rangle = \sum_{\lambda} \lambda^{L'} \quad (1.138)$$

In the thermodynamic limit $L' \rightarrow \infty$, only the biggest eigenvector is relevant since the partition function becomes

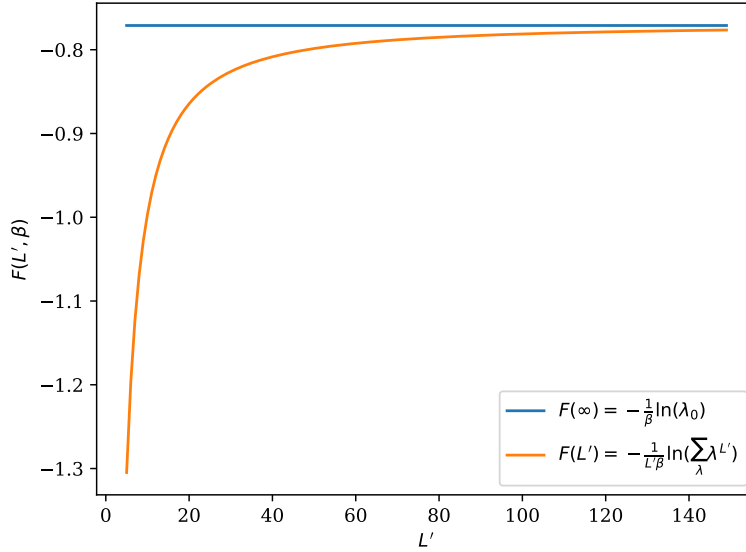
$$Z(L \rightarrow \infty) \simeq \lambda_0^{L'} \quad (1.140)$$

We find that the free energy per site is

$$f = -\frac{1}{L'\beta} \ln(Z) \simeq -\frac{1}{\beta} \ln(\lambda_0) \quad (1.141)$$

$$\mathbf{T} = \begin{bmatrix} \ddots & \vdots & \ddots \\ e^{-\beta H(-1,-1)} & e^{-\beta H(-1,0)} & e^{-\beta H(1,-1)} \\ \dots & e^{-\beta H(0,0)} & \dots \\ e^{-\beta H(1,-1)} & e^{-\beta H(1,0)} & e^{-\beta H(1,1)} \\ \ddots & \vdots & \ddots \end{bmatrix} \quad (1.139)$$

Figure 1.7: Infinite and symmetrical transfer matrix 1.135.


 Figure 1.8: Free energy per site $\Omega(L')$ with respect to the number of sites L' compared to the thermodynamic value $\Omega(\infty)$, for a system of maximum height $L = 100$, $\beta = 1$, $J = 1$ and $V(h_i) = 0$.

In Fig 1.8 the evolution of the free energy per site $\Omega(L')$ is shown without external field, comparing it to the thermodynamic limit. From that figure, the thermodynamic limit becomes valid for $L' > 150$.

To compute the mean height value per site M , the height matrix \hat{M} is introduced and is defined by its action over the vectors $|h\rangle$ in the matrix transfer's base by

$$= \delta_{h,h'} h \quad (1.142)$$

The density is

$$M = \langle h \rangle = \frac{1}{L'} \sum_i h_i = \frac{1}{Z} \sum_{\lambda} \lambda^{L'} \langle \lambda | \hat{M} | \lambda \rangle \simeq \langle \lambda_0 | \hat{M} | \lambda_0 \rangle \quad (1.143)$$

and the mean displacement per site is

$$w^2 = \langle (h - M)^2 \rangle = \frac{1}{Z} \sum_{\lambda} \lambda^{L'} \langle \lambda | \hat{M}^2 | \lambda \rangle - \langle \lambda | \hat{M} | \lambda \rangle^2 \simeq \langle \lambda_0 | \hat{M}^2 | \lambda_0 \rangle - M^2 \quad (1.144)$$

Those two observables are found by computing the first and second moment of the probability distribution that a site i is at height h_i

$$p(h) = \frac{1}{Z} \sum_{\lambda} \lambda^L \langle \lambda | h \rangle^2 \simeq \langle \lambda_0 | h \rangle^2 \quad (1.145)$$

The two-point correlation function of the system is computed by

$$C(r) = \langle h_i h_{i+r} \rangle - M^2 = \frac{1}{Z} \sum_{\lambda \neq \lambda_0} \langle \lambda_0 | M | \lambda \rangle \langle \lambda | M | \lambda_0 \rangle \left(\frac{\lambda}{\lambda_0} \right)^r \quad (1.146)$$

which becomes, in the long distance r limit,

$$C(r) \simeq \langle \lambda_0 | M | \lambda_1 \rangle \langle \lambda_1 | M | \lambda_0 \rangle \left(\frac{\lambda_1}{\lambda_0} \right)^r \quad (1.147)$$

The correlation function has an exponential decay at large distances, which allows us to define the correlation length at large distance ξ

$$\xi = - \frac{1}{\ln(\frac{\lambda_1}{\lambda_0})} \quad (1.148)$$

1.4 Systems driven by imposed hydrodynamic flows

A system which does not respect the Gibbs-Boltzmann distribution is said to be out of equilibrium. The dynamics of the system can lead the configurations from very unlikely ones (for example from initial conditions) to more probable ones. Once the equilibrium state is reached, all the configurations have their Gibbs-Boltzmann probability to occur. Equilibrium and steady-state should thus not be confused. Steady state out of equilibrium systems can be created experimentally by injecting energy into the system with a laser [64], by inducing a shear flow in a Couette cell in liquids [65, 19] or in glassy materials [66, 67]. Those systems should be analysed through model H dynamics which couples diffusive model B dynamics to hydrodynamics in the low Reynolds number Stokes flow regime. In these dynamics the order parameter field will itself induce a hydrodynamics flow which will modify the imposed one. However this full situation is very difficult to analyse and to a first approximation one can assume that the back reaction of the order parameter field on the hydrodynamic flow is small with respect to the imposed hydrodynamic flow and so the Langevin equation is simply

$$\frac{\partial \phi(\mathbf{x}, t)}{\partial t} + \nabla \cdot (\mathbf{v}(\mathbf{x}) \phi(\mathbf{x}, t)) = -L \frac{\delta H}{\delta \phi(\mathbf{x})} + \eta(\mathbf{x}, t), \quad (1.149)$$

where L is given by the underlying model A or B dynamical operator and the noise has the correlation function as given by Eq. (1.26), and $\mathbf{v}(\mathbf{x})$ is the imposed (time independent) hydrodynamic flow or can equally well be an external drive imposed on the particles, due to the gravitational or electric field for example.

The simplest case one can consider is the uniform driving field $\mathbf{v}(\mathbf{x}) = \mathbf{v}_0$ [68, 69]. Unfortunately this simple driving does not lead to a new steady state. Basically all of the colloidal

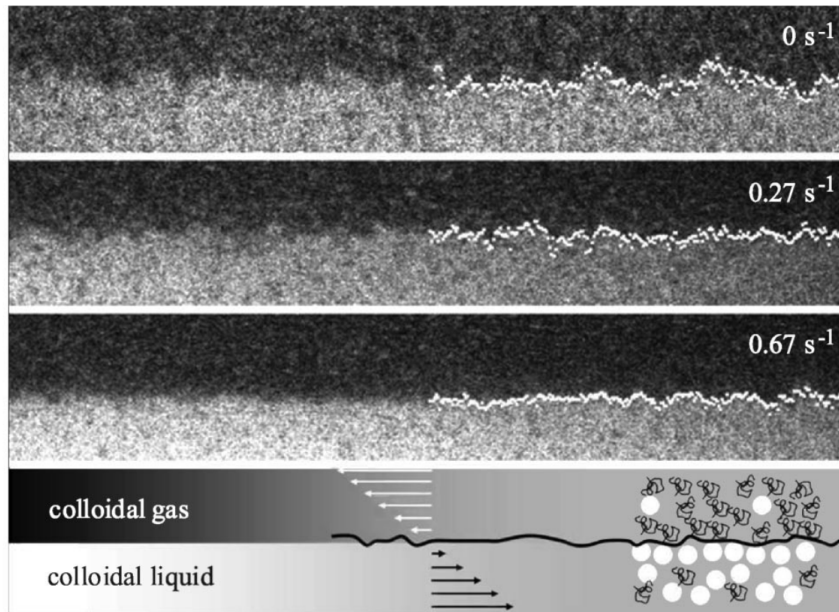


Figure 1.9: Snapshot of the interface a sample of fluorescently labeled poly(methyl methacrylate) (PMMA) colloidal spheres in polystyrene close to the critical point, for different shear rates. The bottom panel schematically shows the flow geometry with the plane of zero velocity located at the interface. From [19].

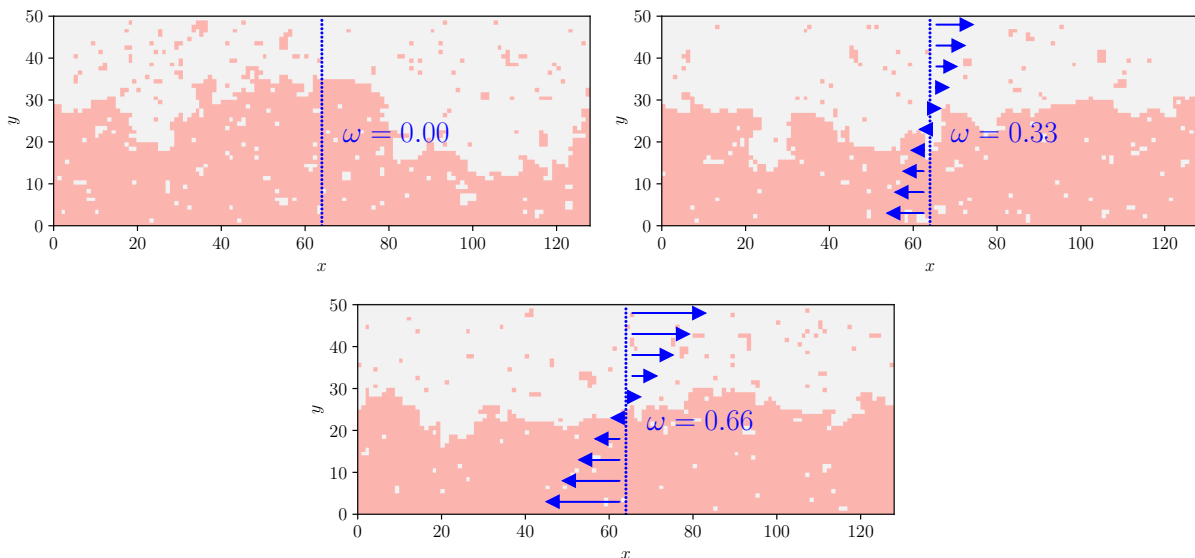


Figure 1.10: Snapshot of a 2D Ising model with respect to the shear (1.151) with Kawasaki dynamics at $T = 0.9T_{2D,C}$.

particles acquire an average velocity \mathbf{v}_0 and so move along at the same speed relative to each other. Mathematically this can be seen by making the Galilean transformation

$$\phi(\mathbf{x}, t) = \phi(\mathbf{x} - \mathbf{v}_0 t, t) = \phi(\mathbf{y}, t) \quad (1.150)$$

This transformation eliminates the driving from the evolution equation (1.149) and so we find an equilibrium system.

The most studied example is where the driving is a shear flow [19, 70]. The effective dynamics of the surface term in the presence of a shear flow, parallel to the interface [9, 29], is written as

$$\mathbf{v}(\mathbf{x}) = \gamma z \mathbf{e}_x \quad (1.151)$$

The addition of a shear flow leads to the appearance of a nonlinear term in h and the interface statistics thus become non-Gaussian. In Fig 1.10 we show the influence of such a shear flow in numerical simulations, which is exactly the behaviour to be seen in capillary waves in polymer melts [65, 19], see Fig 1.9. The shear has a confining effect on the interface [71, 72, 73], thus increasing the effective surface tension of the system. The main result of those two papers is that out of equilibrium steady state systems can behave as equilibrium ones, where the observables are rescaled into effective ones. In Chap 5 we study the effect of a uniform driving $v(\mathbf{x}) = \gamma \mathbf{e}_c$ using a coupling between model A and model B dynamics, and explain theoretically why such systems behave like equilibrium ones.

1.5 Conclusion

Statistical field theory [22] is a powerful tool to study the dynamics of equilibrium fields [36]. The two main models are model A and model B [18], which describe the dynamics of a field respectively in grand-canonical and the canonical ensemble. In the case of phase separated systems, the interface is mostly defined by its surface tension, which is equal to the difference of free energy between the bulk and the interface [25, 5]. From the equations of model A and B we have derived the Edwards-Wilkinson equation [30] for both ensembles. The Ising model [4, 34] provides a good way to study the behaviour of the field by discretization, which is easier to compute in numerical simulations [10]. The same kind of dimensional reduction can be done in order to get an interface lattice model which is called the Solid-On-Solid model [6]. This model allows the use of the transfer method in an easier way than the Ising model [74]. Also, the presence of out-of-equilibrium hydrodynamic flows tend to present interesting features. One such example is the Couette shear [19], which has been found to smoothen the interface [72] and have effective equilibrium properties.

Chapter 2

Numerical methods

In 1949, Metropolis *et.al* [75] presented a method to compute, through Monte Carlo simulations, the expectation value of statistical quantities. If Q is an observable quantity of a statistical system, such as the total energy or density of particles per site, then the expectation value is computed by weighting its value over all configurations C with respect to their statistical weight. Considering the system to be at thermodynamic equilibrium, every configuration C follows the Gibbs-Boltzmann distribution, and the mean value $\langle Q \rangle$ is

$$\langle Q \rangle = \frac{\sum_C Q(C) \exp(-\beta E(C))}{\sum_C \exp(-\beta E(C))} \quad (2.1)$$

For example, in a SOS system of size 100×100 - which is small compared to the thermodynamic limit as discussed in figure 1.8 - there exists 100^{100} different possible configurations. In comparison, numerical simulations can explore up to 10^9 configurations in a reasonable amount of CPU time.

Lattice models are well fitted for Monte Carlo simulations, where the goal is to compute such quantities. In the SOS model, all observables (and even quantities not observable such as the free energy) can be directly computed thanks to the matrix transfer in the grand-canonical ensemble, even though the canonical ensemble stays out of reach of that method.

In this chapter, we start by explaining how Monte Carlo Metropolis algorithms work based upon the statistical ensemble we're interested in, at or out of equilibrium, and then some technical considerations about optimizing numerical simulations are given.

This work was made possible thanks to the Mésocentre de Calcul Intensif Aquitain (MCIA) [20], where I have made the vast majority of the numerical simulations. All the code I have produced can be found on Github [21] under Creative Commons BY 3.0 licence¹. Numerical simulations were made with C++, parallelization with MPI, data treatment with Python, and some minor scripts in Bash.

¹<https://creativecommons.org/licenses/by/3.0/fr/deed.en>

2.1 Estimator

Monte Carlo simulations explore the configurations' space in a random fashion [10] with a probability $p(C)$. By choosing M states C_0, \dots, C_M , the estimator Q_M of Q is given by

$$Q_M = \frac{\sum_{i=0}^M Q(C_i) p(C_i)^{-1} \exp(-\beta E(C_i))}{\sum_{i=0}^M p(C_i)^{-1} \exp(-\beta E(C_i))} \quad (2.2)$$

The bigger the sample number M , the better estimate the estimator provides for $\langle Q \rangle$, up to the limit $Q_{M \rightarrow \infty} = \langle Q \rangle$. If we select the configurations over which the system's sample is done according to the Gibbs-Boltzmann distribution $p(v) = Z^{-1} e^{-\beta E(C)}$, the estimator of $\langle Q \rangle$ is

$$Q_M = \frac{1}{M} \sum_{i=0}^M Q(C_i) \quad (2.3)$$

The error over this estimate is

$$E(Q) = \sqrt{\frac{2\tau}{M} (\langle Q^2 \rangle - \langle Q \rangle^2)} \quad (2.4)$$

This error does depend from the correlation time τ since if two states are really close in time, they would be strongly correlated, adding little information to the estimator. In practice, it is just needed $\frac{\tau}{M} < 10^{-4}$ to obtain an error under 1%. This correlation time τ is computed through the autocorrelation function

$$\mathcal{C}(t) = \langle Q(t')Q(t+t') \rangle - \langle Q \rangle^2 = \frac{1}{t} \int_0^t Q(t')Q(t+t') - \langle Q \rangle^2 dt' \quad (2.5)$$

which behaves as an exponential at long time[76]. A first order estimate of τ is thus given for

$$\tau = \int_0^{\infty} \mathcal{C}(t) / \mathcal{C}(0) dt \quad (2.6)$$

Similarly, the measurement of the correlation length ξ is given at first order by integration the two-point correlation function

$$\mathcal{C}(j) = \frac{1}{L'} \sum_{i=0}^{L'} \langle h_i h_{i+j} \rangle - \langle h \rangle^2 \quad (2.7)$$

2.2 Monte Carlo Metropolis algorithm

A dynamic for systems with a discrete configuration state can be built using Markov chains. Let the dynamic evolve in a discrete time n , and $p_n(C)$ the probability that the system is in configuration C at time n . At that time step, if the system is in state C , it can jump to another state C' with a transition probability $\rho(C \rightarrow C')$. The system at time $n+1$ thus only depends of the state at time n : it is called a Markovian process, and has no inertia nor memory of what have happened prior to time n . The probability $p_{n+1}(C)$ to be in state C at time $n+1$ is equal to the probability that the system was already in state C at time n and stays put with a

transition probability $\rho(C \rightarrow C)$, plus the probability that it was in state C' and jumps towards C with a transition probability $\rho(C' \rightarrow C)$. The master equation of such a dynamic is

$$p_{n+1}(C) = \rho(C \rightarrow C)p_n(C) + \sum_{C' \neq C} \rho(C' \rightarrow C)p_n(C') \quad (2.8)$$

Since $\rho(C' \rightarrow C)$ is a probability, it meets the requirements

$$\sum_{C'} \rho(C' \rightarrow C) = 1 \quad (2.9)$$

Now, if the dynamics describes a system in interaction with a heat bath, the equilibrium distribution is given by

$$p_{eq}(C) = \frac{\exp(-\beta E(C))}{Z} \quad (2.10)$$

with Z the partition function. Since the equilibrium distribution is also stationary, the probability to be at configuration C at time $n + 1$ is

$$p_{eq}(C) = \rho(C \rightarrow C)p_{eq}(C) + \sum_{C' \neq C} \rho(C' \rightarrow C)p_{eq}(C') \quad (2.11)$$

The emergence of equilibrium probability densities ensures that the transition rate from a state to another one is equal to the rate from the reciprocal transition

$$\sum_{C'} p(C)\rho(C \rightarrow C') = \sum_{C'} p(C')\rho(C' \rightarrow C) \quad (2.12)$$

which leads to the detailed balance condition [10]

$$\frac{\rho(C' \rightarrow C)}{\rho(C \rightarrow C')} = \frac{p(C)}{p(C')} = \frac{\exp(-\beta E(C))}{\exp(-\beta E(C'))} \quad (2.13)$$

Hence by adopting the detailed balance condition for the transition probabilities, the steady state distribution computed by Eq (2.11) corresponds to the equilibrium Gibbs-Boltzmann distribution. During a Metropolis step, the transition probability of $C \rightarrow C'$ depends of the probability $g(C \rightarrow C')$ that this transition would be chosen amongst all the other possible transitions, and the acceptance rate $A(C \rightarrow C')$, which gives

$$\rho(C \rightarrow C') = g(C \rightarrow C')A(C \rightarrow C') \quad (2.14)$$

For a lattice model site L' sites, a Monte Carlo time step is done when we have proceeded to L' transition tries.

2.2.1 Glauber dynamics

In the SOS model with L' sites of height comprised in $[0, L]$, sites i are chosen for the Glauber algorithm [77] at random with a uniform probability $\frac{1}{L'}$, plus an integer $\alpha = \pm 1$ with probability $\frac{1}{2}$. If the configuration C has the Hamiltonian $H(h_0, h_1, \dots, h_i, \dots, h_{L'})$, then the new generated configuration will have the Hamiltonian $H(h_0, h_1, \dots, h_i + \alpha, \dots, h_{L'})$. If $\alpha = +1$, then a particle at

site i is added, otherwise it is removed. In the case that $h_i + \alpha \notin [0, L]$, the generated configuration is not valid and discarded. If the generated configuration is valid, the probability of selecting this transition is

$$g(C \rightarrow C') = \frac{1}{2L'} \quad (2.15)$$

From Eq. (2.13), detailed balance gives

$$\frac{\rho(C \rightarrow C')}{\rho(C' \rightarrow C)} = \frac{A(C \rightarrow C')}{A(C' \rightarrow C)} = \exp(-\beta(E(C') - E(C))) \quad (2.16)$$

Is it possible to choose any acceptance rate $A(C \rightarrow C')$ which satisfies detailed balance. A Metropolis algorithm is an algorithm which has the following acceptance rate

$$A(C \rightarrow C') = \begin{cases} \exp(-\beta(E(C') - E(C))) & \text{if } E(C') - E(C) > 0 \\ 1 & \text{otherwise} \end{cases} \quad (2.17)$$

and is said to be the faster acceptance rate in CPU-time. In practice, if $\Delta E > 0$, an integer is uniformly chosen between $r \in [0, 1]$. If $r < A(C \rightarrow C')$ then the transition is accepted, otherwise the transition is rejected and the system stays in the configuration C .

Since $\sum_i h_i$ is not conserved over time, Glauber dynamics corresponds to model A. A snapshot of such a system is showed in Fig 2.1, with peridoci boundary conditions on x .

The energy difference between two configurations is

$$\Delta E = |h_{i-1} - (h_i + \alpha)| + |h_{i+1} - (h_i + \alpha)| - |h_{i-1} - h_i| - |h_{i+1} - h_i| \quad (2.18)$$

It is not needed to compute the total height at each time step. We stock $\sum_i h_i$ in a variable that is updated each time a transition is accepted by

$$\langle h \rangle_{M+1} = \langle h \rangle_M + \alpha \quad (2.19)$$

The same can be done for $\sum_i h_i^2$, which gives the interface's width, and the total energy of the system with $\sum_i |h_i - h_{i+1}|$.

In order to accelerate the equilibration process, we can directly start from the total height computed by the transfer matrix, which is close to the equilibrium states. By looking at the temporal evolution of $E(t)$, one can get the equilibrium time and the correlation time once equilibrium has been reached. It is better practice to study the equilibration time by taking the total energy rather than the number density, or magnetization, since without an external potential, the interface is delocalised and total number of particles is only bounded by the boundary conditions. In Fig 2.2, the energy with respect to time and the autocorrelation function of the system in absence of chemical potential from a ground state $h_i = 0$ for all i are shown. The very small correlation and equilibration times means that numerical simulations reach the equilibrium distribution after 10^3 MC steps, so that 10^7 MC steps will give results accurate up to 1%.

In the SOS model, results from the Glauber dynamics are expected to be exactly the same as the transfer matrix method, as shown in Fig 2.3. Since the interface is not localised for small μ , even though thermal equilibrium is quickly reached, the mean height fluctuates a lot, making its measurement irrelevant in the delocalised limit. Since we can get exact results from the transfer matrix, the Glauber dynamics presents little interest for SOS models in the grand-canonical ensemble. Nevertheless, because there does not exist a transfer matrix formulation of the canonical ensemble, Monte Carlo simulations become interesting.

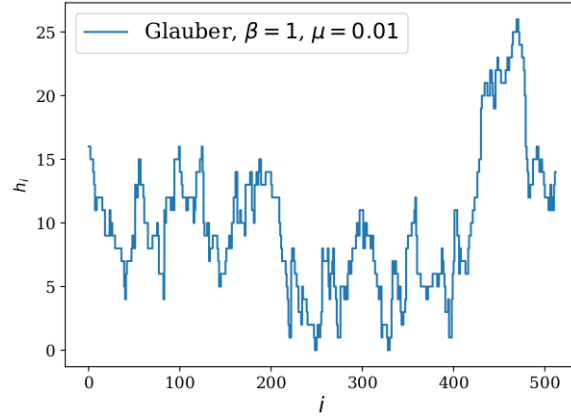


Figure 2.1: Snapshot of a Glauber simulation of a SOS system at $\beta = 1$, $\mu = 0.01$ and $L = \infty$.

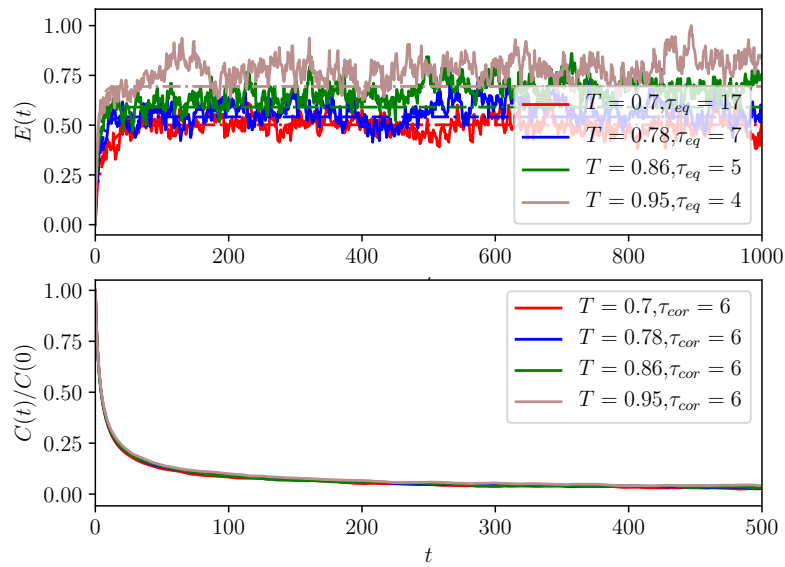


Figure 2.2: Plot of the energy per site (top) and the autocorrelation function (bottom) with Glauber dynamics from an initial state where $h_i = 0$, for different temperatures.

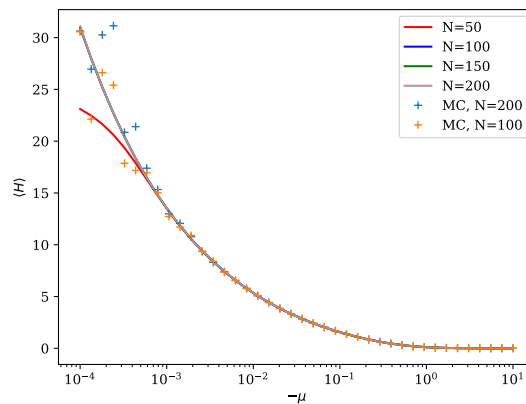


Figure 2.3: Mean height value per site with respect to μ different system size L both by Glauber dynamics and diagonalization of the transfer matrix (which has already been shown in Fig 1.6) for $\beta = 1$ and $L' = 256$.

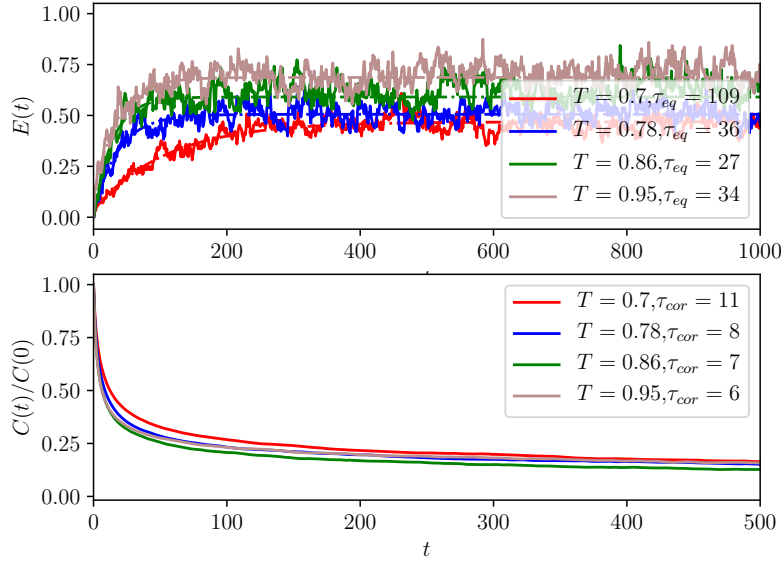


Figure 2.4: Plot of the energy per site (top) and the autocorrelation function (bottom) with Kawasaki dynamics from an initial state where $h_i = 0$, for different temperatures.

2.2.2 Kawasaki dynamics

In the Kawasaki's algorithm [78], a site i is randomly chosen with probability $\frac{1}{L}$, as one of its two nearest neighbors $i - 1$ or $i + 1$ with probability $\frac{1}{2}$. For example, if we take the neighbor site $i - 1$ (it holds the same for the site $i + 1$), a new configuration is generated with Hamiltonian $H(h_0, \dots, h_{i-1} + 1, h_i - 1, \dots, h_L)$, where a particle from site i diffuses it to the neighboring site. A non-local version of this algorithm also exists, but only the local version can implement hydrodynamic flows. The selection probability is

$$g(C \rightarrow C') = \frac{1}{2L'} \quad (2.20)$$

with the same acceptance rate as in Glauber's dynamics (2.17).

Here, the total height is obviously conserved. In the case that a particle is transferred from site i to site $i + 1$, the energy difference is

$$\begin{aligned} \Delta E = & |h_{i-1} - (h_i - 1)| + |h_{i+1} + 1 - (h_i - 1)| + |h_{i+1} + 1 - (h_{i+2})| \\ & - (|h_{i-1} - h_i| + |h_{i+1} - h_i| + |h_{i+1} - h_{i+2}|) \end{aligned} \quad (2.21)$$

In Fig 2.4, we remark that both the equilibration and the correlation times are larger than for non-conserved dynamics, which is normal since the correlation length during coarsening goes as $t^{\frac{1}{2}}$ in model A and as $t^{\frac{1}{3}}$ in model B. Nevertheless they are of the same order of magnitude, which means that numerical simulations will take up roughly the same CPU-time.

This dynamics describes the diffusion of particles at the interface. It is thus possible to add some hydrodynamic flow which breaks equilibrium. Since we have supposed that our configurations obey the Gibbs-Boltzmann distribution, the Metropolis method stays pertinent if we assume that the dynamic is slow compared to the heat exchange with the reservoir.

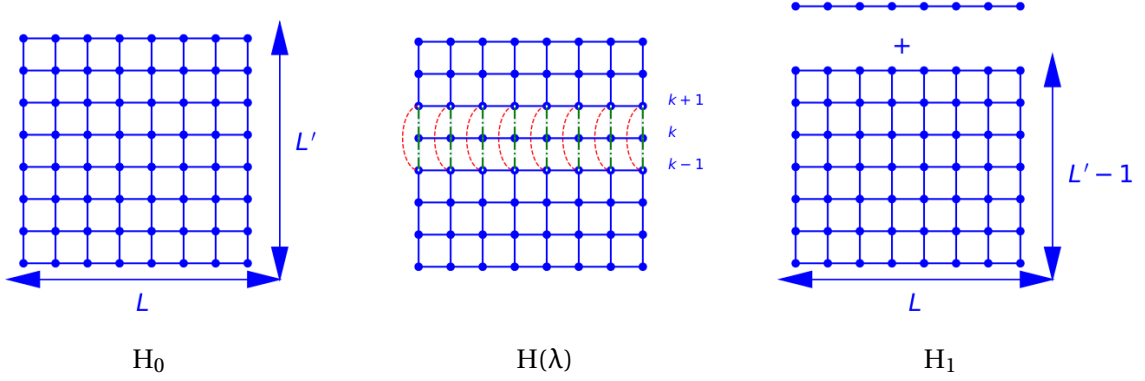


Figure 2.5: Progressive decoupling of the k -th layer of the system in order to compute the free energy through the Crossover Hamiltonian. Blue bonds have an energy of βJ , red ones an energy of $\lambda\beta J$ and the green ones an energy of $(1-\lambda)\beta J$. Reproduction 2D of [11].

2.3 Computing size dependent free energy

2.3.1 The Layer method

It is not possible to compute from Monte Carlo simulations the free energy of a system, since it is not a derivative of the partition function. However, its derivative with respect to the system size can be easily computed. Separating the total free energy of the confined system in a bulk and a singular part

$$F(t, h, L) = L'^2 (L f_{bulk} + \beta^{-1} f_{ex}) \quad (2.22)$$

where f_{bulk} is a bulk term, and f_{ex} the excess free energy due to boundary conditions and to system spanning correlations, we define the thermodynamic force per unit area as

$$p(t, h, L) = -\frac{1}{L'^2} \frac{\partial F}{\partial L} = -f_{bulk} - \beta^{-1} \frac{\partial f_{ex}}{\partial L} \quad (2.23)$$

This force is composed of a bulk term and an excess term defined as the related Casimir force per unit area by

$$f_{casimir} = -\beta^{-1} \frac{\partial f_{ex}}{\partial L} \quad (2.24)$$

In the limit $L \rightarrow \infty$, the excess free energy due to the confinement is zero, so the bulk free energy from Eq (2.22) can be subtracted from the infinite system limit. For two systems of size L_1 and L_2 , where $\left(\frac{L_1}{L_2}\right)^d \ll 1$, at first order the Casimir force is thus

$$f_{ex}(L_1) \simeq -\frac{1}{L'^2} \frac{\partial F(L_1)}{\partial L} + \frac{1}{L'^2} \frac{\partial F(L_2)}{\partial L} \quad (2.25)$$

To compute it, Vasilyev et al. [11] developed a method to compute this derivative thanks to a dummy coupling parameter. Even though the system's size is discrete, it is possible to obtain a continuous-like size of the system thanks to the progressive decoupling the k -th

layer of the system. If H_0 is the Hamiltonian of size L and H_1 the Hamiltonian of size $L-1$ (see Fig 2.5), then they define the crossover Hamiltonian as

$$H_{cr}(\lambda) = (1 - \lambda)H_0 + \lambda H_1 \quad (2.26)$$

with $\lambda \in [0, 1]$, which interpolates from H_0 to H_1 when λ goes from 0 to 1. As λ goes on, the k -th layer of the system is gradually decoupled from it, meaning that the interaction energy of all vertical bonds between layer k and layers $k-1$ and $k+1$ are now equal to $(1-\lambda)\beta J$, while the layers $k+1$ and $k-1$ are gradually couple with an energy $\lambda\beta J$. The crossover Hamiltonian $H_{tr}(\lambda)$ also depends on the position of the decoupled layer $k \in 1, 2, \dots, L$. The free energy associated with this system is

$$F_{cr}(\lambda) = -k_B T \ln \left(\sum_{h_1 \dots h_L} \exp(-\beta H_{tr}(\lambda)) \right) \quad (2.27)$$

The derivative of the free energy with respect to λ is thus

$$\frac{\partial F_{cr}(\lambda)}{\partial \lambda} = \langle H_1 - H_0 \rangle_{H_{cr}(\lambda)} \quad (2.28)$$

where $\langle \cdot \rangle_{H_{cr}(\lambda)}$ represents the statistical mean value in the crossover system, easily computable in numerical simulations. By integrating over the coupling constant, the difference of free energy between the coupled and the fully decoupled systems is

$$F_1 - F_0 = \int_0^1 d\lambda \langle H_1 - H_0 \rangle_{H_{cr}(\lambda)} \quad (2.29)$$

Finally, in the thick limit where $L \gg 1$, the derivative is

$$-\frac{\partial F(t, h, L)}{\partial L} \simeq \int_0^1 d\lambda \langle H_1 - H_0 \rangle_{H_{cr}(\lambda)} \quad (2.30)$$

Even though $H_{cr}(\lambda)$ depends of which layer we decided to decouple, and by transition $H_1 - H_0$ and $\langle H_1 - H_0 \rangle_{H_{cr}(\lambda)}$, the integrand $\int_0^1 d\lambda \langle H_1 - H_0 \rangle_{H_{tr}(\lambda)}$ should be independent of this choice, as long as boundary conditions are not affected by the k -th layer.

For the SOS model, it is possible to exactly compute the energy variation produced by the decoupling, and is equal to

$$H_{cr, \text{SOS}}(\lambda) = H_{0, \text{SOS}} - \frac{\lambda J}{2} \sum_x [\text{sgn}(k-1-h(x)) \text{sgn}(k+1-h(x)) - \text{sgn}(k-h(x)) (\text{sgn}(k-1-h(x)) + \text{sgn}(k+1-h(x)))] \quad (2.31)$$

where the prefactor $\frac{1}{2}$ take into account the prefactor between Ising and SOS models in Hamiltonian (1.125). By doing the table of values, we notice that every term in the sum is equal to -1 independently of k , since contrary to Ising models, SOS models do not possess any bulk energy. We thus have to find another method to compute the thermodynamic force in the SOS model.

2.3.2 The Lopes-Jacquin-Holdsworth method

In the case of a chemical potential conjugated with the total height, Lopes et al. saw that [12]

$$\langle \sum_i h_i \rangle(\mu, L) = -\frac{\delta F(\mu, L)}{\delta \mu} \quad (2.32)$$

Integrating over the chemical potential, we have

$$\Delta F(\mu_1, \mu_2) = F(\mu_1, L) - F(\mu_2, L) = -\int_{\mu_1}^{\mu_2} d\mu' \langle \sum_i h_i \rangle_{\mu'} \quad (2.33)$$

If we know the analytical form of the free energy in the limits $\mu_2 \rightarrow \infty$ or $\mu_1 \rightarrow 0$, this method provides a way to directly measure the free energy of the system for any temperature or size by integrating over the chemical potential.

In the limit $\mu_2 \rightarrow \infty$, the correlation length at the reference state will be small so that the reference free energy will be essentially that of the bulk. As a consequence, it should contain all the information of the Casimir force (2.23). That derivative force can then be computed by

$$\delta L \frac{\partial F(\mu_1, L)}{\partial L} = \Delta F(\mu_1, \mu_2, L) - \Delta F(\mu_1, \mu_2, L - \delta L) \quad (2.34)$$

where δL is the difference thickness between two systems, and which is then independent of μ_2 in the large chemical potential limit as the free energy $F(\mu_2, L)$ converges to the bulk energy. Since in Kawasaki dynamics the total height is constant, this method does work only for model A.

The computation of the difference of free energy depends largely of the chemical potential μ_2 . However, since we are interested in the Casimir force (2.25), it is sufficient to chose a suitable chemical potential μ_2 for which the excess free energy can be safely considered negligible [12]. The dummy function

$$D(\mu, L_1, L_2) = \langle M(L_1) - M(L_1 - 1) - (M(L_2) - M(L_2 - 1)) \rangle \quad (2.35)$$

is thus defined to be the error function of the method, where $M = \sum_i h_i$ are taken at the same temperature and chemical potential, omitted in the notation for the sake of lightness. The contribution of high μ becomes negligible to the Casimir force when the function D becomes null.

The method only makes sense in the Glauber dynamics. In the Kawasaki dynamics, since $\sum_i h_i$ is set to a constant, the integration is done over a constant. We will show in Sec 3.3 a generalized method to bypass this problem.

2.4 Tips and tricks

The simulation's speed of SOS models is so great compared to Ising ones that it is possible to study systems over a wider range of parameters. A SOS simulation of 10^7 MC steps takes roughly 20 minutes to complete once fully optimized. Even though, if we want to launch hundreds of those simulations, it can easily take days, which forces us to optimize the code.

In C++, if compiling with g++, the first thing to do is to compile the programme with the `-O3` flag, which makes you gain an order of magnitude in CPU time.

The most important part of Monte Carlo simulations are the pseudo Random Number Generator (pRNG), which are called at least twice for each transition attempt. The C++ standard library proposes the function `default_random_engine` as the default pRNG. A lot of CPU time can be saved by switching to `sfc64` or `xoroshiro` pRNGs. Furthermore, the generation of ± 1 numbers only require one bit, while the pRNG always generates a 64-bits number, thus wasting 63-bits at each boolean generation. A wasteless method which speeds considerably the simulation's speed can be found in [79].

Lastly, the easiest way to gain real time is to make the code parallel. We can do that either by domain decomposition - which would allow us to simulate larger systems - or parallelise directly over the simulation's parameters (as the temperature or the chemical potential). While the first one is useless in SOS model because of the short correlation length of such systems, the latter can be done via two libraries : OpenMP and MPI. It took me some time to understand that the memory-shared OpenMP protocol has a lot of problems with pRNGs, making this library not suited for Monte Carlo simulations. On the contrary, the MPI library provides impermeability between threads, which makes it the better choice.

2.5 Conclusion

In this chapter, we have explained how to compute expectation values of observables in our system [10], thanks to the Monte Carlo Metropolis algorithm [75]. For that, we need to suppose that the system is in thermal equilibrium with a heat bath, and that it respects detailed balance. We have two different possible algorithms : the Glauber dynamics [77] allows to study the systems in the grand-canonical ensemble, while the Kawasaki dynamics [78] is for canonical ones. Nevertheless, since the transfer matrix method gives exact results for the grand-canonical ensemble, only the Kawasaki dynamics is relevant for SOS models.

In addition to that, measuring the free energy of the system is not an easy task, as we can only compute its derivative. The first method we have presented is about progressively decoupling a layer of the system [11], even though for SOS models, which do not possess a bulk energy, the method does not work. Another method is to integrate over the conjugate variable coupled to the total height [12], which is the chemical potential. This method does not work for Kawasaki algorithms. Since as we have discussed Glauber simulations are not relevant for our models, we find that we have no way to compute the free energy in Monte Carlo methods for the only relevant ensemble which is the canonical one. In a latter chapter, we will see how to fix this issue.

Chapter 3

Equilibrium Interface models and their finite size effects

Models for interfaces arise naturally in phase separated systems, as explained in Chapter 1. Finite size corrections manifest when the correlation length becomes of the order of magnitude of the system's size. When undergoing a continuous phase separation, the system exhibits finite size corrections in the form of a long range critical Casimir interaction, as described in the first section. In the second section we examine finite size effects in continuous interface models in one dimension, and show that while they have similar long-range interactions, the forces induced by interface confinement are quite different. In the low surface tension limit though, a correspondence between interface and critical physics is shown. In the last section, we compute the size-dependent eigenvalues of the transfer matrix for the free SOS model, and compare the results with previous works.

3.1 The Casimir effect

A review about the quantum and the critical Casimir effect is done in this section for completeness, starting from the effect was first observed [14] and describing the basis of the Lifshitz theory that generalises Casimir's contribution to general dielectric materials beyond the perfectly conducting plate paradigm, and ends with the critical Casimir effect.

3.1.1 Quantum Casimir effect

In an ideal conductor, the free charges can move arbitrarily quickly to cancel out any electric charge in the plane [80]. Thus, a perfectly conducting plate in the (x, y) plane imposes boundary conditions on the electromagnetic field

$$\mathbf{E} \times \mathbf{n} = \mathbf{0}; \quad \mathbf{B} \cdot \mathbf{n} = 0 \quad (3.1)$$

The quantum Hamiltonian for the electromagnetic field is given by

$$H = \sum_{\mathbf{k}, \lambda} \hbar \omega(\mathbf{k}, \lambda) \left[a^\dagger(\mathbf{k}, \lambda) a(\mathbf{k}, \lambda) + \frac{1}{2} \right] \quad (3.2)$$

Here λ denotes the polarisation (there are two polarisation states) and \mathbf{k} the wave vector. The dispersion relation for photons is

$$\omega(\mathbf{k}, \lambda) = |\mathbf{k}|c. \quad (3.3)$$

The ground state energy of the electromagnetic field [14] is given by

$$E_0 = \langle 0|H|0 \rangle = H = \sum_{\mathbf{k}, \lambda} \frac{1}{2} \hbar \omega(\mathbf{k}, \lambda) = \sum_{\mathbf{k}} \hbar |\mathbf{k}|c \quad (3.4)$$

The presence of conduction plates at $z = 0$ and $z = L$ means that the wave vectors k_z must be quantised according to $k_z = n\pi/L$ where $n \in \{0, 1, 2, \dots\}$ while if the (x, y) plane has a large area A one can write

$$\sum_{k_x, k_y} \cdot = \frac{A}{(2\pi)^2} \int d^2\mathbf{k}. \quad (3.5)$$

This then gives

$$E_0(L) = \frac{\hbar c A}{(2\pi)^2} \sum_{n=0}^{\infty} \int d^2\mathbf{k} \left(\mathbf{k}^2 + \frac{n^2 \pi^2}{L^2} \right)^{\frac{1}{2}} \quad (3.6)$$

$$= \frac{\hbar c A}{(2\pi)} \sum_{n=0}^{\infty} \int_0^{\infty} k dk \left(\mathbf{k}^2 + \frac{n^2 \pi^2}{L^2} \right)^{\frac{1}{2}} \quad (3.7)$$

The problem with the above expression is that it is clearly divergent. However it can be rendered finite by cutting off the high momentum degrees of freedom by writing

$$E_0(L) = \frac{\hbar c A}{(2\pi)} \sum_{n=0}^{\infty} \int_0^{\infty} k dk \left(\mathbf{k}^2 + \frac{n^2 \pi^2}{L^2} \right)^{\frac{1}{2}} f \left(\left(\mathbf{k}^2 + \frac{n^2 \pi^2}{L^2} \right)^{\frac{1}{2}} \right) \quad (3.8)$$

where f is a smooth function such that $f(p) = 1$ for $p \ll \Lambda$ and $f(p) = 0$ for $p \gg \Lambda$. Here, Λ is an ultraviolet cut-off and f thus only counts the contribution of photons with a momentum less than $\hbar\Lambda$. For this sort of calculation to make physical sense the physical result at the end should be independent of both the choice of f and Λ .

In the limit $L \rightarrow \infty$, the sum over discrete modes is replaced by an integral

$$E_0(L) = \frac{\hbar c A}{(2\pi)} \int_0^{\infty} \frac{L}{\pi} dv \int_0^{\infty} k dk (\mathbf{k}^2 + v^2)^{\frac{1}{2}} f \left((\mathbf{k}^2 + v^2)^{\frac{1}{2}} \right) \quad (3.9)$$

using the relation $dv = \pi/L$. For large L it becomes

$$E_0(L) = AL\epsilon_{bulk} \quad (3.10)$$

where ϵ_{bulk} is a bulk energy density per unit of volume, that is to say the total energy is extensive. The computation above only calculates the energy of the EM field between the plates. If the physical system extends up to $L' \gg L$, then the total energy of both the interior and the exterior of the plates is given by

$$E_{total}(L) = E_0(L) + A(L' - L)\epsilon_{bulk} \quad (3.11)$$

The part of the energy that depends on L is given by

$$U(L) = E_0(L) - AL\epsilon_{bulk} \quad (3.12)$$

It is the derivative of U which gives the physical interaction between the two plates : the pressure associated with this interaction in the colloid science literature is called the disjoining pressure [81], where to compute the effective interaction the bulk pressure has to be subtracted. We write now

$$AL\epsilon_{bulk} = \frac{\hbar cA}{(2\pi)} \int_0^\infty dn \int_0^\infty kdk \left(\mathbf{k}^2 + \frac{n^2\pi^2}{L^2} \right)^{\frac{1}{2}} f \left(\left(\mathbf{k}^2 + \frac{n^2\pi^2}{L^2} \right)^{\frac{1}{2}} \right) \quad (3.13)$$

where the L dependence is in the integral. This then gives

$$U(L) = \frac{\hbar cA}{(2\pi)} \left[\sum_{n=0}^\infty g(n) - \int_0^\infty dn g(n) \right] \quad (3.14)$$

where

$$g(n) = \int_0^\infty kdk \left(\mathbf{k}^2 + \frac{n^2\pi^2}{L^2} \right)^{\frac{1}{2}} f \left(\left(\mathbf{k}^2 + \frac{n^2\pi^2}{L^2} \right)^{\frac{1}{2}} \right) = \frac{1}{2} \int_{\frac{n^2\pi^2}{L^2}}^\infty du u^{\frac{1}{2}} f(u^{\frac{1}{2}}) \quad (3.15)$$

Using the Euler-Maclaurin formula

$$\sum_{n=0}^\infty g(n) - \int_0^\infty dn g(n) = -B_1 g(0) - \frac{1}{2} B_2 g'(0) - \frac{1}{24} B_4 g'''(0) - \dots \quad (3.16)$$

where B_n are the Bernoulli numbers¹, we find that

$$g'(n) = -\frac{\pi^3}{L^3} n^2 f\left(\frac{n\pi}{L}\right) \quad (3.17)$$

Noticing that in the region around $n = 0$, $f = 1$ is a constant, this function has the following properties

$$g'(0) = 0 \quad (3.18)$$

$$g''(0) = 0 \quad (3.19)$$

$$g'''(0) = -\frac{2\pi^3}{L^3} \quad (3.20)$$

Higher order derivatives are zero so the full result is given by the first three terms of the Euler-Maclaurin formula, so the energy becomes

$$U(L) = \frac{\hbar cA}{(2\pi)} \left[-g(0) - \frac{\pi^3}{360L^3} \right] \quad (3.21)$$

The first term independent of L can be interpreted as a surface energy. The effective L dependent interaction is given by

$$U_{int}(L) = -\frac{\hbar\pi^2 cA}{720L^3} \quad (3.22)$$

so the effective interaction is attractive. Interestingly, Casimir thought that his calculation could explain the stability of the electron [14, 82]. The model of the electron is one of a perfectly conducting shell carrying an electric charge e . If the radius of the shell is a then the electrostatic energy of due to the charge is given by

$$E_{Charge} = \frac{e^2}{8\pi a\epsilon_0} \quad (3.23)$$

¹The first Bernoulli numbers are explicitly given by $B_1 = 1$, $B_2 = \frac{1}{2}$, $B_4 = -\frac{1}{30}$

There is thus a repulsive force on the shell which should make it expand. Casimir thought that the Casimir force on a spherical geometry, if it is an attractive force as is the case for the parallel plate geometry, could stabilise the electron. Clearly by dimensional analysis

$$E_{Cas} = -\frac{Z\hbar c}{a} \quad (3.24)$$

the balance of the Casimir and electric forces would then require

$$Z = \frac{e^2}{8\pi\hbar c} \quad (3.25)$$

However, in the case of conducting spherical shell, the constant $Z \simeq -0.046175$ is negative [83, 84, 85], while the same calculation for a cylindrical geometry predicts an attractive force [84].

3.1.2 Lifshitz Theory

The Casimir calculation is based on the boundary conditions imposed on the EM field due to a conductor. However, this is an ideal mathematical limit, conductors being conductors because free charges can move to cancel out the electric field in the conducting surface. The Casimir force can also be seen as due to correlations induced in the charge fluctuations in each plate, allowing for an alternative method based on sources which recovers the Casimir force [86, 87]. In a sense therefore the effect can be interpreted without reference to the zero point energy of the vacuum and the Casimir calculation works due to the fact that the mathematical limit in going to a perfect conductor works. Using a stochastic formulation of electrodynamics by Rytov [88], the Casimir calculation was generalized by Lifshitz for interactions between arbitrary electrical bodies, characterized by their local electric and magnetic response [15]. Even though this theory is very general, the microscopic justification is not completely rigorous, source terms (random currents and dipole fluctuations) are introduced to Maxwell's equations to give a Langevin formulation of Maxwell's equations in the presence of dielectric bodies. The correlation functions of the white noise terms depend on the temperature of the system and are determined via the quantum fluctuation dissipation theorem. The Lifshitz theory is computationally difficult to work with and it was reformulated in a way more useful for practical calculations and that can be applied to experimental setups [89, 90]. Rytov's formulation has the advantage that it can be used to treat out of equilibrium situations where different bodies are held at different temperatures. This allows both the computation of out of equilibrium forces and radiative heat transfer.

The theory in the presence of electromagnetic media is written in terms of the electric and magnetic fields \mathbf{E} and \mathbf{B} and the displacement and magnetizing fields \mathbf{D} and \mathbf{H} which are assumed to obey local relations in real space and Fourier space

$$\tilde{\mathbf{D}}(\omega) = \epsilon(\omega)\tilde{\mathbf{E}}(\omega); \quad \tilde{\mathbf{B}}(\omega) = \mu(\omega)\tilde{\mathbf{H}}(\omega) \quad (3.26)$$

where $\tilde{\epsilon}(\omega)$ and $\tilde{\mu}(\omega)$ are the frequency dependent permittivity and permeability. The boundary conditions at the interface between two materials 1 and 2 are given by

$$B_{1n} = B_{2n} \quad D_{1n} = D_{2n} \quad (3.27)$$

$$E_{1t} = E_{2t} \quad H_{1t} = H_{2t} \quad (3.28)$$

where n denotes the normal component and t the tangential component to the interface.

Forces can be computed using the vacuum (assuming that the surface where the force is computed is next to the vacuum) Maxwell stress tensor.

$$T_{ij} = \epsilon \left(E_i E_j - \frac{1}{2} \delta_{ij} E^2 \right) + \frac{1}{\mu} \left(B_i B_j - \frac{1}{2} \delta_{ij} B^2 \right) \quad (3.29)$$

Notice that the stress tensor is quadratic in the fields \mathbf{E} and \mathbf{B} , this means that even if the fields are on average zero, both thermal and quantum fluctuations give rise to forces.

In media Maxwells equations are

$$\nabla \times \mathbf{E} = -\frac{\partial \mathbf{B}}{\partial t} \quad (3.30)$$

$$\nabla \times \mathbf{H} = \mathbf{J} - \frac{\partial \mathbf{D}}{\partial t} \quad (3.31)$$

$$\nabla \cdot \mathbf{D} = \rho \quad (3.32)$$

$$\nabla \cdot \mathbf{B} = 0 \quad (3.33)$$

In a dielectric medium or conductor where there are no applied external fields there is no free charge or current. As such, the average values of \mathbf{E} and \mathbf{B} are zero. Rytov's idea was to add a random current to induce both thermal and quantum fluctuations into the problem. Assuming that the only contribution to the current comes from a fluctuating polarization density \mathbf{P} , we can write

$$\frac{\partial \rho}{\partial t} + \nabla \cdot \mathbf{J} = 0 \implies \nabla \cdot \left[-\frac{\partial \mathbf{P}}{\partial t} + \mathbf{J} \right] = 0 \quad (3.34)$$

where we have used

$$\rho = -\nabla \cdot \mathbf{P} \quad (3.35)$$

This means that the current is given by

$$\mathbf{J} = \frac{\partial \mathbf{P}}{\partial t} \quad (3.36)$$

or in Fourier space

$$\tilde{\mathbf{J}}(\omega) = i\omega \tilde{\mathbf{P}}(\omega) \quad (3.37)$$

Now if we assume that the fluctuations in the polarization density are uncorrelated in space, the fluctuation dissipation theorem tells us that the correlation function of the polarization density in Fourier space is given by

$$\langle P_\alpha(\omega; \mathbf{x}) P_\beta^\dagger(\omega; \mathbf{x}') \rangle_{sym} = \frac{\hbar \epsilon''(\omega)}{2} \coth\left(\frac{\hbar\omega}{2k_B T}\right) \delta(\omega - \omega') \delta(\mathbf{x} - \mathbf{x}') \delta_{\alpha\beta} \quad (3.38)$$

$$\epsilon(\omega) = \epsilon'(\omega) + i\epsilon''(\omega) \quad (3.39)$$

The Lifshitz calculation for slab geometries gives a force per unit area between two slabs of media separated by a distance L

$$\begin{aligned} \frac{F}{A} &= -\frac{k_B T}{\pi c^3} \sum_{n=0}^{\infty} \omega_n^3 \int_1^{\infty} dp p^2 \left[1 - \frac{(s_1 + p)(s_2 + p)}{(s_1 - p)(s_2 - p)} \exp\left(-\frac{2p\omega_n L}{c}\right) \right] \\ &+ \left[1 - \frac{(s_1 + p\epsilon_1)(s_2 + p\epsilon_2)}{(s_1 - p\epsilon_1)(s_2 - p\epsilon_2)} \exp\left(-\frac{2p\omega_n L}{c}\right) \right] \end{aligned} \quad (3.40)$$

where $\epsilon = \epsilon_0 \epsilon$, $s_i = \sqrt{\epsilon_i - 1 + p^2}$, $\omega = \frac{2\pi n k_B T}{\hbar}$ are the Mastubara frequencies [8] and $\epsilon_i = \epsilon_i(i\omega_n)$. Note that the integral over real frequencies has become a sum over discrete Matsubara frequencies, they come from the poles in the hyperbolic cotangent.

One needs to know the dielectric response at imaginary frequency, this is done using the Kramers-Kronig relation

$$\epsilon(i\omega) = 1 + \frac{2}{\pi} \int_0^\infty d\zeta \frac{\zeta \epsilon''(\zeta)}{\omega^2 + \zeta^2} \quad (3.41)$$

3.1.3 Critical Casimir effect

In systems having a continuous phase transition the correlation length diverges as the critical point is approached. This means that the correlation length has a size comparable to that of the system size, which leads to strong finite-size effects in the free energy. Following the arguments of Fisher and de Gennes [3], we describe how a version of the Casimir effect manifests in critical systems.

3.1.3.1 Bulk scaling for near critical systems

The free energy for a system consisting of N spins has a singular part at a critical temperature T_c which can be written as

$$F(t, h) = N f(t, h) \quad (3.42)$$

where $t = (T - T_c)/T_c$ measures the distance from the critical point and h is the external applied magnetic field. Assuming that the only relevant parameters are T and h (equivalently the concentration or chemical potential of a binary mixture), which is true for $d < 4$ [7], carrying out a renormalisation group transformation blocking spins in blocks of linear size b into new effective spins, we have

$$N f(t, h) = N' f(t', h') \quad (3.43)$$

Clearly the number of spins in the blocked system is given by $b^d N' = N$ and the RG transformation for t and h are given by $t' = b^{y_1} t$ and $h' = b^{y_2} h$, where y_1 and y_2 are positive and are the RG exponents for the fields t and h (from which all critical exponents can be deduced). This means that

$$f(t, h) = \frac{1}{b^d} f(b^{y_1} t, b^{y_2} h) \quad (3.44)$$

We begin by working with $t > 0$ but the arguments here are trivially generalisable to the case $t < 0$. In Eq. (3.44), if b is chosen such that $b^{y_1} t = 1$, then, at the critical field $h = 0$, we find

$$f(t, 0) = t^{\frac{d}{y_1}} f(1, 0) \quad (3.45)$$

The singularity in the specific heat is defined via

$$c \sim \frac{\partial^2}{\partial t^2} f(t, 0) \quad (3.46)$$

and is equal to

$$c \sim t^{\frac{d}{y_1} - 2} \sim t^{-\alpha} \quad (3.47)$$

where α is the exponent associated with the divergence of the specific heat. This means that

$$\alpha = 2 - \frac{d}{y_1} \quad (3.48)$$

The RG transformation for the correlation function has the form

$$C(r, t, h) = \lambda^2(b)C(r/b, b^{y_1}t, b^{y_2}h) \quad (3.49)$$

Clearly length scales transform as $r' = r/b$. Again setting $h = 0$ and choosing $b^{y_1}t = 1$ gives

$$C(r, t, h) = \lambda^2(t^{-\frac{1}{y_1}})C(r/t^{-\frac{1}{y_1}}, 1, 0). \quad (3.50)$$

The correlation function, by definition is given by

$$C(r, t) \sim f(r/\xi), \quad (3.51)$$

where ξ is the correlation length. This immediately tells us that $\xi = t^{-\frac{1}{y_1}}$ and from the usual definition

$$\xi \sim t^{-\nu} \quad (3.52)$$

one have $\nu = 1/y_1$. These two formula for y_1 then give the hyper scaling relation

$$\alpha = 2 - d\nu \quad (3.53)$$

The exponents α and ν are the ones that are important in the critical Casimir effect.

3.1.3.2 Finite size scaling

Consider a system which is finite in one direction with either periodic boundaries or two surfaces. While the critical system has $h = 0$, there can be local surface fields at each surface a and b . This represents a preference of the surfaces for one phase or the other. The finite scaling hypothesis for a slab system of large area A but with finite width L can be stated as

$$f(t, h_a, h_b, L^{-1}) = \frac{1}{b^d} f(b^{y_1}t, b^{y_a}h_a, b^{y_b}h_b, bL^{-1}) \quad (3.54)$$

and see that the field L^{-1} is a relevant field with RG exponent $y_L = 1$. The surface fields are not necessarily relevant so y_a and y_b can be either positive or negative. The important point about finite size scaling is that when L is finite the singularity due to the thermodynamic phase transition is smoothed out by the system's finite size (note that we assume that the system has no two-dimensional phase transition in the region we are looking at). When L is large there should be a bulk contribution to the free energy plus a surface term (so we are considering the limit $L \rightarrow \infty$ before $\xi \rightarrow \infty$)

$$\begin{aligned} f(t, h_a, h_b, L^{-1}) &= f(t, h_a, h_b, 0) + L^{-1} \frac{\partial f(t, h_a, h_b, 0)}{\partial x_4} \\ &= \frac{1}{b^d} f(b^{y_1}t, b^{y_a}h_a, b^{y_b}h_b, 0) + \frac{1}{b^{d-1}} L^{-1} \frac{\partial f(b^{y_1}t, b^{y_a}h_a, b^{y_b}h_b, 0)}{\partial x_4} \end{aligned} \quad (3.55)$$

where we have carried out the Taylor expansion for L^{-1} small using both versions of Eq. (3.59) and $\frac{\partial}{\partial x_n}$ indicates the partial derivative with respect to the n^{th} argument. The second term gives a total contribution to the singular part of the free energy of the order $AL \times L^{-1}$ and is thus a surface tension γ and so we have

$$\gamma = \frac{1}{b^{d-1}} \frac{\partial f(b^{y_1} t, b^{y_a} h_a, b^{y_b} h_b, 0)}{\partial x_4} \quad (3.56)$$

Setting $bt^{y_1} = 1$ then gives close to the critical point

$$\gamma \sim t^{\frac{d-1}{y_1}} \frac{\partial f(1, \lim_{t \rightarrow 0} t^{-\frac{y_a}{y_1}} h_a, \lim_{t \rightarrow 0} t^{-\frac{y_b}{y_1}} h_b, 0)}{\partial x_4} = t^{(d-1)\nu} C' = \xi^{-(d-1)} C' \quad (3.57)$$

The formula relating the surface tension and the correlation length, in the above C' is a constant depending on the universality class.

Now keeping L finite and setting $b^{y_1} t = 1$ in Eq. (3.59) the function can be rewritten as

$$f(t, h_a, h_b, L^{-1}) = t^{\frac{d}{y_1}} f(1, t^{-\frac{y_a}{y_1}} h_a, t^{-\frac{y_b}{y_1}} h_b, t^{-\frac{1}{y_1}} L^{-1}) \quad (3.58)$$

$$f(t, h_a, h_b, L^{-1}) = \frac{1}{\xi^d} f(1, \xi^{y_a} h_a, \xi^{y_b} h_b, \xi/L) \quad (3.59)$$

$$f(t, h_a, h_b, L^{-1}) = \frac{1}{L^d} \theta\left(\frac{L}{\xi}, \xi^{y_a} h_a, \xi^{y_b} h_b\right) \quad (3.60)$$

Now crucially as $\xi \rightarrow \infty$ the function θ is analytic so taking the limit $\xi \rightarrow \infty$ gives

$$f(0, h_a, h_b, L^{-1}) = \frac{1}{L^d} \theta(0, \lim_{\xi \rightarrow \infty} \xi^{y_a} h_a, \lim_{\xi \rightarrow \infty} \xi^{y_b} h_b) \quad (3.61)$$

Clearly for each surface there are 3 possibilities: $\lim_{\xi \rightarrow \infty} \xi^{y_a} h_a = \pm\infty$, if the surface fields are relevant, as well as $\lim_{\xi \rightarrow \infty} \xi^{y_a} h_a = 0$ if the surface fields are irrelevant. There is clearly also a similar argument when the system has periodic boundary conditions and there are no surface fields. Near the critical point depending on the boundary conditions there should be scaling functions when the surface fields attract the same phase $\theta_{++}(x)$, where they attract different phases and $\theta_{+-}(x)$, and $\theta_{pbc}(x)$ when the boundary conditions are periodic. There should also be a zero surface field case θ_{00} when the surfaces fields are irrelevant or zero (this is however unlikely). Fisher and de Gennes argued, without proof, that the force for $(++)$ boundary conditions should be attractive where as the $(+-)$ case should produce repulsive forces [3, 91].

The total singular part of the free energy is thus given by

$$F = ALf(t, h_a, h_b, L^{-1}) = \frac{A}{L^{d-1}} \theta\left(\frac{L}{\xi}, \xi^{y_a} h_a, \xi^{y_b} h_b\right). \quad (3.62)$$

The scale of the energy is set by the energy of thermal fluctuations $k_B T$, so we find the critical Casimir energy

$$F(t=0) = \frac{k_B T A C}{L^{d-1}} \quad (3.63)$$

where C is a constant depending on the surface universality class.

3.2 Finite size scaling in one dimensional interface models

Confining statistical systems generates Casimir forces when the correlation length of the fluctuations becomes of the order of the minimum size of the system, be it for perfect conductor plates in vacuum or in confined critical systems. We have also seen that interfaces between two phases can be described by surface models, so it is physically obvious that finite size effects also arise in those systems. In what follows we will study the size dependence of a number of continuous and discrete interface models (corresponding to the interfaces of two dimensional systems). While long range forces are generated by confinement, we find that those models have quantitatively different behaviours to the critical Casimir effect. However if one assumes a phenomenological proposal by Privman [16] to introduce a finite size correction to the surface tension, the critical Casimir effect can be quantitatively recovered.

3.2.1 Continuous models in one dimension

In one dimension the partition function for a surface model of the type discussed in Sec 1.2 can be written as a path integral

$$Z(t) = \int d[h] \exp\left(-\frac{\beta\sigma}{2} \int_0^t h'^2(x) dx - \beta \int_0^t V(h(x)) dx\right) \quad (3.64)$$

where t is the length of the system and the notation is chosen so the variable x can be thought of as a time in path integral language. It is convenient to fix both the starting point $h(0) = x$ and the end point $h(t) = x$ and define what is known as the propagator [8]

$$K(h, h', t) = \int_{h(0)=h} d[h] \delta(h' - h(t)) \exp\left(-\frac{\beta}{2} \int_0^t \sigma h'^2(x) dx - \beta \int_0^t V(h(x)) dx\right) \quad (3.65)$$

The propagator is an example of a path integral and is the sum over all paths going between h and h' in what can be taken to be the time t . It can be shown [92] that the path integral obeys an imaginary time Schrödinger equation

$$\frac{\partial K(h, h', t)}{\partial t} = -\hat{H}K(h, h', t) \quad (3.66)$$

where \hat{H} is the Hamiltonian operator

$$\hat{H} = -\frac{1}{2\sigma\beta} \frac{\partial^2}{\partial h^2} + \beta V(h) \quad (3.67)$$

and, with a suitable normalisation, the initial condition

$$K(h, h', t) = \delta(h - h') \quad (3.68)$$

If the Hamiltonian operator \hat{H} has eigenfunctions ψ_n , normalised so that

$$\int dh \psi_n^2(h) = 1 \quad (3.69)$$

and with eigenvalues ϵ_n , it is easy to see that the propagator can be written as

$$K(h, h', t) = \sum_n \exp(-t\epsilon_n) \psi_n(h) \psi_n(h') \quad (3.70)$$

If the system has periodic boundary conditions but leave the initial value $h(0)$ of the height to be free, then using the normalisation of the eigenfunctions, we find

$$Z(t) = \int dh K(h, h, t) = \sum_n \exp(-t\epsilon_n) \quad (3.71)$$

Now in the thermodynamic limit $t \rightarrow \infty$ if there is a gap between the ground state energy ϵ_0 and the first excited state, $g = \epsilon_1 - \epsilon_0$ which is non-zero, applying ground state dominance gives

$$Z(t) = \exp(-t\epsilon_0) \quad (3.72)$$

which gives the free energy per unit length as

$$f = \frac{1}{\beta} \epsilon_0 \quad (3.73)$$

As well as the free energy we are interested in the probability distribution of the height at a single point (which is independent of the point chooses due to invariance by translation of the system). For instance the probability distribution of $h(0)$ is given by

$$\begin{aligned} p_1(h) &= \frac{\int d[h] \delta(h(0) - h) \exp\left(-\frac{\beta}{2} \int_0^t h'^2(x) dx - \beta \int_0^t V(h(x)) dx\right)}{Z(t)} \\ &= \frac{K(h, h, t)}{Z(t)} \\ &= \frac{\sum_n \exp(-t\epsilon_n) \psi_n^2(h)}{\sum_n \exp(-t\epsilon_n)} \end{aligned} \quad (3.74)$$

and so as $t \rightarrow \infty$, ground state dominance gives

$$p_1(h) = \psi_0^2(h) \quad (3.75)$$

where the normalisation of the probability density function for h follows from the normalisation of the wave functions.

The joint probability density function for two heights separated by a time or distance x is given by

$$\begin{aligned} p_2(h, h', x) &= \frac{\int d[h] \delta(h(0) - h) \delta(h(x) - h') \exp\left(-\frac{\beta}{2} \int_0^t h'^2(x) dx - \beta \int_0^t V(h(x)) dx\right)}{Z(t)} \\ &= \frac{K(h, h', x) K(h', h, t - x)}{Z(t)} \\ &= \frac{\sum_{nm} \exp(-x\epsilon_n) \psi_n(h) \psi_n(h') \exp(-[L - x]\epsilon_m) \psi_m(h') \psi_m(h)}{\sum_n \exp(-t\epsilon_n)} \end{aligned} \quad (3.76)$$

Due to ground state dominance only the term with $m = 0$ survives in the sum above (as x is taken such that $x \ll t$) so we find

$$p_2(h, h', x) = \sum_n \psi_0(h') \psi_0(h) \psi_n(h') \psi_n(h) \exp(-x[\epsilon_n - \epsilon_0]) \quad (3.77)$$

$$= p_1(h) p_1(h') + \sum_{n>0} \psi_0(h') \psi_0(h) \psi_n(h') \psi_n(h) \exp(-x[\epsilon_n - \epsilon_0]) \quad (3.78)$$

From this we see that when $x[\epsilon_n - \epsilon_0] \gg 1$ for all n , in particular when $x[\epsilon_1 - \epsilon_0] \gg 1$, we have

$$p_2(h, h', x) \sim p_1(h)p_2(h') \quad (3.79)$$

so that the height at large distances are uncorrelated or equivalently are independent random variables. This gives a correlation length

$$\xi = \frac{1}{\epsilon_1 - \epsilon_0} \quad (3.80)$$

3.2.2 The confined elastic line

We consider now the case where $V(h) = 0$ for $0 < h < L$ and $V(h) = \infty$ otherwise. This corresponds to a one dimensional elastic line confined between two impenetrable walls separated by a distance L , as shown in a schematics in Fig 3.1. The Hamiltonian \hat{H} is that for a quantum well of width L and with eigenfunctions [93]

$$\psi(h) = \sqrt{\frac{2}{L}} \sin\left(\frac{\pi(n+1)h}{L}\right) \quad (3.81)$$

where $n \geq 0$ are integers. The ground state energy of such a system is

$$\epsilon_0 = \frac{1}{2\sigma\beta} \frac{\pi^2}{L^2} \quad (3.82)$$

and so, in the thermodynamic limit, the free energy per unit length is

$$f = \frac{1}{2\sigma\beta^2} \frac{\pi^2}{L^2} = \frac{T^2\pi^2}{2\sigma L^2} \quad (3.83)$$

Here the pressure (in this case pressure is a force per unit length) is given by

$$P = -\frac{\partial f}{\partial L} = \frac{\pi^2 T^2}{\sigma L^3} \quad (3.84)$$

which is repulsive. Physically, the fluctuations of the surface repel the walls. The pressure has the Casimir like characteristic that it behaves as a long range power law type interaction, however a two dimensional critical Casimir system (see (3.63)) would have a free energy per unit length $f = CT/L$. We also see that the free energy scales as T^2 rather than T (as is the case for the Casimir interaction).

Since a critical system has zero surface tension, using a model with a finite surface tension for the critical interface is clearly not appropriate. However it has been conjectured by Privman [16] that the term σ , which Privman refers to the stiffness, should be modified by finite size effects (although he considers a case where the height L of the system and the length t are of the same order). The simplest conjecture proposed by Privman[16] is that

$$\sigma(L) \approx \sigma_b + \frac{Ta}{L} \quad (3.85)$$

with a being dimensionless. This amounts to assuming that the corrections are analytic in the variable $1/L$. It seems difficult to justify this from a more microscopic view, however if we use this we find that

$$f = \frac{1}{2\sigma(L)\beta^2} \frac{\pi^2}{L^2} = \frac{T^2\pi^2}{2[\sigma_b + \frac{Ta}{L}]L^2} \quad (3.86)$$

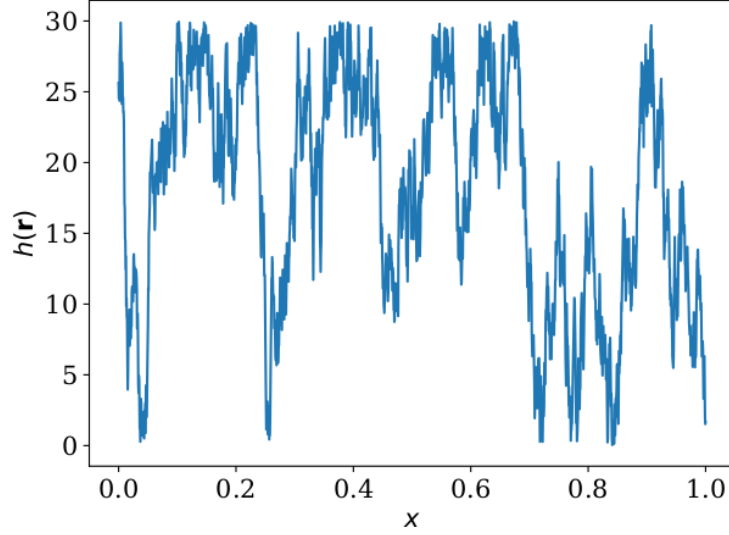


Figure 3.1: Schematics of an interface confined between 0 and $L = 30$ (this is not a numerical simulation).

At the critical point where $\sigma_b = 0$, we find

$$f_c = \frac{T\pi^2}{2aL} \quad (3.87)$$

and this does have exactly the form predicted for a critical system in Eq. (3.63). As such, Casimir-type interactions have an interesting manifestation in interface physics, and deeper development could lead to new interesting physics.

Going back to interface models, using Eq. (3.80) the correlation length is given by

$$\xi = \frac{2\sigma L^2}{3T\pi^2} \quad (3.88)$$

thus it increases as the surface tension is increased or the temperature is lowered. This makes physical sense as the surface should become *flatter* under these conditions. Also, as the system becomes more confined, the correlation length increases, again as confinement kills fluctuations. The correlation length tells us that if we wanted to simulate this system then we need to take

$$t \gg \xi \quad (3.89)$$

in order to be in the thermodynamics limit and so $t \gg \frac{\sigma L^2}{T\pi^2}$. Thus, for L large, in general we would need to simulate rather large systems. The probability distribution function of the height at a single point is given by

$$p_1(h) = \frac{2}{L} \sin^2\left(\frac{\pi h}{L}\right) \quad (3.90)$$

and from this

$$\langle h \rangle = \frac{L}{2} \quad (3.91)$$

which is rather obvious. The width of the interface is given by

$$w = \sqrt{\langle h^2 \rangle - \langle h \rangle^2} \quad (3.92)$$

and here it is given by

$$w = L\sqrt{\frac{1}{12} - \frac{1}{2\pi^2}} = 0.180756 L \quad (3.93)$$

During this thesis we have considered models of surfaces where the overall surface integral is fixed. In magnetic systems this corresponds to systems with conserved magnetisation. It is surprisingly difficult to deal with this constraint in a hard way both for continuous surfaces, treated via the Schrödinger equation, and for discrete systems with the transfer matrix. In principle one can always introduce a magnetic field to fix the average total magnetisation to zero. However, there will always be fluctuations around the average value. If there are N sites, the fluctuations of the magnetisation by site scale as $1/\sqrt{N}$. However, the total magnetisation has fluctuations of the order of \sqrt{N} and so the condition of fixed total magnetisation is only imposed approximately by an applied magnetic field.

In the confined Edwards Wilkinson model we consider the magnetisation M defined by

$$M = \int_0^t dx h(x) \quad (3.94)$$

We know, from symmetry arguments, that without an external applied field we have

$$\langle M \rangle = \frac{tL}{2} \quad (3.95)$$

which can be shown explicitly from the formula

$$\langle M \rangle = t \int_0^L dh h \psi_0^2(h) \quad (3.96)$$

Interestingly, if we write things in terms of the traditional bra and ket notation of quantum mechanics, we see that

$$\langle M \rangle = t \langle 0 | h | 0 \rangle \quad (3.97)$$

and so

$$\langle 0 | h | 0 \rangle = \Delta \epsilon_{0,1}(h) \quad (3.98)$$

where $\Delta \epsilon_{0,1}(h)$ is the shift in the ground state energy to first order in perturbation theory induced by a perturbation of the potential $\Delta V(h) = h$. However this is just the thermodynamic expression

$$\langle M \rangle = -t \frac{\partial}{\partial \lambda} f(\lambda) |_{\lambda=0} \quad (3.99)$$

for a potential $U(h) = V(h) + \lambda h$. The variance of M can be computed by using Eq. (3.78), which gives

$$\begin{aligned} \langle M^2 \rangle_c &= \int_0^t dx dx' [h(x)h(x') - \langle h^2 \rangle] \\ &= \sum_{n>0}^{\infty} \left(\int_0^L dh h \psi_0(h) \psi_n(h) \right)^2 \int_0^t dx dx' \exp(-[\epsilon_n - \epsilon_0]|x - x'|) \end{aligned} \quad (3.100)$$

and for large t carrying out the integration over x and x' gives

$$\langle M^2 \rangle_c = 2t \sum_{n>0} \frac{1}{\epsilon_n - \epsilon_0} \left(\int_0^L dh h \psi_0(h) \psi_n(h) \right)^2 \quad (3.101)$$

From second order perturbation theory we see that this is just equivalent to the thermodynamic identity

$$\langle M^2 \rangle_c = -T t \frac{\partial^2}{\partial \lambda^2} f(\lambda) |_{\lambda=0} \quad (3.102)$$

Using the explicit form of the eigenfunctions we find

$$\langle M^2 \rangle_c = \frac{16L^4 t \sigma \beta}{\pi^2} \sum_{n=1}^{\infty} \frac{1}{(n+1)^2 - 1} \left[\int_0^1 du u \sin(\pi u) \sin(\pi(n+1)u) \right]^2 \quad (3.103)$$

It can then be shown that

$$\int_0^1 du u \sin(\pi u) \sin(\pi(n+1)u) = -\frac{2(n+1)(1 + \cos((n+1)\pi))}{\pi^2[(n+1)^2 - 1]^2} \quad (3.104)$$

From this we see that only the modes where n is odd contribute to the fluctuations of the magnetisation. Consequently we find

$$\langle M^2 \rangle_c = \frac{256L^4 t \sigma \beta}{\pi^6} \sum_{n, \text{ odd}, =1}^{\infty} \frac{(n+1)^2}{[(n+1)^2 - 1]^5} \quad (3.105)$$

$$= \frac{1024L^4 t \sigma \beta}{\pi^6} \sum_{k=0}^{\infty} \frac{(k+1)^2}{[(2k+2)^2 - 1]^5} \quad (3.106)$$

$$= \frac{L^4 t \sigma \beta (15 - \pi^2)}{\pi^4} \quad (3.107)$$

This formula deserves some comment. A first trivial comment is that $\langle M^2 \rangle_c \sim t$ in accordance with the thermodynamic arguments given above. Secondly the variance diverges as $\sigma \beta \rightarrow \infty$, which is normal as the low energy configuration zero mode - a straight line - is unaffected by the confining walls and so in principal this line can lie anywhere on $[0, L]$, explaining the scaling with L^4 .

3.2.3 The Airy line

This is an example of the constant volume ensemble. Physically we could also consider the case of a system which is confined softly by an externally imposed pressure P_0 (which can also be treated as a chemical potential depending on the context) in the constant pressure ensemble. In this case the potential is given by

$$V(h) = \begin{cases} P_0 h & \text{for } h > 0 \\ \infty & \text{for } h \leq 0 \end{cases}$$

The time independent Schrödinger equation for the eigenfunctions here is

$$-\frac{1}{2\sigma\beta} \frac{d^2 \psi_n(h)}{dh^2} + P_0 \beta h \psi_n(h) = \epsilon_n \psi_n(h) \quad (3.108)$$

The corresponding eigenfunctions have boundary conditions $\psi_n(0) = 0$ due to the hard wall potential at $h = 0$ and they must also decay to zero as $h \rightarrow \infty$ so as to be normalisable.

The key to find the eigenfunctions is to transform the Schrödinger into the Airy equation which is

$$\frac{d^2 y(x)}{dx^2} - xy(x) = 0. \quad (3.109)$$

This equation has solutions $\text{Ai}(x)$ which decay as

$$\text{Ai}(x) \sim \frac{\exp(-\frac{2}{3}x^{\frac{3}{2}})\Gamma(\frac{5}{6})\Gamma(\frac{1}{6})}{4\pi^{\frac{3}{2}}x^{\frac{1}{4}}}, \quad (3.110)$$

as $x \rightarrow \infty$ and so are normalizable as eigenfunctions. For $x < 0$ the Airy function oscillates and has an infinite number of negative zeros $-\alpha_n$ such that $\text{Ai}(-\alpha_n) = 0$.

We make the change of variable $h = \ell z'$ to find

$$\frac{1}{2\sigma\beta\ell^2} \frac{d^2 \psi_n(z')}{dz'^2} - P_0\beta\ell(z' - \varepsilon_n)\psi_n(z') = 0, \quad (3.111)$$

where $\varepsilon_n = \varepsilon_n/(P_0\beta\ell)$. Now we choose ℓ so that

$$2\sigma\beta^2 P_0 \ell^3 = 1, \quad (3.112)$$

and we see that

$$\ell = \left(\frac{1}{2\beta^2 \sigma P_0} \right)^{\frac{1}{3}}, \quad (3.113)$$

is an intrinsic length scale.

$$\frac{d^2 \psi_n(z')}{dz'^2} - (z' - \varepsilon_n)\psi_n(z') = 0. \quad (3.114)$$

Finally if we use $z = z' - \varepsilon_n$ we obtain Airy's equation [94]

$$\frac{d^2 \psi_n(z)}{dz^2} - z\psi_n(z) = 0 \quad (3.115)$$

and so

$$\psi_n(z) = c_n \text{Ai}(z), \quad (3.116)$$

where c_n is a normalisation constant. This means that in terms of the original height variable h ,

$$\psi_n(h) = c_n \text{Ai}\left(\frac{h}{\ell} - \varepsilon_n\right) \quad (3.117)$$

The boundary condition $\psi_n(h)$ implies that $\varepsilon_n = \alpha_{n+1}$. This means that the ground state energy is

$$\varepsilon_0 = \alpha_1 P_0 \beta \ell = \frac{\alpha_1 P_0 \beta}{(2\sigma\beta^2 P_0)^{\frac{1}{3}}} = \frac{\alpha_1 P_0^{\frac{2}{3}} \beta^{\frac{1}{3}}}{2^{\frac{1}{3}} \sigma^{\frac{1}{3}}}, \quad (3.118)$$

and where we note that $\alpha_1 = 2.33811$.

$$f = \frac{\alpha_1 P_0^{\frac{2}{3}}}{2^{\frac{1}{3}} \sigma^{\frac{1}{3}} \beta^{\frac{2}{3}}}. \quad (3.119)$$

From the original partition function we see that h is conjugate to P_0 and so we find the average height is given by

$$\bar{h} = \langle h \rangle = \frac{\partial f}{\partial P_0} = \frac{2}{3} \frac{\alpha_1}{2^{\frac{1}{3}} \sigma^{\frac{1}{3}} \beta^{\frac{2}{3}} P_0^{\frac{1}{3}}} = \frac{2}{3} \alpha_1 \ell \quad (3.120)$$

and solving for P_0 in terms of \bar{h} gives

$$P_0 = \frac{4}{27} \frac{\alpha_1^3 T^2}{\sigma \bar{h}^3}, \quad (3.121)$$

We see that P_0 behaves exactly in the same way as the pressure of a confined elastic line in term of the temperature and surface tension. Only the overall numerical prefactor is different.

The correlation length is given by

$$\xi = \frac{2^{\frac{1}{3}} (\sigma T)^{\frac{1}{3}}}{(\alpha_2 - \alpha_1) P_0^{\frac{2}{3}}}. \quad (3.122)$$

When written in terms of \bar{h} the above correlation length behaves in the same way as for the free elastic line, however when P_0 is fixed we see that the behavior as a function of T and σ is quite different. The correlation length still increases with σ but now decreases as the temperature drops.

The probability density function for the height of the interface at a single point is given by

$$p_1(h) = \frac{\text{Ai}^2(\frac{h}{\ell} - \alpha_1)}{\int_0^\infty dh' \text{Ai}^2(\frac{h'}{\ell} - \alpha_1)} \quad (3.123)$$

Writing the height variable in terms of the length scale ℓ , $h(x) = \ell z(x)$, we find that z has the single point probability density function

$$p(z) = \frac{\text{Ai}^2(z - \alpha_1)}{\int_0^\infty dz' \text{Ai}^2(z' - \alpha_1)} = \frac{\text{Ai}^2(z - \alpha_1)}{\text{Ai}'^2(-\alpha_1)} \quad (3.124)$$

Using this we find that the average height is given by

$$\langle h \rangle = \bar{h} = \ell z_0, \quad (3.125)$$

where

$$z_0 = \frac{\int_0^\infty dz z \text{Ai}^2(z - \alpha_1)}{\int_0^\infty dz \text{Ai}^2(z - \alpha_1)}. \quad (3.126)$$

Interestingly comparison with the thermodynamic calculation giving Eq. (3.120) shows that the identity

$$z_0 = \frac{2}{3} \alpha_1, \quad (3.127)$$

must hold - this surprising identity can be verified numerically. Here we find that the average height given by

$$\langle h \rangle = 0.697089 \ell. \quad (3.128)$$

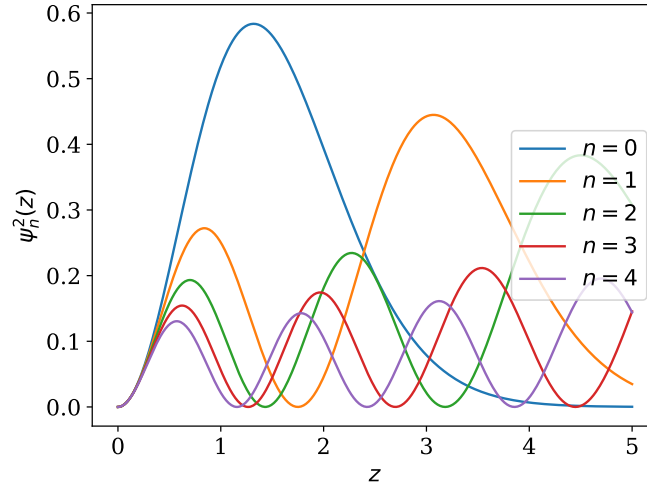


Figure 3.2: The scaled probability density function $p(z)$ for the distribution of the height at a single point for the Airy line given in Eq. (3.124)

The variance of the magnetisation is then given by

$$\langle M^2 \rangle_c = -\text{TL} \frac{\partial^2}{\partial \lambda^2} f(\lambda) |_{\lambda=0} = -\text{TL} \frac{\partial^2}{\partial P^2} f(P) |_{P=P_0} \quad (3.129)$$

$$= L \frac{\alpha_1}{2^{\frac{1}{3}} \sigma^{\frac{1}{3}} \beta^{\frac{5}{3}}} \frac{2}{9} P_0^{-\frac{4}{3}}. \quad (3.130)$$

In terms of the average height this then gives

$$\langle M^2 \rangle_c = \frac{9}{4\alpha_1^3} L \sigma \beta \bar{h}^{-4} \quad (3.131)$$

3.3 The generalized Lopes-Jacquin-Holdsworth Method

In Sec 2.3.2, we have shown a way to numerically compute the free energy of a system at a chemical potential μ in absence of another potential. Here we generalise the method for any kind of external potential. We will explain the method for the Ising model, but the derivation for the SOS model is straightforward.

For any external field which can be written as $BV(\sigma)$, where $V(\sigma)$ is a function of the internal microscopic variables σ_i , the Hamiltonian of the Ising model is

$$H = -J \sum \sigma_i \sigma_j - B \sum_i V(\sigma_i) \quad (3.132)$$

The mean value of the external potential is

$$\begin{aligned} \langle \sum_i V(\sigma_i) \rangle &= \sum_{\mathbf{h}} \sum_i V(\sigma_i) \exp(-\beta H) \\ &= - \frac{\partial F(\mu)}{\partial B} \end{aligned} \quad (3.133)$$

where F is the free energy of the system. For any potential of the form (3.135), we can integrate the previous equation to find

$$F(B_1) - F(B_2) = - \int_{B_1}^{B_2} dB' \langle \sum_i V(\sigma_i) \rangle_{B'} \quad (3.134)$$

If we know the analytical form of the free energy in the limits $B_2 \rightarrow \infty$ or $B_1 \rightarrow 0$, this method provides a way to directly measure it for any temperature or size by integrating over the chemical potential. From the total free energy, we recover the Casimir form through Eq. (2.34). The limit $B_1 \rightarrow 0$ is the free system limit, in which its free energy can not be computed analytically. However, when $B_2 \rightarrow \infty$, for the majority of external fields $BV(\sigma)$ in which we may be interested, there is often a configuration limit whose free energy can be computed analytically. For example, if $V(\sigma) = \sigma$, the configuration limit is the one where all spins point towards the same direction, leading to a free energy of 0. Thus, we have

$$F(B_1) - F_{analytic}(\infty) = - \int_{B_1}^{\infty} dB' \langle \sum_i V(\sigma_i) \rangle_{B'} \quad (3.135)$$

In numerical simulations, it is not possible to range over infinity, and a criterion has to be defined to know the error made between the analytic case $\mu_2 = \infty$ and the maximal μ_2 achieved in simulations. As in Eq (2.35), we define the function

$$D(B, L_1, L_2) = \langle M^*(L_1) - M^*(L_1 - 1) - (M^*(L_2) - M^*(L_2 - 1)) \rangle \quad (3.136)$$

with the generalized magnetization $M^* = \sum_i V(\sigma_i)$. A suitable upper limit of integration if we want to get the Casimir force is when the function D reaches 0 within the precision of the simulation.

For the SOS Hamiltonian

$$H = J \sum_i |h_i - h_{i+1}| + B \sum_i V(h_i) \quad (3.137)$$

we define the generalised mean height as

$$h^* = \langle \sum_i V(h_i) \rangle \quad (3.138)$$

Equation (3.135) writes as

$$F(B_1) - F(B_2) = - \int_{B_1}^{B_2} d\mu' h^*(B') \quad (3.139)$$

which can directly be verified with the transfer matrix for SOS systems. In the limit $B \rightarrow \infty$, the generalised height is zero, while the free energy $F(\infty)$ can often be computed analytically. To minimize the error between the analytical limit and the numerical simulations, a suitable choice of the upper integration's limit B_2 is given by

$$\int_{B_2}^{\infty} dB' h^*(B') \ll \int_{B_1}^{B_2} dB' h^*(B') \quad (3.140)$$

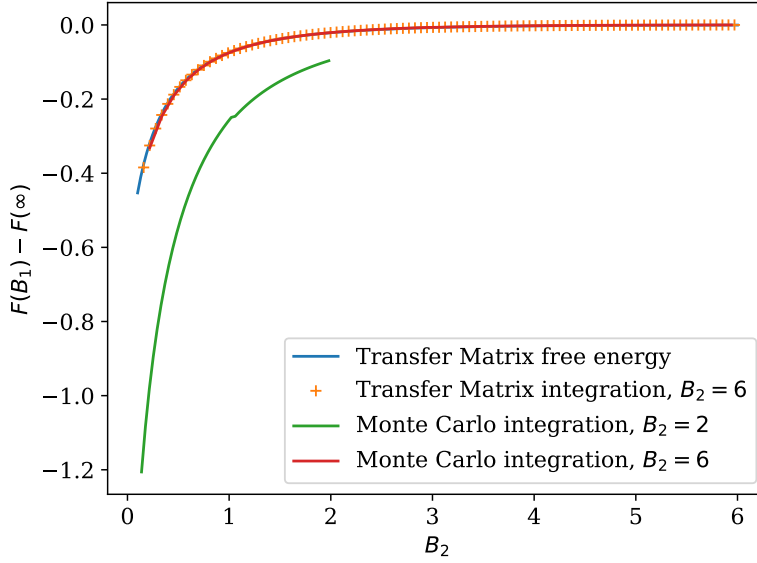


Figure 3.3: Difference in free energy directly computed from transfer matrix, compared to numerical integration over the generalized height, for different upper limit B_2 . The parameters are $L' = 256$, $L = 200$ and $\beta = 1$ for $5e7$ Monte Carlo steps.

An heuristic argument to find a suitable upper limit for integration is when $h^*(B_2) \ll h^*(B_1)$. In Fig 3.3, we see the free energy computed from the matrix transfer, compared to the integration procedure (3.135) for the SOS model for the chemical potential $V(h_i) = h_i$ in Monte Carlo simulations, where we see the agreement for B_2 large enough.

Since the order parameter is conserved in model B, the generalized Lopes-Jacquin-Holdswroth method can be used to compute the free energy for Kawasaki dynamics for potentials different from the chemical potential. As a proof of concept, we take a potential of the form

$$V(h_i) = -|h_i - \frac{L}{2}| \quad (3.141)$$

Such potential will press the interface along $h = 0$ and $h = L$ compared to the classical chemical potential which presses the interface at $h = 0$, as seen in Fig 3.4. Far away from $\frac{L}{2}$, both potentials are equivalent in symmetric fashion, and shall behave similarly for large B , because the free energy only depends on the interface fluctuations and not about the mean height.

In the $B \rightarrow \infty$ limit, the system has two equilibrium positions $h = 0$ et $h = L$, which gives the transfer matrix

$$T = e^{\beta B \frac{1}{2}} \begin{pmatrix} 1 & e^{-\beta JL} \\ e^{-\beta JL} & 1 \end{pmatrix} \quad (3.142)$$

The eigenvalues are $\lambda_{\pm} = e^{\beta B \frac{1}{2}} (1 \pm e^{-\beta JL})$, so the free energy is

$$F(B \rightarrow \infty) = -B \frac{L}{2} \quad (3.143)$$

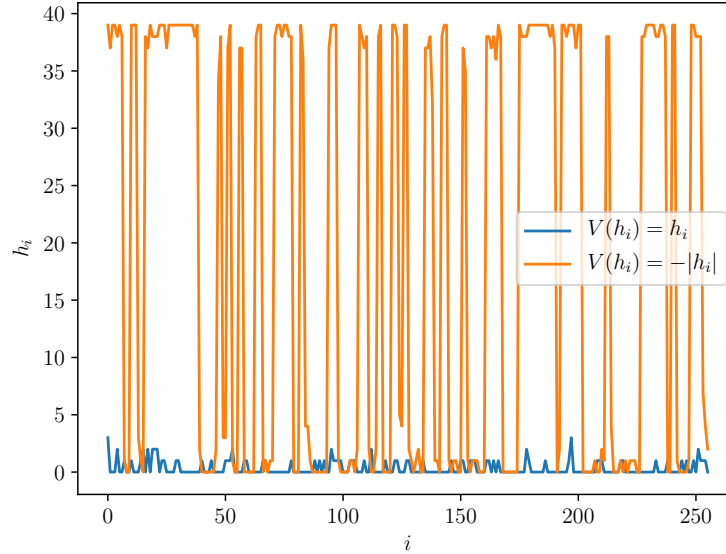


Figure 3.4: Snapshots of systems for the potential (3.141) and the chemical potential for $\beta = 1$ and $B = 2$ with $L = 40$ and $L' = 256$

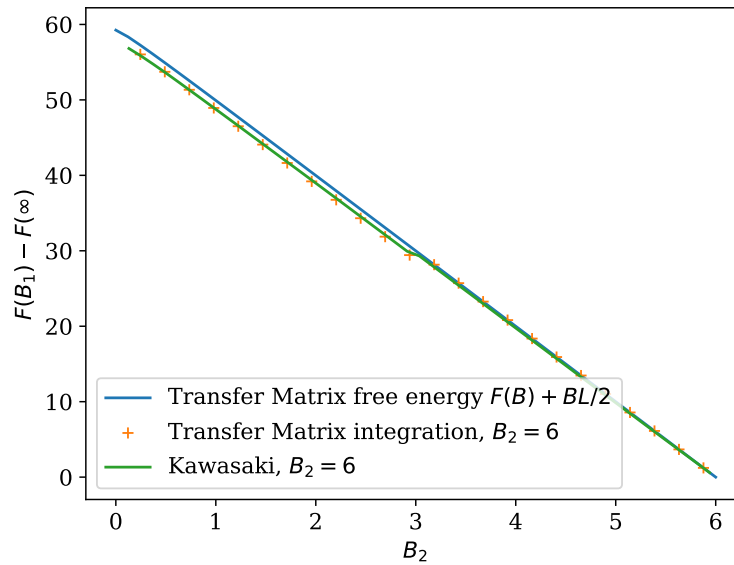


Figure 3.5: Difference in free energy directly computed from transfer matrix with the potential (3.141), compared to numerical integration over the generalized height. The parameters are $L' = 256$, $L = 20$ and $\beta = 1$, $B_2 = 1$ for 10^7 Monte Carlo steps.

In Fig 3.5 we show the difference of free energy computed from the transfer matrix between B_1 finite and $B_2 = 1$, and the integration procedure (3.139) with the generalized height with the matrix transfer and Monte Carlo simulations, both for Glauber and Kawasaki dynamics. The disagreement between the expected value and the simulation results from B_2 are too small, which we also see in the integration of the generalized height from the transfer matrix. We can convince ourselves by doing the integration from the transfer matrix for a larger B_2 . Also, it is worth noting that for this system, there is no significant difference in results for the two different dynamics.

This method opens a new way to compute the free energy for any kind of external potential of the form $BV(h)$, or $BV(\sigma)$ in the case of the Ising or SOS models for conserved and non-conserved dynamics, such as non-uniform external fields [95]. Applied to Ising models, this method allows to check the differences between Glauber and Kawasaki critical Casimir forces, to see if there are any far away from the thermodynamic limit.

3.4 The confined Solid-On-Solid model

From exact diagonalization of the SOS transfer matrix in the infinite case [96], finite-size effects were studied both for the SOS and RSOS model [97, 98]. Nevertheless the derivation of eigenvectors and eigenvalues were not explicit in the latter case. Those eigenvalues are a multiple of an integer, and the study of the eigenvalues issued from an odd integer were not discussed. In addition to redoing properly this computation, we add an analysis to the correlation length and the limits of high and low temperatures for the free energy.

We consider the free interface confined between 0 and L , with no external field. The SOS transfer matrix is thus given by

$$T(h_i, h_j) = \exp(-\beta J |h_i - h_j|) \quad (3.144)$$

Since positions are comprised from 0 to L , the transfer matrix is

$$T_{ij} = \exp(-\beta J |i - j|) = r^{|i-j|} \quad (3.145)$$

where

$$r = \exp(-\beta J) \quad (3.146)$$

To find the eigenvectors of T , we consider the vector denoted by $[a]$ which has components

$$[a]_i = a^i \quad (3.147)$$

where i is an index ranging from 0 to L . The action of the SOS transfer matrix on this vector is given by

$$[T [a]]_i = \sum_{j=0}^L r^{|i-j|} a^j \quad (3.148)$$

so

$$\begin{aligned}
 [T [a]]_i &= r^i \sum_{j=0}^i r^{-j} a^j + r^{-i} \sum_{j=i+1}^L r^j a^j \\
 &= r^i \sum_{j=0}^i r^{-j} a^j + r^{-i} \sum_{k=0}^{L-i-1} r^{i+1+k} a^{i+1+k} \\
 &= r^i \frac{1 - r^{-(i+1)} a^{i+1}}{1 - r^{-1} a} + r a^{i+1} \frac{1 - r^{L-i} a^{L-i}}{1 - r a} \\
 &= \left[\frac{r a}{1 - r a} - \frac{\frac{a}{r}}{1 - \frac{a}{r}} \right] a^i + \frac{r^i}{1 - \frac{a}{r}} - \frac{r^{L+1-i} a^{L+1}}{1 - r a}
 \end{aligned} \tag{3.149}$$

We now define

$$\lambda(a) = \frac{r a}{1 - r a} - \frac{\frac{a}{r}}{1 - \frac{a}{r}} = \frac{\frac{1}{r} - r}{\frac{1}{r} + r - a - \frac{1}{a}} \tag{3.150}$$

and notice that

$$\lambda(a) = \lambda(a^{-1}) \tag{3.151}$$

We can thus write

$$[T [a]]_i = \lambda(a) a^i + \frac{r^i}{1 - \frac{a}{r}} - \frac{r^{L+1-i} a^{L+1}}{1 - r a} \tag{3.152}$$

Now, considering the action of the transfer matrix on the vector $[a^{-1}]$, we get

$$[T [a^{-1}]]_i = \lambda(a) a^{-i} + \frac{r^i}{1 - \frac{1}{r a}} - \frac{r^{L+1-i} a^{-(L+1)}}{1 - \frac{r}{a}} \tag{3.153}$$

Looking for an eigenvector of the form

$$\mathbf{v} = [a] + c[a^{-1}] \tag{3.154}$$

the action of T on \mathbf{v} is

$$[T ([a] + c[a^{-1}])]_i = \lambda(a) [a^i + c a^{-i}] + r^i \left(\frac{1}{1 - \frac{a}{r}} + \frac{c}{1 - \frac{1}{r a}} \right) - r^{L+1-i} \left(\frac{a^{L+1}}{1 - r a} + c \frac{a^{-(L+1)}}{1 - \frac{r}{a}} \right) \tag{3.155}$$

so \mathbf{v} is an eigenvector, with eigenvalue $\lambda(a)$, if

$$\frac{1}{1 - \frac{a}{r}} + \frac{c}{1 - \frac{1}{r a}} = 0 \tag{3.156}$$

$$\frac{a^{L+1}}{1 - r a} + c \frac{a^{-(L+1)}}{1 - \frac{r}{a}} = 0 \tag{3.157}$$

The above equations implies that

$$c = -\frac{r a - 1}{a(r - a)} \tag{3.158}$$

and

$$c^2 = a^{2L} \tag{3.159}$$

Therefore we find

$$v_i = a^i \pm a^{L-i} \tag{3.160}$$

Ground state eigenvector

We expect the ground state eigenvector (corresponding to the largest eigenvalue) to be symmetric with respect to the middle of the system and so

$$v_i = v_{L-i} \quad (3.161)$$

which implies that we should have $c = a^L$.

This then gives the equation determining the values of a the largest eigenvalue, and in general for the eigenvalues which are symmetric ($c = 1$),

$$a^{L+1} = \frac{1 - ra}{r - a}. \quad (3.162)$$

As a check on the above derivation we consider the case $L = 1$ where there are only two sites. In this case, the transfer matrix is given explicitly by

$$T = \begin{pmatrix} 1 & r \\ r & 1 \end{pmatrix} \quad (3.163)$$

and the largest eigenvector is easily seen to be given by

$$\lambda_0 = 1 + r \quad (3.164)$$

In this case, we see that Eq. (3.162) gives

$$a^2 = \frac{1 - ra}{r - a} \quad (3.165)$$

which has three solutions

$$a_1 = -1 \quad (3.166)$$

$$a_2 = \frac{1}{2} \left(-\sqrt{r^2 + 2r - 3} + r + 1 \right) \quad (3.167)$$

$$a_3 = \frac{1}{2} \left(\sqrt{r^2 + 2r - 3} + r + 1 \right) \quad (3.168)$$

We see that $a_2 = 1/a_3$, and $|a_2| = |a_3| = 1$, and that

$$\lambda(-1) = \frac{1 - r}{1 + r} \quad (3.169)$$

while

$$\lambda(a_2) = \lambda(a_3) = 1 + r \quad (3.170)$$

corresponds to the maximal eigenvalue. Note that $\lambda(-1)$ is not the other eigenvalue of the transfer matrix, this has to be found by considering solutions with $c = -1$, as we will see later.

The equation (3.162) determining a can also be written as

$$a^L = -\frac{r - \frac{1}{a}}{r - a} \quad (3.171)$$

From this we see that if a is a solution then $1/a$ and $a = -1$ are always a solution.

We now introduce θ and

$$a = \exp(i\theta) \quad (3.172)$$

Then the parameter of the eigenvector is

$$\exp(iL\theta) = -\frac{r - \exp(-i\theta)}{r - \exp(i\theta)} \quad (3.173)$$

From Eq. (3.150), we have

$$\lambda(\theta) = \frac{\sinh(\beta J)}{\cosh(\beta J) - \cos(\theta)}. \quad (3.174)$$

Notice that in order to construct a real eigenvector corresponding to λ_0 we can use the fact that $v_i(a) = a^i + a^{L-i}$ and $v_i(a^{-1}) = a^{-i} + a^{-L+i}$ are both eigenvectors with the same eigenvalue. This means that $u_i(a) = v_i(a) + v_i(-a)$ is also an eigenvector and all its components are real.

Clearly the largest eigenvalue corresponds to the value of θ closest to 0, so we look for an eigenvalue such that $L\theta \sim 1$. Writing

$$\phi = L\theta \quad (3.175)$$

this gives for L large

$$\exp(i\phi) \approx -\frac{r-1+i\frac{\phi}{L}}{r-1-i\frac{\phi}{L}} \approx -1 + 2i\frac{\phi}{L(1-r)} \quad (3.176)$$

and so we find to leading order in $1/L$

$$\theta = \frac{(2n+1)\pi}{L} \quad (3.177)$$

We notice that this approximation is only valid if $L(1-r) \gg 1$. For large β this approximation is simply equivalent to $L \gg 1$, while when β is small it requires that $H\beta \gg 1$.

The closest eigenvector to the real axis has $n = 0$ so we have

$$\lambda_0 \approx \frac{\sinh(\beta J)}{\cosh(\beta J) - \cos(\frac{\pi}{L})} \approx \frac{\sinh(\beta J)}{\cosh(\beta J) - 1 + \frac{\pi^2}{2L^2}} \approx \coth\left(\frac{\beta J}{2}\right) \left(1 - \frac{\pi^2}{4 \sinh^2(\frac{\beta J}{2}) L^2}\right) \quad (3.178)$$

In the limit $L \rightarrow \infty$, the ground-state eigenvalue is the same as the Sine-Gordon chain of length $L' \rightarrow \infty$ fixed at $h(0) = h(L') = 0$ with a SOS interaction between nearest neighbors [96], which is normal since boundary conditions on the x -axis are negligible in the thermodynamic limit.

First excited state eigenvector

In order to compute the second eigenvalue λ_1 we look for an odd or antisymmetric solution with $c = -1$. We thus find

$$\exp(iL\theta) = \frac{r - \exp(-i\theta)}{r - \exp(i\theta)} \quad (3.179)$$

For large L we look for a solution of the form $\theta = \phi/L$ and this gives

$$\exp(i\phi) \approx 1 \quad (3.180)$$

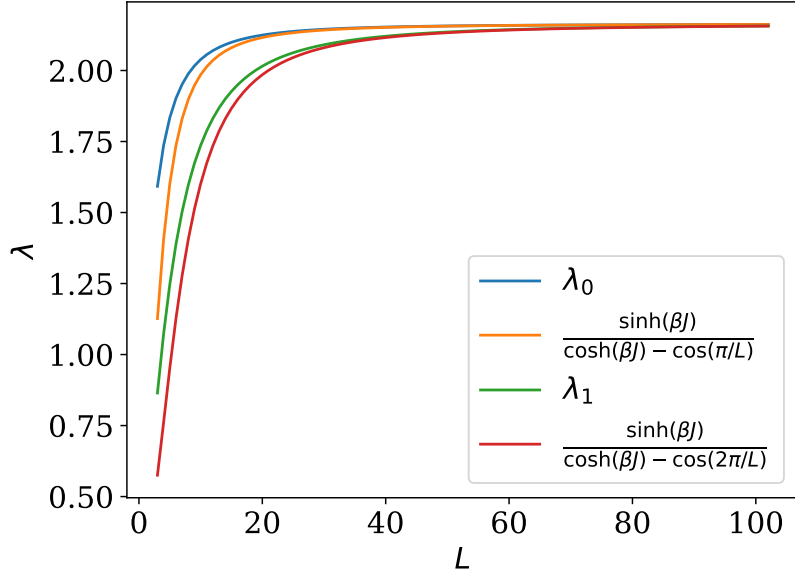


Figure 3.6: λ_0 and λ_1 as a function of L computed by numerical diagonalisation of the transfer matrix, compared to the analytical approximations for large L : Eq. (3.178) and Eq. (3.181). Here we have chosen for $J = 1$ and $\beta = 1$.

and so we chose solutions $\phi = 2n\pi$ for integer n . However the solution $n = 0$ which corresponds to $a = 1$ has $v(i) = a^i - a^{L-i} = 0$ and so does not correspond to an eigenvector. We thus take the next solution $\phi = 2\pi$ which gives

$$\lambda_1 \approx \frac{\sinh(\beta J)}{\cosh(\beta J) - \cos(\frac{2\pi}{L})} \approx \frac{\sinh(\beta J)}{\cosh(\beta J) - 1 + \frac{2\pi^2}{L^2}} \approx \coth(\frac{\beta J}{2}) \left(1 - \frac{\pi^2}{\sinh^2(\frac{\beta J}{2})L^2}\right) \quad (3.181)$$

In Fig 3.6, we show the agreement between the computation of the first two eigenvalues computed by numerical diagonalisation and compared with the analytical approximations Eq. (3.178) and Eq. (3.181) which are valid for the large L limit.

The correlation length is now given by

$$\xi = \frac{1}{\ln(\frac{\lambda_0}{\lambda_1})} = \frac{1}{\ln(\frac{\cosh(\beta J) - \cos(\frac{\pi}{L})}{\cosh(\beta J) - \cos(\frac{2\pi}{L})})} \approx \frac{4 \sinh^2(\frac{\beta J}{2})L^2}{3 \pi^2} \quad (3.182)$$

and we see that this has the same form as that for the free elastic line in Eq. (3.88). Furthermore, the free energy per site is given in the thermodynamic limit and for large L by

$$f = -\frac{1}{\beta} \ln(\lambda_0) \approx -\frac{1}{\beta} \left[\ln(\coth(\frac{\beta J}{2})) - \frac{\pi^2}{4 \sinh^2(\frac{\beta J}{2})L^2} \right] \quad (3.183)$$

and this gives a pressure

$$P = -\frac{\partial f}{\partial L} = \frac{T\pi^2}{2 \sinh^2(\frac{\beta}{2})L^3} \quad (3.184)$$

This has the same form as the pressure for the elastic line in Eq. (3.84) if we make the identification of the effective surface tension to be used in the elastic line model

$$\sigma_{eff} = \frac{2}{\beta} \sinh^2\left(\frac{\beta J}{2}\right) \quad (3.185)$$

We should note that this is also consistent with the equality deduced by comparing the correlation length of the two models.

We see that in the limit of large L and for appropriately low temperatures, the finite size SOS model reproduces the phenomenology of the elastic line (confined Edwards-Wilkinson surface). This is not surprising as at low temperatures, jumps of more than two lattice spacings in the height are suppressed by a factor of $\exp(-\beta J)$ with respect to staying at the same height moving up or down by one site. The low temperature SOS model thus becomes effectively equivalent to the RSOS model and thus is equivalent to a local random walk model.

High temperature limit

To explore the high temperature limit we can note that if we write

$$z = r - \exp(-i\theta) \quad (3.186)$$

we can write Eq. (3.173) as

$$\exp(iL\theta) = -\frac{z}{\bar{z}} = \exp(2i\psi + i\pi) \quad (3.187)$$

where

$$\tan(\psi) = \frac{\sin(\theta)}{r - \cos(\theta)} \quad (3.188)$$

This then gives

$$L\theta = 2\psi + \pi \quad (3.189)$$

and so

$$\tan(\psi) = \frac{\sin(\theta)}{r - \cos(\theta)} = \tan\left(\frac{L\theta}{2} + \frac{\pi}{2}\right) = -\cot\left(\frac{L\theta}{2}\right) \quad (3.190)$$

which finally gives

$$\tan\left(\frac{L\theta}{2}\right) = \frac{\cos(\theta) - r}{\sin(\theta)} \quad (3.191)$$

In this form we see that our calculations agree with those of Svrvick et al [97]. Furthermore when $\beta \rightarrow 0$ we know that the elements of the transfer matrix all tend to one and that the largest eigenvalue has all components equal. This means that in the infinite temperature limit, $\theta = 0$. Therefore in Eq. (3.191) we look for solutions where θ is small. Taylor expanding gives to leading order

$$\frac{L\theta^2}{2} \approx 1 - r - \frac{\theta^2}{2} \quad (3.192)$$

which gives

$$\theta \approx \sqrt{\frac{2(1-r)}{L+1}} \quad (3.193)$$

However the above expansion assumes that $\theta L \ll 1$ and so

$$\sqrt{2L(1-r)} \ll 1 \quad (3.194)$$

This means that the height can fluctuate by of order L from site to site. The high temperature approximation is thus equivalent to

$$\theta \approx \sqrt{\frac{2\beta J}{L+1}}. \quad (3.195)$$

Therefore at high temperature this means that $L\beta J \ll 1$, which gives a maximal eigenvalue

$$\lambda_0 = L + 1 \quad (3.196)$$

and a free energy

$$f = -\frac{1}{\beta} \ln(L + 1) \quad (3.197)$$

which is the obvious result coming from the infinite temperature entropy. This result suggests that the solution for θ at small β can be written as a perturbation series of the form

$$\theta = \sqrt{\beta J} \sum_{n=0}^{\infty} b_n (\beta J)^n \quad (3.198)$$

The first two terms give

$$\theta = \sqrt{\beta J} \left[\sqrt{\frac{2\beta J}{L+1}} - \beta J \frac{2+2L+L^2}{6\sqrt{2}(1+L)^{\frac{3}{2}}} \right] \quad (3.199)$$

and from this we find

$$f = -\frac{1}{\beta} \ln\left(L + 1 - \beta J \frac{L^2 + 2L}{3}\right) \quad (3.200)$$

and where we show in Fig 3.7 the agreement of the high-temperature approximation (3.200) with respect to the direct diagonalization of the transfer matrix. As pointed out above this result gives the high temperature entropy but it also exhibits the correct average energy ϵ per unit length at high temperature. To see this we note that all values of h are equiprobable at infinite temperature and so

$$\epsilon = \frac{1}{(L+1)^2} J \sum_{i,j=0}^L |i-j| = J \frac{L^2 + 2L}{3} \quad (3.201)$$

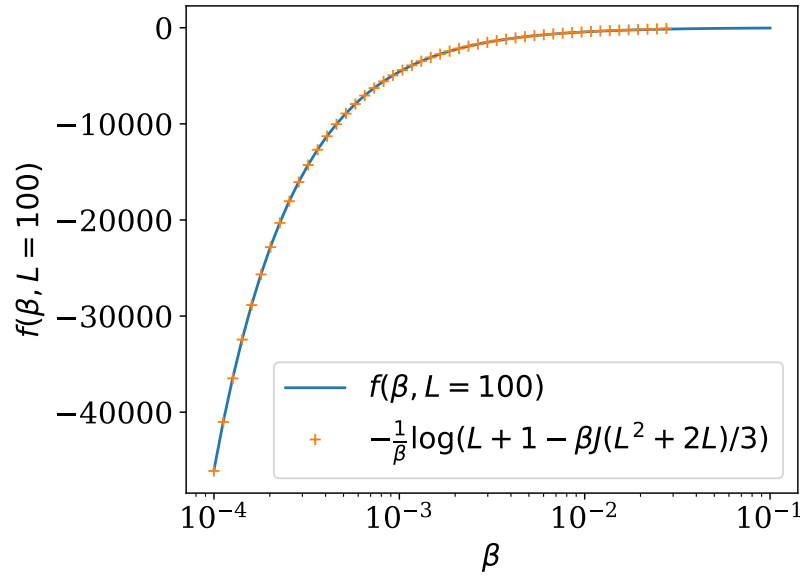


Figure 3.7: Free energy with respect to β for $L = 100$ and $J = 1$ in the high-temperature limit, by direct diagonalization of the transfer matrix and by Eq (3.200).

3.5 Conclusion

Finite-size effects corrections in the free energy are important when the correlation length becomes of the order of magnitude of the system's size. The derivative of the free energy with respect to the system size yields a confinement pressure, which can be seen for electromagnetic fields [14, 88, 15] and for critical systems [3], which has long-range interaction.

For continuous 1D interface systems, we use the path integral method [8] to compute the energy of all states, which gives us in the thermodynamic limit $f = \frac{1}{\beta} \epsilon_0$ and $\xi = \frac{1}{\epsilon_1 - \epsilon_0}$. The computation of the free energy of a continuous 1D interface is thus mapped to a 1D quantum problem. This method can be used for all potentials $V(h)$, and so we apply it to two specific cases. In the confined elastic line, we find the free energy per unit length $f = \frac{\Gamma^2 \pi^2}{2\sigma L^2}$, which gives a different power-law than the critical Casimir force, which is to be expected since critical systems have no surface tension. Using a conjecture [16] about the finite-size corrections on the surface tension, we show the correspondence between both models in the case $\sigma = 0$, and thus that interface physics exhibits Casimir-like interactions in the right limit : this relationship between interface and critical systems could lead to interesting new physics. In the semi-infinite geometry though, we compute the average height when the interface is under pressure.

For discrete Solid-On-Solid models, the path integral cannot be directly applied, and methods adapted to discrete systems must be used. The first method is to compute the free energy through numerical simulations. We generalize the LJH method [12] to any external potential both for Ising and SOS models, and compare it to the transfer matrix in the case of SOS for Kawasaki dynamics in the SOS model - which was the special case where neither the Layer method nor the LJH method were pertinent. This generalised method opens new ways

to study finite-size effects on critical systems under different thermodynamical ensembles, namely the critical Casimir force in Kawasaki Ising systems.

For the confined SOS interface, we followed Švrakić [97] to obtain the exact eigenvalues and eigenvectors of the transfer matrix in the case $V(h) = 0$. This gives us a free energy which has a the same dependence to the system's size than the confined elastic line.

Chapter 4

Beyond Solid-On-Solid : the Particles-Over-Particles model

While Ising models describe bulk behaviour of magnetic systems [4, 34] and interfaces between two coexisting phases [46], a direct interface lattice models exists, which is called Solid-On-Solid. This model was first studied by Gilmer and Bennema [99, 6] as a way to compute the crystal growth, whose dynamical equation will be later known as the Edwards-Wilkinson equation [30, 31]. In a second time, correspondance between SOS and the highly anisotropic Ising model at low temperature where found [47, 96], with the exact derivation of the SOS hamiltonian from the Ising one explained in Sec 1.3.2. When using an exponent of 2 in the interaction between nearest sites, the Gaussian SOS exhibits similar behavior to fluid interfaces [100, 101]. In Monte Carlo simulations for the Ising model, spins are taken with a uniform probability [75, 10], allowing the study of interface dynamics [102, 103, 72, 104]. On the contrary in the SOS approximation it is the heights which are taken with a uniform probability [50, 62], thus discarding bulk information.

Driven by this lack of correspondence between both models, in this chapter we modernize Temperley's model [105] with a model that we call **Particles-Over-Particles** which takes into account combinatorial terms, giving rise to an entropic contribution. By noticing that the height h of the interface is the sum of all particles of size $a = 1$ which are put under it, we first develop the partition function and transfer matrix of our model and compare it to SOS, then we develop the M-particles system where we introduce multiple types of particles stacked vertically, where each type may obey to a different dynamic, kinetic coefficient or diffusive constant.

4.1 The model

In a SOS system of size L' , the height of the interface at site i is noted $h_i \in [0, L]$ at site i , and fixing the total number of particles to be N the partition function is given by

$$Z_{\text{SOS}}(N) = \sum_{h_0 h_1 \dots h_{L'}} \delta_{\sum_i h_i, N} \exp \left(-\beta J \sum_{i=1}^{L'} |h_{i+1} - h_i| - \beta B \sum_{i=1}^{L'} V(h_i) \right) \quad (4.1)$$

where $V(h)$ is a function of the internal variables h_i and B the coupling parameter which has the dimension of energy. As done in the case of a perfect gas, if the height profiles represent

particle numbers which are all identical, the partition function is given by

$$Z_{\text{POP}}(N) = \frac{1}{N!} \sum_{h_1, h_2 \dots h_{L'}} \delta_{\sum_{i=1}^{L'} h_i, N} \frac{N!}{\prod_{i=1}^{L'} h_i!} \exp\left(-\beta J \sum_{i=1}^{L'} |h_{i+1} - h_i| - \beta B \sum_{i=1}^{L'} V(h_i)\right) \quad (4.2)$$

Here the combinatorial term $\frac{N!}{\prod_{i=1}^{L'} h_i!}$ represents the number of ways that the h_i particles on each site can be chosen from the N particles available. In the same fashion as the Solid-On-Solid, we call this model the **Particles-Over-Particles model**, since particles are stacked in columns of height h_i . The constraint on the particle number makes the computation of the partition function at fixed N complicated both analytically and numerically. However, changing into the grand canonical ensemble using the formula

$$\Xi = \sum_N \exp(\beta \mu N) Z_{\text{POP}}(N) \quad (4.3)$$

where Ξ is the grand partition function and μ the chemical potential, we find

$$\Xi_{\text{POP}} = \sum_{h_1, h_2 \dots h_{L'}} \frac{1}{\prod_{i=1}^{L'} h_i!} \exp\left(-\beta J \sum_{i=1}^{L'} |h_{i+1} - h_i| - \beta B \sum_{i=1}^{L'} [V(h_i) - \mu h_i]\right) \quad (4.4)$$

The model differs from the usual solid on solid model in that a number of particle configurations give rise to the same height configurations. The grand partition function can then be written as

$$\Xi = \sum_{h_1, h_2 \dots h_{L'}} \exp(-\beta H_{\text{eff}}(h_1, h_2 \dots h_{L'})) \quad (4.5)$$

where

$$H_{\text{eff}} = J \sum_{i=1}^{L'} |h_{i+1} - h_i| + \sum_{i=1}^{L'} [BV(h_i) - \mu h_i + \frac{1}{\beta} \ln(h_i!)] \quad (4.6)$$

The transfer matrix is

$$T_{\text{POP}}(h, h') = T_{\text{SOS}}(h, h') \exp\left(-\frac{\ln(h) + \ln(h')}{2}\right) \quad (4.7)$$

Contrary to the SOS model where there needs to be a confining external field in order to localize the interface [106, 107], the entropic term gives a stable position for the interface. In absence of external field $B = 0$, the effective potential is given by

$$V_{\text{eff}}(h) = -\mu h + \frac{1}{\beta} \ln(h!) \quad (4.8)$$

If the chemical potential is large enough, the number of particles N is large enough to use Stirling's formula and approximate a continuous derivative with the finite-difference in h , so

$$V_{\text{eff}}(h)' = -\mu + \frac{1}{\beta} \ln(h) \quad (4.9)$$

which gives the mean height

$$\langle h \rangle = \exp(\beta \mu) \quad (4.10)$$

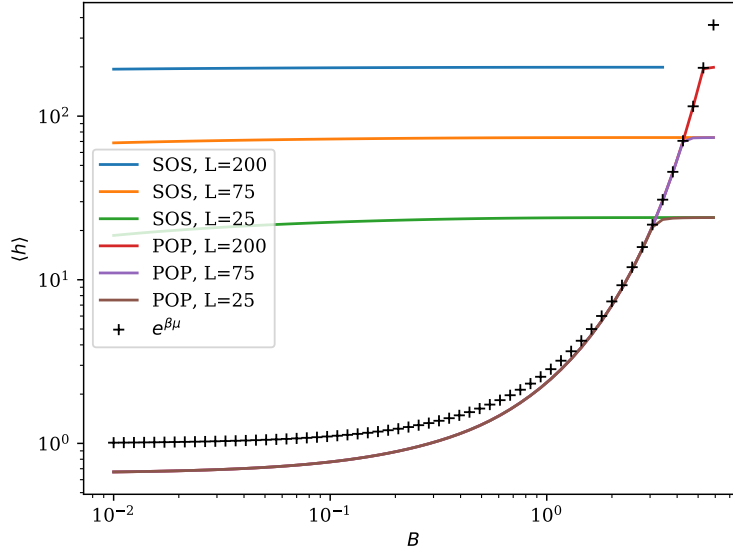


Figure 4.1: Mean height of the SOS (for reference) and POP model with respect the chemical potential μ through transfer matrix with different maximal heights in the thermodynamic limit $L' \rightarrow \infty$, compared to the Stirling's approximation Eq (4.10), at $\beta = 1$.

In Fig 4.1, we show the mean height (4.10) compared to the transfer matrix diagonalisation with different matrix size and the Monte Carlo simulations at $\beta = 1$. When $\langle h \rangle \gg 1$, the Stirling's formula becomes valid and Eq. (4.10) becomes accurate. Since $\langle h \rangle$ cannot exceed the maximum size of the system, saturation occurs at large μ . SOS mean height is also plotted as a reference, where we see that even in the limit $\mu = 0$, the mean height is equal to $\langle h \rangle(\mu = 0) = \frac{1}{2}$.

The Kawasaki implementation is straightforward, a particle n is chosen with probability $\frac{1}{N}$ at each Monte Carlo step, then an attempt to move the particle to the left or right using Metropolis acceptance rate is made.

The Glauber case is trickier. At equilibrium, we expect that as many particles are added as subtracted, so an attempt with probability 0.5 to add a particle is made, and the attempt to remove one is done with the same probability. When adding a particle, a site i is chosen with uniform probability $1/L'$, so the selection rate is

$$g(h_i \rightarrow h_i + 1) = \frac{1}{2L'} \quad (4.11)$$

To remove a particle¹, a particle n is chosen with uniform probability $1/N$, meaning that the selection probability is

$$g(h_i \rightarrow h_i - 1) = \frac{h_i}{2N} \quad (4.12)$$

¹In C++, we can use a `std::vector` in which we add or remove particles. After each success attempt, we rebuild the distribution `std::uniform_int_distribution(0, N - 1)`, where N is the number of particles. This operation is lightweight and should not cause any slowing down. For the next section's algorithm with multiple particle types, we use `std::discrete_distribution<>`.

In the case that there is no particle in the system, that phase is skipped and we immediately proceed to attempt to add a new particle. In order to satisfy detailed balance, acceptance rates need to verify

$$\begin{aligned} \frac{g(h_i \rightarrow h_i + 1) A(h_i \rightarrow h_i + 1)}{g(h_i + 1 \rightarrow h_i) A(h_i \rightarrow h_i + 1)} &= \frac{N}{L'(h_i + 1)} \frac{A(h_i \rightarrow h_i + 1)}{A(h_i \rightarrow h_i + 1)} \\ &= \exp(-\beta(E(h_i + 1) - E(h_i))) \end{aligned} \quad (4.13)$$

Choosing an acceptance rate that satisfies this condition is not as easy as the Metropolis acceptance rate [75], and we provide no clear answer as to how to solve this problem. Using the Metropolis acceptance rate ($A(\mu \rightarrow \nu) = 1$ if $\Delta_E < 0$) does not provide the correct equilibrium averages expected by the transfer matrix.

Here, the combinatoric term is directly taken into account in the selection probability, which is why it is difficult to find a good acceptance rate. Nevertheless, it is possible to use uniform selection probability as with SOS and introduce the combinatoric term in the energy.

4.2 M-particles POP system

The Ising model with spins $\sigma = \pm 1$ has a direct mapping with liquid/gas and binary mixtures systems [2], which are systems with two types of particles (for the liquid/gas model σ is a "density of particles"). On the contrary, SOS models only need the existence of one type of particles, since everything that is over the interface is not taken into account. We can imagine multi-layering of non-miscible liquids having different densities [108, 109], forming many layers with $M - 1$ interfaces, M being the number of particles' type. We can decide to study one specific interface between two particle types, and in such case the classic SOS model would be enough, with J being the surface energy cost between both liquids.

In this multi-layered system, we consider a model of a surface delimiting a bulk phase of L' sites which contains M different particle types $p_1 \dots p_M$. N_m is the total number of particles of type m and $n_{m,i}$ denotes the number of particles of type m at site i . The interface height is $h_i = \sum_m n_{m,i}$. Taking into account the entropic contribution, the effective Hamiltonian for the model is

$$H[M] = J \sum_i |h_i - h_{i+1}| + B \sum_i V(h_i) - \sum_m \mu_m \sum_i n_{m,i} + \frac{1}{\beta} \sum_m \sum_i \ln(n_{m,i}) \quad (4.14)$$

We assume that the particles in each column are demixed, i.e. the permitted particle configurations are taken to be stacked vertically such that the stack of p_{m+1} particles lies on top of the p_m particles, as seen in Fig 4.2 for $M = 2$. This assumption is not particularly necessary when considering that the energy interaction between layers is zero. The first term in the Hamiltonian corresponds to the surface tension with a gas phase above the stacks of particles. As discussed with the SOS model, a restricted or gaussian version of Eq. (4.14) can be made.

The grand partition function is given by

$$\Xi = \sum_{\mathbf{n}_1 \dots \mathbf{n}_M} \exp(-\beta H[M]) \quad (4.15)$$

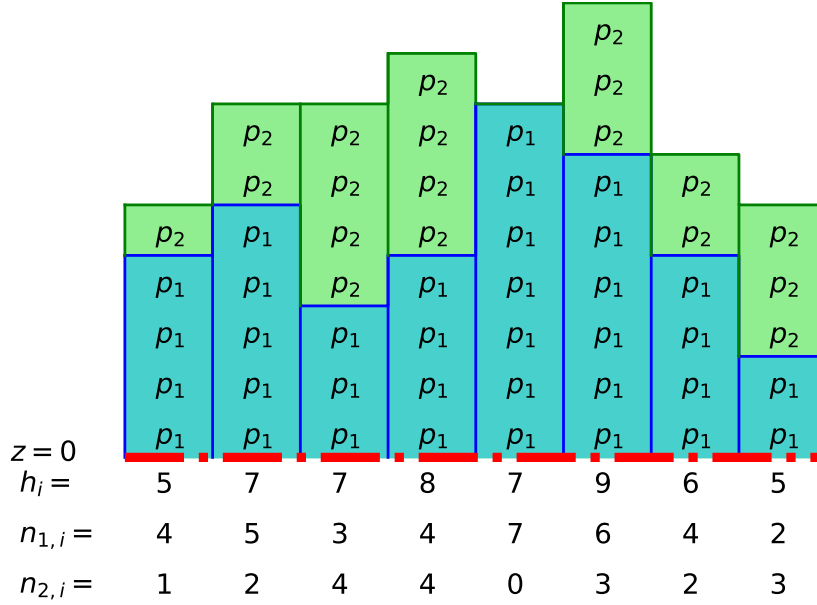


Figure 4.2: Possible POP configuration with two types of particles p_1 and p_2 . The red line shows the origin $z = 0$. In the i -th column the interface is at height h_i , with $n_{1,i}$ particles of type p_1 at site i , and same for particles p_2 . There are no particles at the top of the interface.

If $M = 2$, the the statics of the above can be reduced to the study of a single particle model by making the change of variable $n_{2,i} = h_i - n_{1,i}$. Using the binomial relation $(a + b)^{n_1} = \sum_{h'=0}^{n_1} \frac{n_1!}{h'!(n_1-h')!} a^{h'} b^{n_1-h'}$ the sum over the variables $n_{1,i}$ can be trivially carried out and we find

$$\begin{aligned} \Xi &= \sum_{\mathbf{h}} \exp \left(-\beta J \sum_i |h_i - h_{i+1}| - \beta B \sum_i V(h_i) - \sum_i \ln(h_i!) + \beta \mu_e \sum_i h_i \right) \\ &= \sum_{\mathbf{h}} \exp(-\beta H_{eff}(h_1, h_2 \dots h_{L'})) \end{aligned} \quad (4.16)$$

where $\mu_e = \frac{1}{\beta} \ln(\exp(\beta \mu_1) + \exp(\beta \mu_2))$ is the effective chemical potential for the variables h_i . If we add a third type of particle, we clearly see that the same reduction can be carried out. Thus, by recursivity, for any number of particle type M , we have the same effective Hamiltonian as the single particle system (4.6), with an effective chemical potential

$$\mu_e = \frac{1}{\beta} \ln \left(\sum_m \exp(\beta \mu_m) \right) \quad (4.17)$$

An interesting thing to remark is that even if the chemical potential of a particle type $\mu_m = 0$, its contribution to the effective chemical potential is nonzero. This reduced theory can be numerically solved in equilibrium by transfer matrix methods.

Now let the subset \bar{M} of particle types from the M particle types be in the canonical ensemble, while all the other ones are in the grand-canonical one. This is the so-called model C [18], which describes the coupling between conserved and non-conserved fields, such as impurities in liquids [110] or ionic conductors moving through a lattice set up by different

types of ions [111, 112]. The total partition function is then

$$\Xi = \sum_h \exp(-\beta H_{eff}(h_1, h_2 \dots h_{L'})) \prod_{m \in M} \delta_{\sum_{i=1}^{L'} h_i, N_m} \quad (4.18)$$

with the average number of particles per site being

$$\begin{aligned} \langle n_m \rangle &= \frac{1}{\beta L'} \frac{\partial}{\partial \mu_m} \ln(\Xi) \\ &= \frac{1}{\beta L'} \frac{\partial \mu_e}{\partial \mu_m} \frac{\partial}{\partial \mu_e} \ln(\Xi) \\ &= \frac{\exp(\beta \mu_m)}{\sum_m \exp(\beta \mu_m)} \end{aligned} \quad (4.19)$$

where $\langle \sum_m n_m \rangle$.

Mixing Glauber and Kawasaki dynamics for different particle types could be implemented using the following algorithm. Each non-conserved particle type possess a kinetic coefficient α_m , while each conserved particle type has a diffusive coefficient D_m . We set $p_m = \alpha_m$ if the particle is non-conserved, and $p_m = D_m$ otherwise, and we normalize it in order to have $\sum_m p_m = 1$. At each Monte Carlo step, a particle of type m is chosen with probability p_m , and then we proceed with Glauber or Kawasaki dynamics for a single-type particle system, as described in the previous section. To satisfy detailed balance, we have to understand how this coefficient p_m changes the selection probability g , and we get the same difficulties as in the single-particle type Glauber case.

Nevertheless, when all particles are under Kawasaki dynamics and $p_m = 1/M$ is a constant, then the ratio between selection rates is equal, which solves all the issues.

This algorithm could prove useful for studying multi-particle systems where each particle type is under different potentials (think of an ion in a neutral solvent under magnetic field) or different temperature [113], some of them which are under non-equilibrium forces like shearing.

4.3 Continuum Theory

In order to understand the statics of the model we write a continuum version of the theory with M field $n_m(x)$ and we take the a Gaussian form for the surface energy

$$H = \int dx \frac{\sigma}{2} \left[\frac{d}{dx} \left(\sum_m n_m \right) \right]^2 + V(n_1(x), \dots, n_M(x)) \quad (4.20)$$

where σ is the surface tension and

$$V(n_1(x), \dots, n_M(x)) = \sum_m -\mu_m n_m(x) + T n_m(x) [\ln(n_m(x)) - 1] \quad (4.21)$$

We have used Stirlings formula and thus assumed that the typical value of $n_m(x)$ are large. We now expand $V(n_1(x), \dots, n_M(x))$ by writing $n_m(x) = \bar{n}_m + \phi_m(x)$ where $(\bar{n}_1, \dots, \bar{n}_M)$ is the minimum of $V(n_1, \dots, n_M)$. Here we find

$$\bar{n}_m = \exp(\beta \mu_m) \quad (4.22)$$

This gives an effective Hamiltonian for the fluctuations of the fields ϕ_m

$$H_f = \frac{\sigma}{2} \int dx \left[\frac{d}{dx} \left(\sum_m \phi_m \right)^2 + \sum_m r_m \phi_m^2(x) \right] \quad (4.23)$$

where

$$r_m = \frac{T}{\sigma \bar{n}_m} \quad (4.24)$$

A straight-forward calculation then shows that the Fourier transform of the connected height-height fluctuation correlation function is

$$\tilde{C}_{hh}(k) = \frac{T}{\sigma} \frac{1}{k^2 + r_e} \quad (4.25)$$

where $r_e = \prod_m r_m / \sum_m r_m$. We thus find

$$= \frac{T}{2\sigma m_e} = \frac{1}{2} \sqrt{\frac{T\bar{h}}{\sigma}}, \quad (4.26)$$

where $\bar{h} = \sum_m \bar{n}_m$.

4.4 Conclusion

There are two ways of interpreting the interface's description through its height $\{h_i\}$. The first one is to only see the height as the interface's degrees of freedom [99, 6], while the second one is to interpret that height as a number of particles of type A which are below the interface with particles of type B, which is the physical phenomenon happening in crystal growth. This interpretation requires the addition of an entropic term [105], which localises the free interface in a semi-infinite geometry, contrary to SOS models [107]. The system can also be composed of multiple layers of different particles [multilayer], and this new model can take that into account for numerical simulations. The problem lies in the numerical algorithm. Taking a height with non-uniform probability is tricky, as it changes the selection probability $g(C \rightarrow C')$, so the acceptance probability $A(C \rightarrow C')$ is not as simple as the Metropolis one [75, 10]. We let the resolution of this problem - and as such the study of new physics through numerical simulations of this model - to the community.

Chapter 5

Driven interfaces

One of the most natural ways of creating a non-equilibrium steady state is by applying external driving forces, as shown in Fig 5.1. Driving arises naturally in sedimenting systems due to gravity, in systems with free charges under the action of an electric field, and also due to the radiation pressure exerted by a laser. Experiments where a phase separated colloidal system is sheared parallel to the interface show that driving due to shear tends to suppress surface fluctuations [19], and similar results are found where Ising models are numerically sheared [73, 104]. These results are somewhat surprising, for instance they are contrary to the observation that wind generates waves on the ocean. One may think that the precise nature of the driving plays a role, for instance uniformly driving a system may be intrinsically different to applying a shear field which is manifestly nonuniform.

In this chapter we investigate driving using three different methods. In the first section - which is almost a verbatim of a paper we have published [17] - we develop model C interfaces (model B interface is invariant under Galilean transformation under driving) and find that the height fluctuations are suppressed and the correlation length of the fluctuations is increased. In the second section, we discuss driving in the SOS model, where the Galilean invariance is broken by the discrete-time nature of numerical simulations, and find an increase of the interface width with respect to driving.

5.1 The effect of driving on model C interfaces

Constructing a continuum model which is analytically tractable and is also affected by uniform driving is straightforward but contains some subtleties. In a continuum system it is clear that uniform driving can only move a system away from equilibrium when the driving acts differently on different particle types. For instance, consider a system of identical interacting Brownian particles driven by a uniform force. The force will induce the same average velocity on all the particles, consequently, in the frame moving with this average velocity, we will recover the unmodified equilibrium state. However, when multiple particle types are present, the mean velocity induced on different species are different and no Galilean transformation is possible. Perhaps the first such study of this phenomenon was due to Onsager [114], who studied the conductivity of electrolytes and in doing so showed how the correlation functions in the steady state were modified by the electric field. Recently there have been many studies of driven multi-particle Brownian systems [115, 116, 117, 118, 119, 120], including the elec-

trolyte problem, and rich new physics has been found, even in the case of purely Gaussian theories [121, 122] based on stochastic density functional theory [123].

The dynamics of discrete particle systems is however affected by uniform driving of identical particles. The study of driven lattice gases has revealed a wide range of intriguing physical phenomena and indeed shown how driving can even lead to phase separation [112, 124, 125, 102]. The discrete nature of the dynamics of these systems, both in space and time, means that no Galilean transformation to an equilibrium state exists. Analytical studies of these systems require a phase ordering kinetics description in terms of a continuum order parameter. In order to break Galilean invariance the local mobility of the particles can be taken to be dependent on the local order parameter, this is then sufficient to induce non-trivial steady states under driving [112, 125, 73, 104]. Interfaces between the separated phases in uniformly driven systems have non capillary behaviors which are, even today, not fully understood [125]. Taking random driving in a given direction also leads to non-equilibrium steady states, if the noise is Gaussian and white, the fluctuation dissipation theorem is violated and novel interface fluctuations are induced which, again, are not of the capillary type [124].

Driving can also be deterministic but space dependent, for instance if one considers applied shear flows, the spatial dependence of the flow means no Galilean transformation to an equilibrium steady state is possible and this therefore leads to non-equilibrium steady states. The effect of shear on interfaces in these type of systems yields interface equations of the stochastic Burgers type and the statistics are no thus longer Gaussian due to the presence of nonlinearities [9, 29, 73, 104, 70, 126]

In this chapter we analyse what is known, in the classification of Hohenberg and Halperin [18], as model C type dynamics for two fields, one with conserved model B type dynamics, which is in addition convected at a uniform velocity to mimic driving. We refer to this first field as the colloid field. This colloid field is coupled to an additional field which undergoes model A non-conserved dynamics and which is not subjected to the driving. The model A field can be thought of a passive solvent and its coupling to the model B field is chosen in such a way that it has no influence on the non-driven equilibrium steady state. We then derive the effective dynamics between two separated low temperature phases by using a method introduced in [9, 29] for the study of interfaces under shear flow. This method yields a Gaussian theory for the interface statistics and driving introduces interesting new physics, notably we find that the effective surface tension of the system is increased but also the correlation length of interface fluctuations (due to an effective gravitational term) are increased. These observations are in qualitative agreement with experimental results on sheared low tension interfaces in phase separated colloidal systems [19]. In this experimental system the interface fluctuations were also found to be well described by Gaussian statistics and this is our principal motivation for studying theories which remain Gaussian but are modified by driving. While the long wavelength theory we find is of a capillary type, we also find new, higher derivative terms, which are generated in the spectrum of the height fluctuations.

As an aside, we also show how the model introduced here can be used to analyse the effect of activity on the dynamics of the surface between two phases of active colloids. The activity is implemented by taking a different temperature for the colloid and solvent fields, this difference in temperatures leads to significantly modified surface statistics which again develop dependencies on static and dynamical variables of the model which otherwise remain hidden for the equilibrium version of the problem.

5.1.1 The underling two field model

We consider a coarse grained model for two scalar fields ψ and ϕ with Hamiltonian

$$H[\psi, \phi] = H_1[\psi] + H_2[\psi, \phi] \quad (5.1)$$

The Hamiltonian H_1 is of the classic Landau-Ginzburg form

$$H_1[\psi] = \int d\mathbf{x} \left[\frac{\kappa}{2} [\nabla\psi(\mathbf{x})]^2 + V(\psi(\mathbf{x})) - gz\psi(\mathbf{x}) \right] \quad (5.2)$$

The last term represents the energy due to a gravitational field and will introduce a finite correlation length in the fluctuations between the two phases. We assume that the above Hamiltonian has two stable phases with average concentrations of the field $\phi(\mathbf{x})$ given by the constant values ψ_1 and ψ_2 , the difference between the order parameter in the two different phases is denoted by $\Delta\psi = \psi_2 - \psi_1 > 0$. This means that we find the phase 1 as $z \rightarrow \infty$ and the phase 2 as $z \rightarrow -\infty$. The term H_2 is taken to be a simple quadratic coupling between the fields

$$H_2 = \int d\mathbf{x} \frac{\lambda}{2} (1 - \psi(\mathbf{x}) - \phi(\mathbf{x}))^2 \quad (5.3)$$

which is an approximative conservation law of total volume fraction of the phases. The field ϕ can be thought of as the local volume fraction of the solvent in a colloidal system. However the presence of this solvent field does not change the effective equilibrium statistical mechanics of the colloid field ψ as the partition function can be written as

$$Z = \int d[\phi] d[\psi] \exp(-\beta H_1[\psi] - \beta H_2[\psi, \phi]) = CZ_{eff} \quad (5.4)$$

where Z_{eff} is the effective partition function for the field ψ , after we have integrated out the degrees of freedom corresponding to the field ϕ , and C is a constant term resulting from this integration. The effective partition function is thus simply given by

$$Z_{eff} = \int d[\psi] \exp(-\beta H_1[\psi]) \quad (5.5)$$

and, as stated above, we see that the field ϕ thus has no effect on the equilibrium statistical mechanics of the field ψ .

We now consider the dynamics of the fields. We take local diffusive model B dynamics for the field ψ and non-conserved model A dynamics for the field ϕ

$$\frac{\partial\psi(\mathbf{x}, t)}{\partial t} + \mathbf{v} \cdot \nabla\psi(\mathbf{x}, t) = D\nabla^2 \frac{\delta H}{\delta\psi(\mathbf{x})} + \sqrt{2DT}\nabla \cdot \boldsymbol{\eta}_1(\mathbf{x}, t) \quad (5.6)$$

$$\frac{\partial\phi(\mathbf{x}, t)}{\partial t} = -\alpha \frac{\delta H}{\delta\phi(\mathbf{x})} + \sqrt{2\alpha T}\eta_2(\mathbf{x}, t). \quad (5.7)$$

The first equation corresponds to standard model B dynamics but with an advection term by a constant velocity field \mathbf{v} . In Fig 5.1, we show the effect of that advection term in the presence of an interface. Since phase 1 is more diluted than phase 2, there are less particles which are driven at constant velocity \mathbf{v} . The second equation has no advection term and is simple model A dynamics. In principle we can also treat the case where the dynamics of the

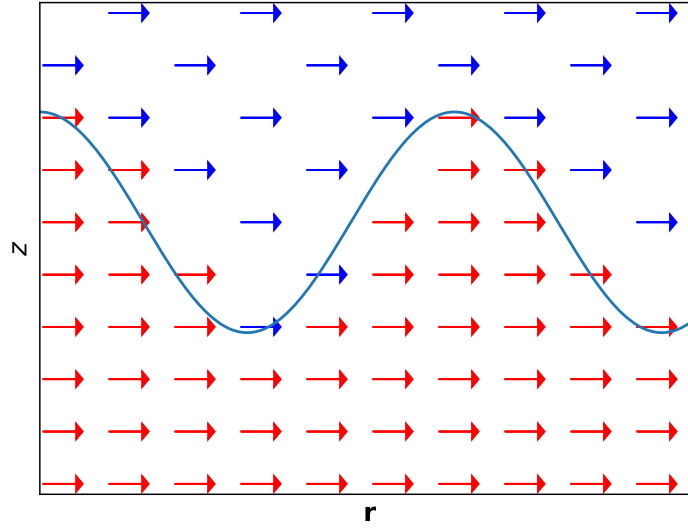


Figure 5.1: Schematics of the advection term $\mathbf{v} \cdot \nabla\psi(\mathbf{x}, t)$ for a field under the interface approximation (5.18). The red and blue phase respectively correspond to ϕ_2 and ψ_1 , with $\phi_2 > \psi_1$, and the solid line the interface between phases.

field ϕ is also diffusive and thus of model B type, the analysis given here can be extended to this case but the analysis of the resulting equations is considerably more complicated. The use of model A dynamics for the solvent is justified by assuming that its dynamics is faster than that of the colloids and that the volume fraction can vary due to local conformational changes rather than diffusive transport.

The noise terms above are uncorrelated and Gaussian with zero mean, their correlation functions are given by

$$\langle \eta_{1i}(\mathbf{x}, t) \eta_{1j}(\mathbf{x}', t') \rangle = \delta_{ij} \delta(t - t') \delta(\mathbf{x} - \mathbf{x}') \quad (5.8)$$

$$\langle \eta_2(\mathbf{x}, t) \eta_2(\mathbf{x}', t') \rangle = \delta(t - t') \delta(\mathbf{x} - \mathbf{x}'), \quad (5.9)$$

and T is the temperature in units where $k_B = 1$. These dynamical equations are thus explicitly given by

$$\frac{\partial \psi(\mathbf{x}, t)}{\partial t} + \mathbf{v} \cdot \nabla \psi(\mathbf{x}, t) = D \nabla^2 \left[\frac{\delta H_1}{\delta \psi(\mathbf{x})} + \lambda(\phi(\mathbf{x}, t) + \psi(\mathbf{x}, t)) \right] + \sqrt{2DT} \nabla \cdot \boldsymbol{\eta}_1(\mathbf{x}, t) \quad (5.10)$$

and

$$\frac{\partial \phi(\mathbf{x}, t)}{\partial t} = -\alpha \lambda [\phi(\mathbf{x}, t) + \psi(\mathbf{x}, t)] + \sqrt{2\alpha T} \eta_2(\mathbf{x}, t). \quad (5.11)$$

Taking the temporal Fourier transform, defined with the convention

$$\tilde{F}(\mathbf{x}, \omega) = \int_{-\infty}^{\infty} dt \exp(-i\omega t) F(\mathbf{x}, t), \quad (5.12)$$

we can eliminate the field $\tilde{\phi}$ which is given by

$$\tilde{\phi}(\mathbf{x}, \omega) = \frac{-\alpha \lambda \tilde{\psi}(\mathbf{x}, \omega) + \sqrt{2\alpha T} \tilde{\eta}_2(\mathbf{x}, \omega)}{i\omega + \alpha \lambda}, \quad (5.13)$$

this then gives the closed equation for $\tilde{\psi}$:

$$\left[1 - \frac{\lambda D \nabla^2}{i\omega + \alpha\lambda}\right] i\omega \tilde{\psi}(\mathbf{x}, \omega) + \mathbf{v} \cdot \nabla \tilde{\psi}(\mathbf{x}, \omega) = D \nabla^2 \tilde{\mu}(\mathbf{x}, \omega) + \tilde{\zeta}(\mathbf{x}, \omega), \quad (5.14)$$

where

$$\mu(\mathbf{x}, t) = \frac{\delta H_1}{\delta \psi(\mathbf{x}, t)} \quad (5.15)$$

is the effective chemical potential associated with the field ψ and the noise term is given by

$$\tilde{\zeta}(\mathbf{x}, \omega) = \frac{\sqrt{2\alpha T D} \lambda}{i\omega + \alpha\lambda} \nabla^2 \tilde{\eta}_2(\mathbf{x}, \omega) + \sqrt{2D T} \nabla \cdot \tilde{\eta}_1(\mathbf{x}, \omega). \quad (5.16)$$

Inverting the temporal Fourier transform then gives the effective evolution equation

$$\frac{\partial \psi(\mathbf{x}, t)}{\partial t} - \lambda D \nabla^2 \int_{-\infty}^t dt' \exp(-\alpha\lambda(t-t')) \frac{\partial \psi(\mathbf{x}, t')}{\partial t} + \mathbf{v} \cdot \nabla \psi(\mathbf{x}, t) = D \nabla^2 \mu(\mathbf{x}, t) + \zeta(\mathbf{x}, t). \quad (5.17)$$

5.1.2 Effective interface dynamics

Following Sec 1.2.2, we derive the dynamical equation for the interface $h(\mathbf{r})$, where

$$\psi(\mathbf{x}, t) = f(z - h(\mathbf{r}, t)) \quad (5.18)$$

and $f(z) \rightarrow \psi_2$ as $z \rightarrow -\infty$ and $f(z) \rightarrow \psi_1$ as $z \rightarrow \infty$, and we use the sharp interface approximation

$$f'(z) = \Delta \psi \delta(z) \quad (5.19)$$

We also assume that the driving is in the $\mathbf{r} = (x, y)$. The dynamical evolution for the field ψ in Eq. (5.17) is first written as

$$\nabla^{-2} \left[\frac{\partial \psi(\mathbf{x}, t)}{\partial t} + \mathbf{v} \cdot \nabla \psi(\mathbf{x}, t) \right] - \lambda D \int_{-\infty}^t dt' \exp(-\alpha\lambda(t-t')) \frac{\partial \psi(\mathbf{x}, t')}{\partial t} = D \mu(\mathbf{x}, t) + \nabla^{-2} \zeta(\mathbf{x}, t) \quad (5.20)$$

Using the relations (1.57) and (1.59), where $V(\psi(\mathbf{x})) = V(\psi(\mathbf{x})) - gz\psi(\mathbf{x})$, multiplying both sides by $f'(z - h(\mathbf{r}, t))$ and integrating over z as in Eq (1.57) and (1.59), we obtain

$$\begin{aligned} \int_{-\infty}^{\infty} dz f'(z - h(\mathbf{r}, t)) \mu(\mathbf{x}, t) &= \kappa \nabla^2 h(\mathbf{r}, t) \int_{-\infty}^{\infty} dz f'(z - h(\mathbf{r}, t))^2 - \int_{-\infty}^{\infty} dz g z f'(z - h(\mathbf{r}, t)) \\ &= \kappa \nabla^2 h(\mathbf{r}, t) \int_{-\infty}^{\infty} dz' f'(z')^2 - \int_{-\infty}^{\infty} dz' g(z' + h(\mathbf{r}, t)) f'(z') \\ &= \kappa \nabla^2 h(\mathbf{r}, t) \int_{-\infty}^{\infty} dz' f'(z')^2 - \Delta \psi g h(\mathbf{r}, t). \end{aligned} \quad (5.21)$$

By using the Cahn-Hilliard estimate of the surface tension (1.41), we thus find

$$\int_{-\infty}^{\infty} dz f'(z - h(\mathbf{r}, t)) \mu(\mathbf{x}, t) = \sigma [\nabla^2 h(\mathbf{r}, t) - m^2 h(\mathbf{r}, t)] \quad (5.22)$$

where $m^2 = \Delta \psi g / \sigma$.

We now carry out the same operation on the left hand side of Eq. (5.20). First we have

$$\begin{aligned}
 \nabla^{-2} \frac{\partial \psi(\mathbf{x}, t)}{\partial t} + \mathbf{v} \cdot \nabla \psi(\mathbf{x}, t) + \lambda D \int_{-\infty}^t dt' \exp(-\alpha \lambda (t - t')) \frac{\partial \psi(\mathbf{x}, t')}{\partial t'} = \\
 - \nabla^{-2} f'(z - h(\mathbf{r}, t)) \left[\frac{\partial h(\mathbf{r}, t)}{\partial t} + \mathbf{v} \cdot \nabla h(\mathbf{r}, t) \right] + \lambda D \int_{-\infty}^t dt' \exp(-\alpha \lambda (t - t')) f'(z - h(\mathbf{r}, t')) \frac{\partial h(\mathbf{r}, t')}{\partial t'} \\
 \approx - \nabla^{-2} f'(z) \left[\frac{\partial h(\mathbf{r}, t)}{\partial t} + \mathbf{v} \cdot \nabla h(\mathbf{r}, t) \right] + \lambda D \int_{-\infty}^t dt' \exp(-\alpha \lambda (t - t')) f'(z) \frac{\partial h(\mathbf{r}, t')}{\partial t'}
 \end{aligned} \tag{5.23}$$

where in the last line above we have neglected terms quadratic in h . Note that the neglecting of these additional terms is not strictly justified, they could potentially induce non-perturbative effects which render the surface fluctuations non-Gaussian. However we see here that the first order computation we carry out tends to reduce fluctuations with respect to equilibrium or non-driven interfaces and so if the equilibrium theory can be described by an equation which is linear in height fluctuations, it seems physically reasonable to assume that the approximation also holds for the driven interface. Again, we multiply the above by $f'(z)$ and integrate over z .

Putting this all together we obtain

$$\Delta \psi^2 \int d\mathbf{r} G(0, \mathbf{r} - \mathbf{r}') \left[\frac{\partial h(\mathbf{r}, t)}{\partial t} + \mathbf{v} \cdot \nabla h(\mathbf{r}, t) \right] + \frac{\sigma \lambda D}{\kappa} \int_{-\infty}^t dt' \exp(-\alpha \lambda (t - t')) \frac{\partial h(\mathbf{r}, t')}{\partial t'} = \sigma [\nabla^2 h(\mathbf{r}, t) - m^2 h(\mathbf{r}, t)] + \xi(\mathbf{r}, t) \tag{5.24}$$

where $G = -\nabla^{-2}$, or more explicitly

$$\nabla^2 G(z - z', \mathbf{r} - \mathbf{r}') = -\delta(z - z') \delta(\mathbf{r} - \mathbf{r}') \tag{5.25}$$

The noise term ξ is given by

$$\xi(\mathbf{r}, t) = \int_{-\infty}^{\infty} dz f'(z - h(\mathbf{r}, t)) \nabla^{-2} \zeta(\mathbf{x}, t). \tag{5.26}$$

Now, as the equations of motion have been derived to first order in h and we wish to recover the correct equilibrium statistics for the non-driven system, we ignore the h dependence in the noise and make the approximation

$$\xi(\mathbf{r}, t) \approx \int_{-\infty}^{\infty} dz f'(z) \nabla^{-2} \zeta(\mathbf{x}, t). \tag{5.27}$$

The correlation function of this noise is most easily evaluated in terms of its Fourier transform with respect to space and time defined by

$$\hat{F}(\mathbf{q}, \omega) = \int dt d\mathbf{r} \exp(-i\omega t - i\mathbf{q} \cdot \mathbf{r}) F(\mathbf{r}, t). \tag{5.28}$$

Using the relations Eqs. (1.41) and (5.19) one can show that

$$\langle \hat{\xi}(\mathbf{q}, \omega) \hat{\xi}(\mathbf{q}', \omega') \rangle = 2T (2\pi)^d \delta(\omega + \omega') \delta(\mathbf{q} + \mathbf{q}') \left[\frac{\sigma}{\kappa} \frac{\alpha D^2 \lambda^2}{\omega^2 + \alpha^2 \lambda^2} + \frac{D \Delta \psi^2}{2q} \right] \tag{5.29}$$

In full Fourier space the equation of motion for the field ψ then reads

$$\left[i(\omega + \mathbf{q} \cdot \mathbf{v}) \frac{\Delta\psi^2}{2q} + \frac{D\sigma\lambda}{\kappa} \frac{i\omega}{\alpha\lambda + i\omega} \right] \hat{h}(\mathbf{q}, \omega) = -D\sigma(q^2 + m^2) \hat{h}(\mathbf{q}, \omega) + \hat{\xi}(\mathbf{q}, \omega) \quad (5.30)$$

From this, the full Fourier transform of the correlation function of the interface height is given by

$$\hat{C}(\mathbf{q}, \omega) = 2TD \frac{\left[\frac{\Delta\psi^2}{2q} (\omega^2 + \alpha^2\lambda^2) + \frac{\sigma\alpha D\lambda^2}{\kappa} \right]}{\left| i \left[\frac{\alpha\lambda\Delta\psi^2}{2q} (\omega + \mathbf{q} \cdot \mathbf{v}) + \frac{\lambda\sigma D}{\kappa} \omega + D\sigma(q^2 + m^2)\omega \right] + [\alpha\lambda D\sigma(q^2 + m^2) - \frac{\Delta\psi^2}{2q} \omega(\omega + \mathbf{q} \cdot \mathbf{v})] \right|^2} \quad (5.31)$$

Using the above we can extract the equal time height-height correlation function in the steady states. Its spatial Fourier transform can shown to be given by

$$\tilde{C}_s(\mathbf{q}) = \frac{1}{2\pi} \int d\omega \hat{C}(\mathbf{q}, \omega) \quad (5.32)$$

This integral has the same form as

$$I(f(\omega)) = \int \frac{d\omega}{2\pi} \frac{f(\omega)}{|i(A\omega + B) + (C - D\omega - E\omega^2)|} \quad (5.33)$$

so we see that the integral we need to evaluate can be written in the form

$$I = aI(\omega^2) + bI(1) \quad (5.34)$$

The calculation of Eq. (5.32) can be carried out in the presence of a forcing term on the height profile in order to compute the response function for the surface which has a denominator of the form

$$\text{Den} = i(A\omega + B) + (C - D\omega - E\omega^2) \quad (5.35)$$

and due to causality the above only has poles in the upper complex plane (due to the convention of Fourier transforms used here). Consequently we find that

$$\int \frac{d\omega}{2\pi} \frac{1}{i(A\omega + B) + (C - D\omega - E\omega^2)} = 0 \quad (5.36)$$

as one may close the integration contour in the lower half of the complex plane. Taking the real and imaginary part of Eq. (5.36) leads to

$$CI(1) - DI(\omega) - EI(\omega^2) = 0 \quad (5.37)$$

$$AI(\omega) + BI(1) = 0 \quad (5.38)$$

Using this we can express $I(\omega^2)$ as a function of $I(1)$, and explicitly we have

$$I(\omega^2) = \frac{I(1)}{E} \left[C + \frac{DB}{A} \right] \quad (5.39)$$

To evaluate $I(1)$ we now use

$$I(1) = -\text{Im} \int \frac{d\omega}{2\pi} \frac{1}{A\omega + B} \frac{1}{i(A\omega + B) + (C - D\omega - E\omega^2)} \quad (5.40)$$

The integrand above has no poles in the lower half of the complex plane but has a *half pole* at $\omega = -B/A$ on the real axis, thus using standard complex analysis we find

$$I(1) = \frac{1}{2(CA + BD - \frac{EB^2}{A})} \quad (5.41)$$

Then after some laborious, but straightforward algebra, we obtain that

$$\tilde{C}_s(\mathbf{q}) = T \frac{(2D\sigma q(\kappa[q^2 + m^2] + \lambda) + \alpha\kappa\lambda\Delta\psi^2)^2 + \kappa^2\Delta\psi^4(\mathbf{q} \cdot \mathbf{v})^2}{\sigma[q^2 + m^2] \left((2Dq\sigma(\kappa[q^2 + m^2] + \lambda) + \alpha\kappa\lambda\Delta\psi^2)^2 + \kappa(\kappa\sigma[q^2 + m^2] + \lambda\sigma)\Delta\psi^4(\mathbf{q} \cdot \mathbf{v})^2 \right)} \quad (5.42)$$

In the absence of driving, *i.e.* when $\mathbf{v} = \mathbf{0}$ we recover the equilibrium correlation function

$$\tilde{C}_s(\mathbf{q}) = \tilde{C}_{eq}(\mathbf{q}) = \frac{T}{\sigma[q^2 + m^2]}, \quad (5.43)$$

here we see that $1/m = \xi_{eq}$ is the so called capillary length, which is the equilibrium correlation length of the height fluctuations. We also notice that the correlation function for wave vectors perpendicular to the driving direction is simply the equilibrium one.

If we write $C_s(\mathbf{q}) = T/H_s(\mathbf{q})$ we can interpret $H_s(\mathbf{q})$ as an effective quadratic Hamiltonian for the height fluctuations, it is thus given by

$$H_s(\mathbf{q}) = \sigma[q^2 + m^2] + \frac{\kappa\lambda\sigma\Delta\psi^4(\mathbf{q} \cdot \mathbf{v})^2}{(2D\sigma q(\kappa[q^2 + m^2] + \lambda) + \alpha\kappa\lambda\Delta\psi^2)^2 + \kappa^2\Delta\psi^4(\mathbf{q} \cdot \mathbf{v})^2} \quad (5.44)$$

For small q we find

$$H_s(\mathbf{q}) = \sigma m^2 + \sigma q^2 \left(1 + \frac{v^2 \cos^2(\theta)}{\alpha^2 \lambda \kappa} \right), \quad (5.45)$$

where θ is the angle between the wave vector \mathbf{q} and the direction of the driving. This thus gives a direction dependent surface tension

$$\sigma_s(\theta) = \sigma \left(1 + \frac{v^2 \cos^2(\theta)}{v_0^2} \right) \quad (5.46)$$

where we have introduced the intrinsic velocity $v_0 = \sqrt{\alpha^2 \lambda \kappa}$ which depends on the microscopic *dynamical* quantity α associated with the model A dynamics of the field ϕ , as well as the microscopic static quantities κ (which generates the surface tension) and λ the coupling between the field ψ and ϕ . This appearance of dynamical and static quantities that are otherwise hidden in equal time correlation functions in equilibrium is already implicit in the works of Onsager [114] where it is used to compute the conductivity of Brownian electrolytes and the explicit expressions were derived using stochastic density functional theory in [121]. We also note that the universal thermal Casimir effect between model Brownian electrolyte systems driven by an electric field exhibits similar features, developing a dependency on both additional static and dynamical variables with respect to the equilibrium case [127]

However for this small q expansion we see that the microscopic quantities D , the diffusion constant of the field ϕ , and the order parameter jump $\Delta\psi$ do not appear.

From the above, we see that in the direction of the driving the surface tension increases and the fluctuations of the surface are thus suppressed. We may also write

$$H_s(\mathbf{q}) = \sigma_s(\theta)[q^2 + m_e^2(\theta)], \quad (5.47)$$

with

$$m_s^2(\theta) = \frac{m^2}{1 + \frac{v^2 \cos^2(\theta)}{v_0^2}}, \quad (5.48)$$

this corresponds to a correlation length

$$\xi_s = \xi_{eq} \sqrt{1 + \frac{v^2 \cos^2(\theta)}{v_0^2}}, \quad (5.49)$$

and we see that it is increased in the direction of the driving.

As we have just remarked that the above results appear to be independent of the order parameter jump $\Delta\psi$ and the diffusion constant D , however the next order correction to H_s for small q is given by

$$H_s(\mathbf{q}) = \sigma_s(\theta)[q^2 + m_e^2(\theta)] - \frac{4Dq\sigma^2(\lambda + \kappa m^2)(\mathbf{q} \cdot \mathbf{v})^2}{\alpha^3 \kappa^2 \lambda^2 \Delta\psi^2}, \quad (5.50)$$

and so the small \mathbf{q} expansion breaks down at $\Delta\psi = 0$, indeed one can see that the system has exactly the equilibrium correlation function when $\Delta\psi = 0$.

In the limit of large q we see that the effective Hamiltonian is given, to leading order, by the original equilibrium Hamiltonian and so the out of equilibrium driving has no effect on the most energetic modes of the system.

The results here predict that for unconfined surfaces the long range height fluctuations are described by an isotropic form of capillary wave theory with an anisotropic surface tension which is largest in the direction of driving. Numerical simulations of driven lattice gases in two dimensions [125] show a more drastic change upon driving and find $C_s(q) \sim 1/q$.⁶⁶ and thus a strong deviation from capillary wave theory.

5.1.3 A model of active interfaces

We can apply the results derived in the previous section to analyse a simple model for surfaces formed between two phases of active colloids. Activity is modelled by assuming that the colloidal field ψ has a temperature different to that of the solvent field ϕ . This models the effect that activity leads to enhanced colloidal diffusivity over and above the Brownian motion of particles due to thermal fluctuations [113].

In the absence of any driving the dynamical equations for the field ψ and ϕ become

$$\frac{\partial\psi(\mathbf{x}, t)}{\partial t} = D\nabla^2 \frac{\delta H}{\delta\psi(\mathbf{x})} + \sqrt{2DT_1} \nabla \cdot \boldsymbol{\eta}_1(\mathbf{x}, t) \quad (5.51)$$

$$\frac{\partial\phi(\mathbf{x}, t)}{\partial t} = -\alpha \frac{\delta H}{\delta\phi(\mathbf{x})} + \sqrt{2\alpha T_2} \eta_2(\mathbf{x}, t). \quad (5.52)$$

Following the same arguments as above we find that

$$\hat{C}(\mathbf{q}, \omega) = 2D \frac{\left[T_1 \frac{\Delta\psi^2}{2q} (\omega^2 + \alpha^2 \lambda^2) + T_2 \frac{\sigma \alpha D \lambda^2}{\kappa} \right]}{\left| i\omega \left[\frac{\alpha \lambda \Delta\psi^2}{2q} + \frac{\lambda \sigma D}{\kappa} + D\sigma(q^2 + m^2) \right] + [\alpha \lambda D\sigma(q^2 + m^2) - \frac{\Delta\psi^2}{2q} \omega^2] \right|^2}. \quad (5.53)$$

The equal time steady state height fluctuations thus have correlation function

$$\tilde{C}_s(q) = \frac{T_1}{\sigma(q^2 + m^2)} \left[1 - \left(1 - \frac{T_2}{T_1}\right) \frac{\lambda \sigma}{\kappa} \frac{1}{\frac{\alpha \lambda \Delta\psi^2}{2Dq} + \frac{\lambda \sigma}{\kappa} + \sigma(q^2 + m^2)} \right]. \quad (5.54)$$

We see, again, that the inclusion of a non-equilibrium driving changes the statistics of height fluctuations and leads to a steady state that depends on both dynamical variables D and α as well as static ones $\Delta\psi$, λ and κ that remain hidden in the equilibrium case. This phenomenon is again seen in the behavior of the universal thermal Casimir force between Brownian conductors held at different temperatures [128].

If we assume strong activity we can take the limit $T_1 \gg T_2$, in this case we find

$$\tilde{C}_s(q) = \frac{T_1}{\sigma(q^2 + m^2)} \frac{\frac{\alpha \lambda \Delta\psi^2}{2Dq} + \sigma(q^2 + m^2)}{\frac{\alpha \lambda \Delta\psi^2}{2Dq} + \frac{\lambda \sigma}{\kappa} + \sigma(q^2 + m^2)}. \quad (5.55)$$

Interpreted in terms of an effective Hamiltonian for an equilibrium system at the temperature T_1 the above gives

$$H_s(q) = \sigma(q^2 + m^2) \left[1 + \frac{\lambda \sigma}{\kappa} \frac{q}{\frac{\alpha \lambda \Delta\psi^2}{2D} + q\sigma(q^2 + m^2)} \right]. \quad (5.56)$$

In the case of an unconfined interface (where there is no gravitational effect on the surface fluctuations) *i.e.* $m = 0$ we see that for small q

$$H_s(q) \approx \sigma q^2 + \frac{2D\sigma^2}{\kappa \alpha \Delta\psi^2} q^3. \quad (5.57)$$

We see that the effective surface tension is not modified but a reduction of fluctuations due to the presence of the term in q^3 arises. As in the case of a driven system, we see that the large q behavior of the effective Hamiltonian is given by the equilibrium case where $T = T_1 = T_2$.

In the case where the interface is confined, we see that for small q one obtains

$$H_s(q) \approx \sigma m^2 \left[1 + \frac{2D\sigma}{\kappa \alpha \Delta\psi^2} q \right], \quad (5.58)$$

and thus at the largest length scales of the problem there is a qualitative departure from capillary wave behavior induced by activity, and the correlation length of height fluctuations at the largest length scales is given by

$$\xi_a = \frac{2D\sigma}{\kappa \alpha \Delta\psi^2}. \quad (5.59)$$

The above result should be compared with that obtained in [124] for systems with anisotropic thermal white noise, which breaks detailed balance and mimics random driving of the system parallel to the interface; for free interfaces it was found that $C_s(q) \sim 1/q$.

5.1.4 Conclusion

We have presented a model to analyse the effect of uniform driving on the dynamics of the interface in a two phase system. In order to generate a non-equilibrium state a second *hidden* order parameter was introduced. This models the behaviour of a local or solvent degree of freedom which is not influenced by the driving field. In this way, we obtain out of equilibrium interface fluctuations which are described by Gaussian statistics as found in the experimental study of [19]. The agreement with this experimental study also extends to qualitative agreement with the increase of the effective surface tension in the direction of driving and also an increase in the correlation length of the height fluctuations with respect to a non-driven equilibrium interface. However, we note that numerical simulations of a sheared Ising interface [72, 104] also reveal a reduction of interface fluctuations but the lateral correlation length is found to be reduced.

The basic idea underlying this study would be interesting to apply to a number of possible variants of this model, for instance both the dynamics of the main field ϕ and the solvent field ϕ could be varied. To make a direct link with driven colloidal interfaces one should study model H type dynamics for the main field ϕ and other variants for the dynamics of the solvent field ϕ could also be considered.

As mentioned above, in lattice based models driving induces non-equilibrium states even in the simple Ising lattice gas. A model analogous to that studied here can be formulated in a lattice based systems using the Hamiltonian

$$H = -J \sum_{(ij)} S_i S_j (1 + \sigma_{(ij)}), \quad (5.60)$$

where $S_i = \pm 1$ are Ising spins at the lattice sites i , and $\sigma_{(ij)} = \pm 1$ are Ising like dynamical solvent variables associated with the lattice links (ij) . The static partition function is given by

$$Z = \text{Tr}_{\sigma_{ij}, S_i} \exp \left[\beta J \sum_{(ij)} S_i S_j (1 + \sigma_{(ij)}) \right], \quad (5.61)$$

and the trace over the solvent variables can be trivially carried out to give

$$Z = \text{Tr}_{S_i} \left(\exp \left[\beta J \sum_{(ij)} S_i S_j \right] \prod_{(ij)} 2 \cosh(\beta J S_i S_j) \right) = [2 \cosh(\beta J)]^L \text{Tr}_{S_i} \exp(\beta J \sum_{(ij)} S_i S_j), \quad (5.62)$$

where L is the number of links on the lattice of the model. We thus see that the underlying effective static model is precisely the zero field Ising model.

This model can then be driven in a number of ways, for instance using conserved Kawasaki dynamics for the Ising spins to model diffusive dynamics in the presence of a uniform driving field parallel to the surface between the two phases at a temperature below the ferromagnetic ordering temperature T_c . The dynamics of the Ising spins on the lattice links can be given by non-conservative single spin flip, for instance Glauber, dynamics to keep the analogy with the continuum model discussed in the paper but diffusive dynamics or indeed a mixture of diffusive and non-conserved dynamics could be implemented. It would be interesting to see to what extent this modification of the driven lattice gas model affects the non-equilibrium driven states that arise.

It is also clear that this lattice model can be used to simulate the effect of activity where the Ising spins S_1 corresponding to the colloid field undergo Kawasaki dynamics at the temperature T_1 where as the link variables $\sigma_{(ij)}$ undergo single spin flip non-conserved dynamics at the temperature T_2 .

5.2 Driven SOS model

Common experience with wind generated waves shows us that the effective surface tension of driven interfaces decrease with driving, as seen in a homemade wind generation system in Fig 5.2. The difference in this kind of system comes from the way the interface is driven. In the previous section, the whole system was driven, while in wind generated waves only the upper phase has an hydrodynamic flow, meaning that the velocity field is

$$\mathbf{v}(\mathbf{x}, t) = \Theta(h(\mathbf{r}, t))\mathbf{e}_x \quad (5.63)$$

where $\Theta(\cdot)$ is the Heaviside step function. While in the previous section, in order to break the Galilean invariance, we were forced to couple the colloidal field $\phi(\mathbf{x}, t)$ with a solvent field $\phi(\mathbf{x}, t)$, this kind of velocity field does not require such artifact to give out-of-equilibrium steady states only with the colloidal field. Even though the full computation for this new system was not carried, numerical simulations on SOS models under Kawasaki dynamics allows for direct study. In the case of a uniform driving in lattice based numerical simulations, the invariance is broken because of the discrete-time nature of the algorithm. In a SOS model under Kawasaki dynamics, the implementation of a constant driving flow is as follows. From the configuration C a configuration C' is chosen as explained in Sec 2.2.2, meaning a random site i and its nearest neighbor $i \pm 1$ are chosen in such a way that the first one give one of its particles to the second. Under a flow, the difference of energy between both states is

$$\Delta E_d = \Delta E_{eq} \pm v \quad (5.64)$$

where v is the intensity of the drive, and the sign depends on the direction of the flow. For example, if the flow goes to the right, then every configuration which moves a particle to the right will have an additional energy $+v$, while if the particle goes against the flow, it will have an additional energy $-v$. We suppose here that the uniform driving in SOS systems is equal to driving in Eq. (5.63) since there is no bulk behaviour.

Implementing a shear $v|L/2 - y|$ as in Fig 1.10 is tricky, because it requires to know the height of the particle and thus have access to bulk information which does not exist in SOS models. Here, only the particles at the interface can move and change height accordingly to the interface's height of the neighboring site. The vertical movement of the particle, couple to the horizontal one, is what makes the SOS model different to the Ising one, and physical arguments forbids the use of h_i , h_{i+1} or even the average $\frac{h_i + h_{i+1}}{2}$ as the shear contribution might be zero depending of the configuration, even though it should always be present.

Under periodic boundary conditions, the direction of the flow should not alter the steady state. The average total energy has thus to be an even function with respect to the drive v , ie

$$\langle E(v) \rangle = \langle E(-v) \rangle \quad (5.65)$$

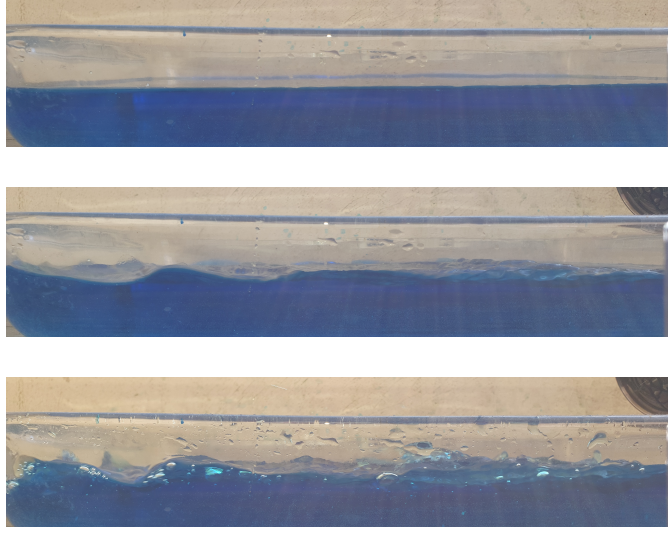


Figure 5.2: Homemade wind generated waves with a hair dryer, where the water has been coloured in blue for contrast. The stronger the wind output, the larger the interface width becomes.

and same goes for the surface tension $\sigma(\nu)$. From Eqs. (1.41) and (1.43), the surface tension is

$$\sigma(\nu) = \int_{-\infty}^{\infty} dz J \left(\frac{d \tanh\left(\frac{z}{\xi_{\perp}(\nu)}\right)}{dz} \right)^2 = \int_{-\infty}^{\infty} dz J \frac{1}{\cosh^4\left(\frac{z}{\xi_{\perp}(\nu)}\right) \xi_{\perp}^2} \quad (5.66)$$

where $\xi_{\perp}(\nu)$ is the interfacial correlation length. This interface width has the same qualitative behaviour as the interface width $\langle w \rangle = \sqrt{\langle h^2 \rangle - \langle h \rangle^2}$.

In Fig 5.3 we show some snapshots of numerical simulations under Kawasaki dynamics, and visually see how the interface width effectively increases with the driving for the same mean value $\langle h \rangle$, while in Fig 5.4 we plot the interface width and the surface tension with respect to the drive. The first thing we notice is that the interface width increases with the imposed driving in an almost linear way, as does the mean height of wind generated waves with respect to the wind surface velocity [129]. The second thing we notice is that there are a change of regime at $\nu = 2J$ and $\nu = 4J$, with a net change in the derivative. The change of energy ΔE has values in $[-4, -2, 0, 2, 4]$, so we see that there are three regimes : the weak driving regime for $\nu < 2J$, the middle regime for $2J < \nu < 4J$ where some moves with adding energy to the system are always accepted, and the strong driving regime for $\nu > 4J$ where all moves adding energy are accepted, ending with a saturation when the bond energy becomes negligible with respect to the driving. This discontinuity in the derivative of the interface width is not seen in the GSOS model, which exhibits a smoother while qualitatively similar behaviour.

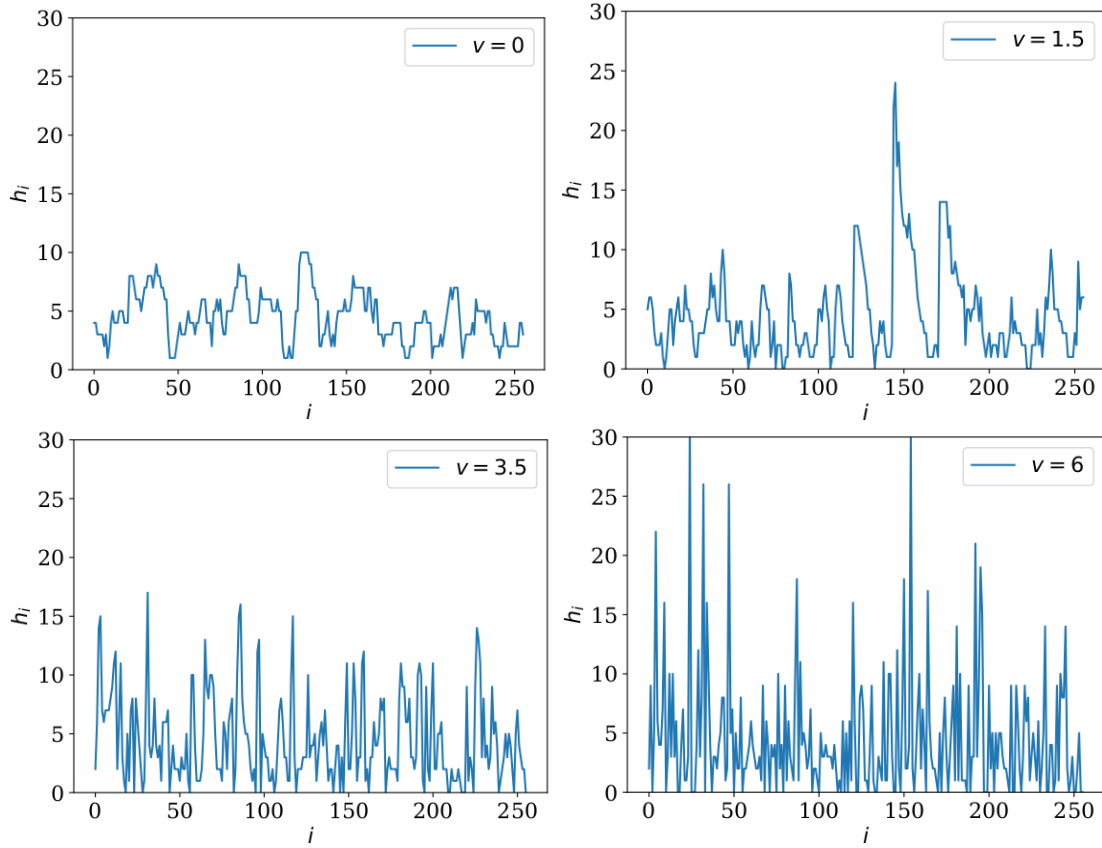


Figure 5.3: Snapshot of the SOS interface with Kawasaki dynamics at $\beta = 1$ and $\langle h \rangle = 4.51$ for different drivings using Eq (5.64).

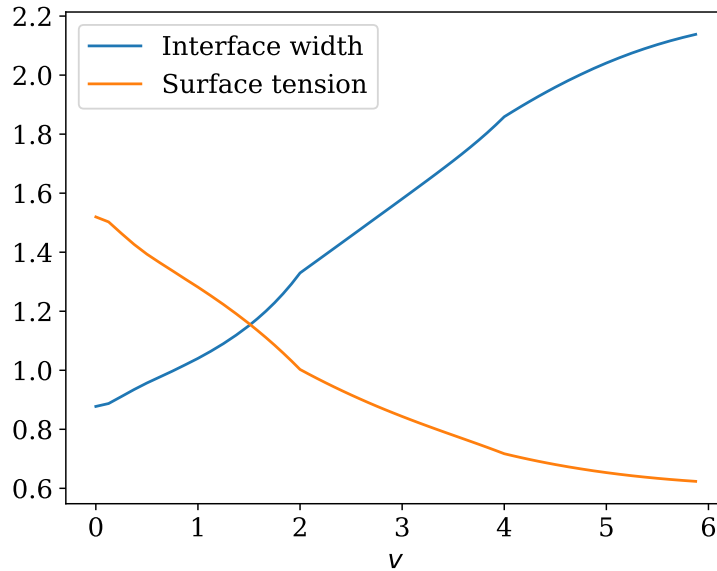


Figure 5.4: Interface width $w = \sqrt{\langle h^2 \rangle - \langle h \rangle^2}$ and surface tension σ computed from the integral (5.66) with respect to the drive v , with $L' = 256$, $L = 200$, $\langle h \rangle = 4.5$, and $\beta = J = 1$ for $5 \cdot 10^7$ MC steps.

5.3 Conclusions

We presented two models to analyse the effect of uniform driving on the dynamics of the interface in a two phase system. Using dynamics derived from model B [9, 29] and adding a coupling field from model A in order to remove galilean invariance in the equations, we found that the driving does increase the effective surface tension in the direction of driving and increases the correlation length along the interface with respect to a non-driven equilibrium interface, as seen in colloid experiments [19] and numerical simulations [104]. This work resulted in a published article [17].

We also studied the effect of driving in SOS models, and found that contrary to Ising systems [72] and model C systems, the driving does reduce the surface tension in a similar fashion as wind generated waves [129]. We conjecture that solving model B with the velocity field $\mathbf{v}(\mathbf{x}, t) = \Theta(h(\mathbf{r}, t))\mathbf{e}_x$ would lead to similar behaviour, and that the physical difference between the two systems is how the interface is sheared : in the model C case the bulk is driven while in wind generated waves only particles at the interface are driven. SOS models provide a direct way to simulation such driving, and we propose the following implementation for the Ising model. At low temperature in a phase separated system, the interface height at point \mathbf{r} is defined as $h(\mathbf{r}) = \sum_{z=0}^L \sigma(\mathbf{r}, z)$. To mimic wind driving, only spins which are over the interface would be affected by the driving.

In this chapter, we have shown how out-of-equilibrium steady states can exhibit similar behaviour as equilibrium systems, with a rescaling of the system's observables. The primary goal of the thesis was to study the effect of out-of-equilibrium steady states in confined geometry, and the results shown in the chapter show no compelling evidence of new physics to be found there.

Bibliography

- [1] L. Landau and E. Lifchitz. *Physique théorique - T9 Physique Statistique*. Éditions Mir Moscou. 1990. [xiii](#), [5](#)
- [2] N. Goldenfeld. *Lectures on Phase Transitions and the Renormalization Group*. CRC Press, 1 edition, March 2018. [xiii](#), [16](#), [70](#)
- [3] A. Gambassi. The Casimir effect: From quantum to critical fluctuations. *Journal of Physics: Conference Series*, 161:012037, April 2009. [xiii](#), [42](#), [44](#), [64](#)
- [4] M. Niss. History of the Lenz-Ising Model 1920–1950: From Ferromagnetic to Cooperative Phenomena. *Arch. Hist. Exact Sci.*, 59(3):267–318, March 2005. [xiii](#), [15](#), [26](#), [67](#)
- [5] D. B. Abraham and A. Martin-Löf. The transfer matrix for a pure phase in the two-dimensional Ising model. *Commun.Math. Phys.*, 32(3):245–268, September 1973. [xiii](#), [18](#), [22](#), [26](#)
- [6] G. H. Gilmer and P. Bennema. Simulation of Crystal Growth with Surface Diffusion. *Journal of Applied Physics*, 43(4):1347–1360, April 1972. [xiii](#), [20](#), [26](#), [67](#), [73](#)
- [7] D. J. Amit and V. M. Mayor. *Field theory, the renormalization group, and critical phenomena: graphs to computers*. World Scientific, Singapore ; New Jersey, 3rd ed edition, 2005. [xiii](#), [42](#)
- [8] T. Matsubara. A New Approach to Quantum-Statistical Mechanics. *Progress of Theoretical Physics*, 14(4):351–378, October 1955. [xiii](#), [42](#), [45](#), [64](#)
- [9] A. J. Bray, A. Cavagna, and R. D. M. Travasso. Interface fluctuations under shear. *Phys. Rev. E*, 64(1):012102, June 2001. [xiv](#), [xv](#), [10](#), [26](#), [76](#), [89](#)
- [10] M. E. J. Newman and G. T. Barkema. *Monte Carlo Methods in Statistical Physics*. Oxford University Press, Oxford, New York, February 1999. [xiv](#), [26](#), [28](#), [29](#), [36](#), [67](#), [73](#)
- [11] O. Vasilyev, A. Gambassi, A. Maciołek, and S. Dietrich. Universal scaling functions of critical Casimir forces obtained by Monte Carlo simulations. *Physical Review E*, 79(4), April 2009. [xiv](#), [33](#), [36](#)
- [12] D. Lopes Cardozo, H. Jacquin, and P. C. W. Holdsworth. Critical Casimir forces in a magnetic system: An experimental protocol. *Physical Review B*, 90(18), November 2014. [xiv](#), [xv](#), [35](#), [36](#), [64](#)

- [13] K. A. Milton. *The Casimir effect: Physical manifestation of zero-point energy*. World Scientific Pub, 1st edition, 2001. [xiv](#)
- [14] H. B. G. Casimir. On the attraction between two perfectly conducting plates. *Royal Netherlands Academy of Arts and Sciences*, 51(7):793–498, 1948. [xiv](#), [37](#), [38](#), [39](#), [64](#)
- [15] I. M. Lifshitz and A. M. Kosevich. On the theory of magnetic susceptibility of metals at low temperatures. *Zh. Eksp. Teor. Fiz.*, 53(6):730–742, 1955. [xiv](#), [40](#), [64](#)
- [16] V. Privman. Finite-Size Properties of the Angle-Dependent Surface Tension of Rough Interfaces. *Physical Review Letters*, 61(2):4, 1988. [xiv](#), [xv](#), [45](#), [47](#), [64](#)
- [17] D. S. Dean, P. Gersberg, and P. C. W. Holdsworth. The effect of driving on model C interfaces. *Journal of Statistical Mechanics: Theory and Experiment*, 2020(3):033206, March 2020. [xv](#), [75](#), [89](#)
- [18] P. C. Hohenberg and B. I. Halperin. Theory of dynamic critical phenomena. *Rev. Mod. Phys.*, 49(3):435–479, July 1977. [xv](#), [1](#), [6](#), [26](#), [71](#), [76](#)
- [19] D. Derks, D. G. A. L. Aarts, D. Bonn, H. N. W. Lekkerkerker, and A. Imhof. Suppression of Thermally Excited Capillary Waves by Shear Flow. *Physical Review Letters*, 97(3), July 2006. [xv](#), [24](#), [25](#), [26](#), [75](#), [76](#), [85](#), [89](#)
- [20] Mésocentre de Calcul Intensif Aquitain. <https://redmine.mcia.fr/projects/mcia>. [xv](#), [27](#)
- [21] P. Gersberg. Github with all my programs, 2020. <https://github.com/Bulbille/Curta>. [xv](#), [27](#)
- [22] A. J. Bray. Theory of phase-ordering kinetics. *Advances in Physics*, 43(3):357–459, June 1994. [1](#), [26](#)
- [23] L. Onsager. Crystal Statistics. I. A Two-Dimensional Model with an Order-Disorder Transition. *Physical Review*, 65(3-4):117–149, February 1944. [2](#), [16](#)
- [24] J. A. Tuszyński, R. Paul, and R. Chatterjee. Exact solutions to the time-dependent Landau-Ginzburg model of phase transitions. *Physical Review B*, 29(1):380–386, January 1984. [7](#)
- [25] J. W. Cahn and J. E. Hilliard. Free Energy of a Nonuniform System. I. Interfacial Free Energy. *The Journal of Chemical Physics*, 28(2):11, February 1958. [7](#), [8](#), [26](#)
- [26] Y. Hennequin, D. G. A. L. Aarts, J. H. van der Wiel, G. Wegdam, J. Eggers, H. N. W. Lekkerkerker, and Daniel Bonn. Drop Formation by Thermal Fluctuations at an Ultralow Surface Tension. *Physical Review Letters*, 97(24), December 2006. [8](#)
- [27] J. Atencia and D. J. Beebe. Controlled microfluidic interfaces. *Nature*, 437(7059):648–655, September 2005. [8](#)
- [28] H. W. Diehl, D. M. Kroll, and H. Wagner. The interface in a Ginsburg-Landau-Wilson model: Derivation of the drumhead model in the low-temperature limit. *Zeitschrift fur Physik B Condensed Matter and Quanta*, 36(4):329–333, December 1980. [9](#)

- [29] A. J. Bray, A. Cavagna, and R. D. M. Travasso. Interface fluctuations, Burgers equations, and coarsening under shear. *Physical Review E*, 65(1), December 2001. [10](#), [26](#), [76](#), [89](#)
- [30] S. F. Edwards and D. R. Wilkinson. The Surface Statistics of a Granular Aggregate. *Proceedings of the Royal Society of London. Series A, Mathematical and Physical Sciences*, 381(1780):17–31, 1982. [11](#), [26](#), [67](#)
- [31] T. Halpin-Healy and Y-C. Zhang. Kinetic roughening phenomena, stochastic growth, directed polymers and all that. Aspects of multidisciplinary statistical mechanics. *Physics Reports*, 254(4-6):215–414, March 1995. [11](#), [67](#)
- [32] R. Paul, S. Puri, and H. Rieger. Domain growth in Ising systems with quenched disorder. *Physical Review E*, 71(6), June 2005. [12](#)
- [33] D. A. Huse. Corrections to late-stage behavior in spinodal decomposition: Lifshitz-Slyozov scaling and Monte Carlo simulations. *Physical Review B*, 34(11):7845–7850, December 1986. [15](#)
- [34] M. Niss. History of the Lenz–Ising Model 1950–1965: from irrelevance to relevance. *Arch. Hist. Exact Sci.*, 63(3):243, May 2009. [xiii](#), [15](#), [26](#), [67](#)
- [35] R. Gupta, J. DeLapp, G. G. Batrouni, G. C. Fox, C. F. Baillie, and J. Apostolakis. Phase Transition in the 2 D XY Model. *Physical Review Letters*, 61(17):1996–1999, October 1988. [15](#)
- [36] M. Le Bellac, F. Mortessagne, and G. G Batrouni. *Equilibrium and Non-Equilibrium Statistical Thermodynamics*. Cambridge University Press, 2004. [15](#), [26](#)
- [37] M. Aizenman. Proof of the Triviality of ϕ^4 Field Theory and Some Mean-Field Features of Ising Models for $d > 4$. *Physical Review Letters*, 47(1):1–4, July 1981. [15](#)
- [38] L.J. de Jongh and A.R. Miedema. Experiments on simple magnetic model systems. *Advances in Physics*, 23(1):1–260, January 1974. [16](#)
- [39] W.P. Wold. The Ising Model and Real Magnetic Materials. *Brazilian Journal of Physics*, 30(4):794–810, December 2000. [16](#)
- [40] H. Ikeda and K. Hirakawa. Neutron scattering study of two-dimensional Ising nature of K₂CoF₄. *Solid State Communications*, 14:529–532, November 1973. [16](#)
- [41] J. Frohlich. On the triviality of $\lambda\phi^4$ theories and the approach to the critical point in $D > 4$ dimensions. *Nuclear Physics B*, 200:281–296, August 1981. [16](#)
- [42] A. L. Talapov and H. W. J. Blöte. The magnetization of the 3D Ising model. *Journal of Physics A: Mathematical and General*, 29(17):5727–5733, September 1996. [16](#)
- [43] T. Preis, P. Virnau, W. Paul, and J. J. Schneider. GPU accelerated Monte Carlo simulation of the 2D and 3D Ising model. *Journal of Computational Physics*, 228(12):4468–4477, July 2009. [16](#)

- [44] J. Stecki, A. Maciol/ek, and K. Olausson. Magnetization profiles of the planar fluctuating interface in a $d = 2$ Ising strip. *Physical Review B*, 49(2):1092–1103, January 1994. [17](#)
- [45] H. L. Richards, M. A. Novotny, and P. E. Rikvold. Numerical transfer-matrix study of surface-tension anisotropy in Ising models on square and cubic lattices. *Phys. Rev. B*, 48(19):14584–14598, November 1993. [18](#)
- [46] D. B. Abraham and P. Reed. Interface profile of the Ising ferromagnet in two dimensions. *Commun.Math. Phys.*, 49(1):35–46, February 1976. [18](#), [67](#)
- [47] R. H. Swendsen. Roughening transition in the solid-on-solid model. *Physical Review B*, 15(2):689–692, January 1977. [19](#), [67](#)
- [48] J. M. J. van Leeuwen and H. J. Hilhorst. Pinning of a rough interface by an external potential. *Physica A: Statistical Mechanics and its Applications*, 107(2):319–329, June 1981. [19](#)
- [49] M. Elwenspoek and J. P. van der Eerden. Kinetic roughening and step free energy in the solid-on-solid model and on naphthalene crystals. *Journal of Physics A: Mathematical and General*, 20(3):669–678, February 1987. [20](#)
- [50] M. R. Wilby, D. D. Vvedensky, and A. Zangwill. Scaling in a solid-on-solid model of epitaxial growth. *Phys. Rev. B*, 46(19):12896–12898, November 1992. [20](#), [67](#)
- [51] D. Boal. *Mechanics of the Cell: Second edition*. page 624, 2012. [20](#)
- [52] G Gompper and D. M. Kroll. Steric Interactions in Multimembrane Systems: A Monte Carlo Study. *Europhysics Letters (EPL)*, 9(1):59–64, May 1989. [20](#)
- [53] M. E. Fisher. Walks, walls, wetting, and melting. *Journal of Statistical Physics*, 34(5/6):63, October 1983. [20](#)
- [54] V. Privman and N. M. Švrakić. Transfer-Matrix Spectrum for Systems with Interfaces. *Phys. Rev. Lett.*, 62(6):633–636, February 1989. [20](#)
- [55] Y. Kim, D. K. Park, and L. M. Kim. Conserved growth in a restricted solid-on-solid model. *J. Phys. A: Math. Gen.*, 27(15):L533, 1994. [20](#)
- [56] I. Vaysburd. Critical RSOS models in external fields. *Nuclear Physics B*, 446(3):387–404, July 1995. [20](#)
- [57] H. J. F. Knops. Exact Relation between the Solid-on-Solid Model and the XY Model. *Phys. Rev. Lett.*, 39(12):766–769, September 1977. [20](#)
- [58] G. Schehr and S. N. Majumdar. Universal asymptotic statistics of maximal relative height in one-dimensional solid-on-solid models. *Phys. Rev. E*, 73(5):056103, May 2006. [21](#)
- [59] R. H. Swendsen. Monte Carlo studies of the interface roughening transition. *Physical Review B*, 15(11):5421–5431, June 1977. [20](#)

- [60] A. L. Owczarek and T. Prellberg. Exact solution of the discrete (1+1)-dimensional SOS model with field and surface interactions. *J Stat Phys*, 70(5-6):1175–1194, March 1993. [21](#)
- [61] S. N. Majumdar and A. Comtet. Airy Distribution Function: From the Area Under a Brownian Excursion to the Maximal Height of Fluctuating Interfaces. *J Stat Phys*, 119(3-4):777–826, May 2005. [21](#)
- [62] M. Siegert and M. Plischke. Scaling behavior of driven solid-on-solid models with diffusion. *J. Phys. I France*, 3(6):1371–1376, June 1993. [22](#), [67](#)
- [63] P. A. Pearce and K. A. Seaton. Exact solution of cyclic solid-on-solid lattice models. *Annals of Physics*, 193(2):326–366, August 1989. [22](#)
- [64] A. Girot, J. Petit, R. Saiseau, T. Guérin, H. Chraïbi, U. Delabre, and J. P. Delville. Conical Interfaces between Two Immiscible Fluids Induced by an Optical Laser Beam. *Physical Review Letters*, 122(17), May 2019. [24](#)
- [65] D. Derks, H. Wisman, A. van Blaaderen, and A. Imhof. Confocal microscopy of colloidal dispersions in shear flow using a counter-rotating cone-plate shear cell. *Journal of Physics: Condensed Matter*, 16(38):S3917–S3927, September 2004. [24](#), [26](#)
- [66] L. Berthier and J-L. Barrat. Nonequilibrium dynamics and fluctuation-dissipation relation in a sheared fluid. *The Journal of Chemical Physics*, 116(14):6228–6242, April 2002. [24](#)
- [67] L Berthier and J-L. Barrat. Shearing a Glassy Material: Numerical Tests of Nonequilibrium Mode-Coupling Approaches and Experimental Proposals. *Physical Review Letters*, 89(9), August 2002. [24](#)
- [68] K-T. Leung and J. L. Cardy. Field theory of critical behavior in a driven diffusive system. *J Stat Phys*, 44(3-4):567–588, August 1986. [24](#)
- [69] A. J. Bray and a. Cavagna. Coarsening dynamics of a nonconserved field advected by a uniform shear flow. *Journal of Physics A: Mathematical and General*, 33(33):L305–L311, August 2000. [24](#)
- [70] M. Thiébaud and T. Bickel. Nonequilibrium fluctuations of an interface under shear. *Physical Review E*, 81(3), March 2010. [26](#), [76](#)
- [71] T. H. R. Smith. *Driven interfaces in the Ising model*. PhD thesis, University of Bristol, 2010. [26](#)
- [72] T. H. R. Smith, O. Vasilyev, D. B. Abraham, A. Maciołek, and M. Schmidt. Interfaces in Driven Ising Models: Shear Enhances Confinement. *Phys. Rev. Lett.*, 101(6):067203, August 2008. [26](#), [67](#), [85](#), [89](#)
- [73] T. H. R. Smith, O. Vasilyev, D. B. Abraham, A. Maciołek, and M. Schmidt. Interfaces in confined Ising models: Kawasaki, Glauber and sheared dynamics. *Journal of Physics: Condensed Matter*, 20(49):494237, December 2008. [26](#), [75](#), [76](#)

- [74] V. Privman and N. M. Švrakić. Asymptotic degeneracy of the transfer matrix spectrum for systems with interfaces: Relation to surface stiffness and step free energy. *J Stat Phys*, 54(3-4):735–754, February 1989. [26](#)
- [75] N. Metropolis and S. Ulam. The Monte Carlo Method. *Journal of the American Statistical Association*, 44(247):335–341, September 1949. [27](#), [36](#), [67](#), [70](#), [73](#)
- [76] S. Wansleben and D. P. Landau. Monte Carlo investigation of critical dynamics in the three-dimensional Ising model. *Physical Review B*, 43(7):6006–6014, March 1991. [28](#)
- [77] R. J. Glauber. Time-Dependent Statistics of the Ising Model. *Journal of Mathematical Physics*, 4(2):294–307, February 1963. [29](#), [36](#)
- [78] K. Kawasaki. Diffusion Constants near the Critical Point for Time-Dependent Ising Models. I. *Physical Review*, 145(1):224–230, May 1966. [32](#), [36](#)
- [79] M. Ankerl. Fast random bool in C++. <https://martin.ankerl.com/2018/12/08/fast-random-bool/>. [36](#)
- [80] R. Feynman. Feynman Lectures on Physics, Mainly Electromagnetism and Matter., 1963. [37](#)
- [81] C. Stubenrauch and R. von Klitzing. Disjoining pressure in thin liquid foam and emulsion films—new concepts and perspectives. *Journal of Physics: Condensed Matter*, 15(27):R1197–R1232, July 2003. [39](#)
- [82] B. Carazza and G. P. Guidetti. The Casimir Electron Model. *Archive for History of Exact Sciences*, 35(3):273–279, 1986. [39](#)
- [83] T. H. Boyer. Quantum Electromagnetic Zero-Point Energy of a Conducting Spherical Shell and the Casimir Model for a Charged Particle. *Physical Review*, 174(5):1764–1776, October 1968. [40](#)
- [84] K. A. Milton, L. L. DeRaad, and J. Schwinger. Casimir self-stress on a perfectly conducting spherical shell. *Annals of Physics*, 115(2):388–403, October 1978. [40](#)
- [85] M. E. Bowers and C. R. Hagen. Casimir energy of a spherical shell. *Physical Review D*, 59(2), December 1998. [40](#)
- [86] J. Schwinger, L. L. DeRaad, and K. A. Milton. Casimir Effect in Dielectrics. *Annals of Physics*, pages 1–23, 1978. [40](#)
- [87] J. Schwinger. Casimir energy for dielectrics. *Proceedings of the National Academy of Sciences*, 89(9):4091–4093, May 1992. [40](#)
- [88] S.M. Rytov, Y. A. Kravtsov, and V.I. Tatarskii. *Principles of Statistical Radiophysics Vol 3. Elements of Random Fields*. Springer, Berlin, 1989. [40](#), [64](#)
- [89] N.G. Van Kampen, B.R.A. Nijboer, and K. Schram. On the macroscopic theory of Van der Waals forces. *Physics Letters A*, 26(7):307–308, February 1968. [40](#)

- [90] B. W. Ninham and V. A. Parsegian. van der Waals Forces. 10:18, 1970. [40](#)
- [91] A. Gambassi, A. Maciołek, C. Hertlein, U. Nellen, L. Helden, C. Bechinger, and S. Dietrich. Critical Casimir effect in classical binary liquid mixtures. *Physical Review E*, 80(6), December 2009. [44](#)
- [92] H. Kleinert. *Path Integrals in Quantum Mechanics, Statistics, Polymer Physics, and Financial Markets*. World Scientific, Singapore, 5th edition, 2009. [45](#)
- [93] C. Cohen-Tannoudji, B. Diu, and F. Laloë. *Mécanique quantique*, volume 1. EDP-Sciences, 2018. [47](#)
- [94] J. R. Albright. Integrals of products of Airy functions. *Journal of Physics A: Mathematical and General*, 10(4):485–490, April 1977. [51](#)
- [95] R. Bissacot and L. Cioletti. Phase Transition in Ferromagnetic Ising Models with Non-uniform External Magnetic Fields. *J Stat Phys*, 139(5):769–778, June 2010. [57](#)
- [96] R. A. Guyer. Sine-Gordon chain as a model for a two-dimensional interface. *Phys. Rev. B*, 20(10):4375–4381, November 1979. [57](#), [60](#), [67](#)
- [97] N. M. Švrakić, V. Privman, and D. B. Abraham. Finite-size corrections for inclined interfaces in two dimensions: Exact results for Ising and solid-on-solid models. *Journal of Statistical Physics*, 53(5-6):1041–1059, December 1988. [57](#), [62](#), [65](#)
- [98] V. Privman and N. M. Švrakić. Finite-size scaling for the restricted solid-on-solid model of the two-dimensional wetting transition. *Physical Review B*, 37(7):3713–3715, March 1988. [57](#)
- [99] G.H. Gilmer and P. Bennema. Computer simulation of crystal surface structure and growth kinetics. *Journal of Crystal Growth*, 13-14:148–153, May 1972. [67](#), [73](#)
- [100] H. Müller-Krumbhaar. Kinetic Gaussian model. *Zeitschrift für Physik B*, 25:287–292, 1976. [67](#)
- [101] C.F. Baillie, W. Janke, and D.A. Johnston. Solid on solid on fluid lattices. *Physics Letters B*, 318(3):424–432, December 1993. [67](#)
- [102] B. Schmittmann and R.K.P Zia. Driven diffusive systems. An introduction and recent developments. *Physics Reports*, 301(1-3):45–64, July 1998. [67](#), [76](#)
- [103] M. Müller and G. Münster. Profile and Width of Rough Interfaces. *J Stat Phys*, 118(3-4):669–686, February 2005. [67](#)
- [104] T. H. R. Smith, O. Vasilyev, A. Maciołek, and M. Schmidt. Lateral transport of thermal capillary waves. *EPL*, 89(1):10006, 2010. [67](#), [75](#), [76](#), [85](#), [89](#)
- [105] H. N. V. Temperley. Statistical mechanics and the partition of numbers II. The form of crystal surfaces. *Mathematical Proceedings of the Cambridge Philosophical Society*, 48(4):683–697, October 1952. [67](#), [73](#)

- [106] T. W. Burkhardt. Localisation-delocalisation transition in a solid-on-solid model with a pinning potential. *J. Phys. A: Math. Gen.*, 14(3):L63, 1981. [68](#)
- [107] S. T. Chui and J. D. Weeks. Pinning and roughening of one-dimensional models of interfaces and steps. *Phys. Rev. B*, 23(5):2438–2441, March 1981. [68](#), [73](#)
- [108] C. K. Wang, J. J. Seaborg, and S. P. Lin. Instability of multi-layered liquid films. *Physics of Fluids*, 21(10):1669, 1978. [70](#)
- [109] M. Bonizzi and R.I. Issa. On the simulation of three-phase slug flow in nearly horizontal pipes using the multi-fluid model. *International Journal of Multiphase Flow*, 29(11):1719–1747, November 2003. [70](#)
- [110] A. Crisanti, M. Falcioni, A. Provenzale, P. Tanga, and A. Vulpiani. Dynamics of passively advected impurities in simple two-dimensional flow models. *Physics of Fluids A: Fluid Dynamics*, 4(8):1805–1820, August 1992. [71](#)
- [111] W. Dieterich, P. Fulde, and I. Peschel. Theoretical models for superionic conductors. *Advances in Physics*, 29(3):527–605, June 1980. [72](#)
- [112] S. Katz, J. L. Lebowitz, and H. Spohn. Nonequilibrium steady states of stochastic lattice gas models of fast ionic conductors. *Journal of Statistical Physics*, 34(3-4):497–537, February 1984. [72](#), [76](#)
- [113] A. Y. Grosberg and J.-F. Joanny. Nonequilibrium statistical mechanics of mixtures of particles in contact with different thermostats. *Physical Review E*, 92(3), September 2015. [72](#), [83](#)
- [114] L. Onsager, P. C. Hemmer, and H. Holden. *The Collected Works of Lars Onsager: With Commentary*, volume 17. World Scientific, world scientific series in 20th century physics edition, 1996. [75](#), [82](#)
- [115] J. Dzubiella, G. P. Hoffmann, and H. Löwen. Lane formation in colloidal mixtures driven by an external field. *Physical Review E*, 65(2), January 2002. [75](#)
- [116] J. Chakrabarti, J. Dzubiella, and H. Löwen. Dynamical instability in driven colloids. *Europhysics Letters (EPL)*, 61(3):415–421, February 2003. [75](#)
- [117] J. Chakrabarti, J. Dzubiella, and H. Löwen. Reentrance effect in the lane formation of driven colloids. *Physical Review E*, 70(1), July 2004. [75](#)
- [118] K. R. Sütterlin, A. Wysocki, A. V. Ivlev, C. R ath, H. M. Thomas, M. Rubin-Zuzic, W. J. Goedheer, V. E. Fortov, A. M. Lipaev, V. I. Molotkov, O. F. Petrov, G. E. Morfill, and H. Löwen. Dynamics of Lane Formation in Driven Binary Complex Plasmas. *Physical Review Letters*, 102(8), February 2009. [75](#)
- [119] T. Glanz and H. Löwen. The nature of the laning transition in two dimensions. *Journal of Physics: Condensed Matter*, 24(46):464114, November 2012. [75](#)

- [120] K. Klymko, P. L. Geissler, and S. Whitelam. Microscopic origin and macroscopic implications of lane formation in mixtures of oppositely driven particles. *Physical Review E*, 94(2), August 2016. [75](#)
- [121] V. Démery and D. S. Dean. The conductivity of strong electrolytes from stochastic density functional theory. *J. Stat. Mech.*, 2016(2):023106, 2016. [76](#), [82](#)
- [122] A. Poncet, O. Bénichou, V. Démery, and G. Oshanin. Universal Long Ranged Correlations in Driven Binary Mixtures. *Physical Review Letters*, 118(11), March 2017. [76](#)
- [123] D. S. Dean, I. T. Drummond, and R. R. Horgan. Renormalization of drift and diffusivity in random gradient flows. *Journal of Physics A: Mathematical and General*, 29(24):7867–7879, December 1996. [76](#)
- [124] R. K. P. Zia and K-T. Leung. Interfacial correlation and dispersion in a non-equilibrium steady state system. *Journal of Physics A: Mathematical and General*, 24(24):L1399–L1404, December 1991. [76](#), [84](#)
- [125] K-T. Leung and R. K. P. Zia. Anomalous interfacial correlations in non-equilibrium anisotropic systems. *Journal of Physics A: Mathematical and General*, 26(16):L737–L741, August 1993. [76](#), [83](#)
- [126] M. Thiébaud, Y. Amarouchene, and T. Bickel. Nonlinear Brownian dynamics of interfacial fluctuations in a shear flow. *Journal of Statistical Mechanics: Theory and Experiment*, 2014(12):P12011, December 2014. [76](#)
- [127] D. S. Dean, B-S. Lu, A. C. Maggs, and R. Podgornik. Nonequilibrium Tuning of the Thermal Casimir Effect. *Physical Review Letters*, 116(24), June 2016. [82](#)
- [128] B.-S. Lu, D. S. Dean, and R. Podgornik. Out-of-equilibrium thermal Casimir effect between Brownian conducting plates. *EPL (Europhysics Letters)*, 112(2):20001, October 2015. [84](#)
- [129] N. Maat, C. Kraan, and W. A. Oost. The roughness of wind waves. *Boundary-Layer Meteorology*, 54(1-2):89–103, January 1991. [87](#), [89](#)